Technische Universität München

Fakultät für Medizin

Functional and metabolic fitness of human CD4$^+$ T lymphocytes under mitochondrial and nutrient stress

Lisa Holthaus

Vollständiger Abdruck der von der Fakultät für Medizin der Technischen Universität München zur Erlangung des akademischen Grades eines Doktors der Naturwissenschaften (Dr. rer. nat.) genehmigten Dissertation.

Vorsitzender: Prof. Dr. Percy A. Knolle

Prüfende/-r der Dissertation:

1. Prof. Dr. Anette-Gabriele Ziegler

2. Prof. Dr. Martin Hrabě de Angelis

Die Dissertation wurde am 20.02.2019 bei der Technischen Universität München eingereicht und durch die Fakultät für Medizin am 08.10.2019 angenommen.

Table of Content

List of Figures

LIST OF TABLES

ABBREVIATION

2-DG	2-desoxyglucose
3PG	3-Phosphoglyceric acid
ACC1	acetyl-CoA Carboxylase I
Akt	activated protein kinase B
AMPK	AMP-activated protein kinase
AP-1	activator protein 1
ATP	Adenosine triphosphate
Bcl-6	B-cell lymphoma 6 protein
Ca^{2+}	Calcium
CD	Cluster of differentiation
CoA	coenzyme A
CPT1	carnitine palmitoyl transferase I
DAG	diacylglycerol
DC	Dentritic cell
DHA	Dihydroxyacetone phosphate
DMSO	Dimethyl sulfoxide
DNA	Deoxyribonucleic acid
EAE	experimental autoimmune encephalomyelitis
ECAR	extracellular acidification rate
elF2a	eukaryotic initiation factor 2a
Elk-1	ETS domain-containing protein
ER	Endoplasmatisches Reticulum
ETC	Electron transport chain
FA	Fatty acid
FACS	Fluorescence-activated cell sorting
FAD/FADH2	flavin adenine dinucleotide
FAO	Fatty acid oxidation
FAS	Fatty acid synthesis
FASN	fatty acid synthase
FBP	Fructose bisphosphatase
FFA	Free fatty acids
FoxP3	Forkhead box P3
FSC	Forward scatter
G3P	Glyceraldehyde 3-phosphate
G6P	glucose-6-phosphate
GAPDH	Glyceraldehyde 3-phosphate dehydrogenase
GCK	Glucokinase
Glut1	Glucose transporter 1
GM-CSF	Granulocyte-macrophage colony-stimulating factor
GOT1/2	aspartate aminotransferase
GPCR	G protein coupled receptor
GTP	Guanosine triphosphate
HDAC	histone deacetylase
HIFα	hypoxia-inducible factor 1-alpha

HMGRCR	hydroxymethylglutaryl-CoA reductase
HSP	Heat shock protein
IκB	Inhibitor of κB
ICOS	inducible co-stimulator
IFN	Interferons
IKK	IκB kinase
IL	Interleukin
IMM	inner mitochondrial membrane
IP_3	inositol triphosphate
ITAM	immunoreceptor tyrosin-based activation motifs
JNK	Jun kinase
LAT	linker of activation of T cells
Lck	lymphocyte-specific protein tyrosine kinase
LDH	Lactate dehydrogenase
MACS	Magnetic activated cell sorting
MAPK	mitogen-associated protein kinases
MDH2	Malate dehydrogenase, mitochondrial
MHC	Major Histocompatibility Complex
MFI	Mean fluorescence intensity
mTOR	mammalian target of rapamycin
NAD/ NADH	Nicotinamide adenine dinucleotide
NADP/ NADPH	Nicotinamide adenine dinucleotide phosphate
NCID	NAD^+-induced cell death
NFkB	nuclear factor kappa-light-chain-enhancer of activated B cells
NFAT	nuclear factor of activated T cell
OCAR	oxygen consumption rate
OXPHOS	oxidative phosphorylation
PI3K	phosphatidylinositol 3-kinase
PBMC	peripheral blood mononuclear cell
PCA	Principle component analysis
PHD	prolyl hydroxylase domain proteins
PIP_2	Phosphatidylinositol 4,5-bisphosphate
PLC	phospholipase C
PPP	Pentose phosphate pathway
PKC-θ	protein kinase C-θ
pVHL	Hippel-Lindau tumor suppressor protein
RasGRP	guanine-nucleotide exchange factor
RCF	Relative centrifugal force
RNA	Ribonucleic acid
RORγt	orphan nuclear hormone receptor
ROS	Reactive oxygen species
SIRT1	Sirtuin 1
SLP-76	lymphocyte cytosolic protein 2
SRC	Spare respiratory capacity
SREBP	sterol regulatory element binding protein
SSC	Side scatter

STAT	signal transducer and activator of transcription
TCA cycle	Tricarboxylic acid cycle
TCR	T cell receptor
T_{FH} cell	T follicular helper cells
T_H cells	T helper cells
TNF	tumor necrosis factor
TRAF-6	TNF receptor associated factor 6
T_{reg}	regulatory T cell
Zap-70	Zeta-chain-associated protein kinase 70

SUMMARY

Molecular metabolism drives cellular function. A precise regulation of metabolic pathways supports cell-type specific energy demands for their functional properties. In T cell biology, metabolism was shown to be directly linked to T cell activation, function, differentiation and survival. In comparison to many other cell types, immune cells frequently switch between resting and active stages and adjust their functional profiles for host immunity. This functional rewiring in a T cell life cycle is accompanied by metabolic rewiring. In the absence of antigen exposure, naive T cells display a metabolic quiescent phenotype. In optimal environmental conditions, activation of T cells initiates a metabolic switch from catabolic metabolism to anabolic metabolism. The available nutrients are used to maximize energy production by engaging oxidative phosphorylation (OXPHOS). Antigen recognition initiates signaling cascades and metabolic reprogramming to support cell growth and proliferation. Anabolic pathways such as glycolysis are stimulated to meet the energy demand for adjusted function. Primed memory T cells remain after terminated immune challenges. Just like naive T cells, memory T cells display a catabolic metabolism, relying on the oxidation of glucose and fatty acids. Moreover, T cells encounter and operate in conditions with limited nutrient supply and need to respond to and transduce a variety of external signals. Nutrients are the basis of cellular metabolism and can act as important cues that influence immune cell function. Adaptation mechanisms to discrete microenvironments are pivotal for effective adaptive immune responses.

The aim of my thesis was to determine the metabolic requirements for human $CD4^+$ T cell functions. I used *in vitro* measures of T cell response in the presence of metabolic perturbations as my model. I described $CD4^+$ T cell functional adaptation in the presence of different environmental factors such as nutrient scarcity and mitochondrial stress. The impact of nutrient availability was simulated with fluctuating glucose concentrations. Mitochondrial stress was induced by specific inhibitors targeting the electron transport chain (ETC) and the ATP synthase.

$CD4^+$ T cell functional changes were aligned to distinct metabolic pathways by using an *in vitro* model of human $CD4^+$ T cell function, including T cell activation, proliferation and cytokine production. Metabolic alterations were reported by real time extracellular flux analysis, glucose uptake assays and reactive oxygen species production. Genomic changes under these conditions in the different $CD4^+$ T cell subsets were investigated by RNA sequencing (RNAseq) to understand the underlying mechanism of T cell fitness.

I could show that T cell activation, proliferation but not cytokine production relied on mitochondrial function. Moreover, T lymphocytes did not compensate for mitoenergetic dysfunction by increasing glycolytic rates as many other cell types. Induction of mitochondrial stress was further linked to increased ROS production. This was particularly evident in naive T cells which were already shown to be functionally more sensitive compared to their memory counterparts. Limiting glucose

concentration alone did not affect T cell function but I identified a synergistic role of glucose deprivation and mitochondrial dysfunction. I was able to support the functional and metabolic data with findings at the transcriptional level. The expression of glycolytic genes remained stable, indicating that metabolic adaptation mechanism was not observed on a transcriptional level. However, mitochondrial dysfunction led to a decrease in the expression of genes downstream of interferon signaling in naive, memory and regulatory $CD4^+$ T cells.

Furthermore, molecular chaperones were shown to be highly induced especially in naive T cells, supporting their functional sensitivity. The natural occurring polyphenol resveratrol has been reported to interfere directly with mitochondrial function. My investigations of T cell function in the presence of resveratrol found no alteration in metabolic flux, suggested a mechanism of action that is upstream of mitochondrial function. I found that resveratrol markedly impaired $CD4^+$ T cell proliferation and cytokine production, had little effect on T cell activation, and reduced ROS production. These findings were further supported by a decrease in the expression of several cytokines at the transcriptional level and many genes which are known activators of NFκB.

My thesis presents a detailed description of T cell functional and metabolic interplay. My findings show how three quintessential aspects of T cell function are differently affected by nutrient availability and mitochondrial processes. Activation and proliferation, but not effector function, were critically dependent upon intact electron chain transport and ATP synthase. The findings provide new understanding as to how adaptive immunity may be compromised by stress and potentially modulated via therapy that targets metabolic pathways.

ZUSAMMENFASSUNG

Die bioenergetischen und biosynthetischen Produktionswege einer Zelle sind genauestens an ihre Funktionen angepasst. Dies gilt in besonderem Maße für Immunzellen, die im Gegensatz zu den meisten anderen Zelltypen, ihre Aktivität den gegebenen Anforderung und Umweltbedingungen anpassen können. Diese funktionale Umstrukturierung erfordert auch eine Umprogrammierung des Stoffwechsels.

Ruhende T-Zellen nutzen vorhandene Nährstoffe ausschließlich zur Energieproduktion, indem sie Energie in Form von ATP durch oxydative Phosphorylierung in den Mitochondrien bereitstellen. Die Aktivierung der T-Zellen löst einen Wechsel von katabolen zu anabolen Stoffwechseln aus. Die oxydative Phosphorylierung wird durch eine gesteigerte Verbrennung von Glukose mittels aerober Glykolyse ersetzt. Hierdurch erhöht sich die Produktion von essentiellen molekularen Bausteinen, welche das Zellwachstum und die Proliferation unterstützt.

Die Milieus, in denen T-Zellen ihre Funktion ausüben, sind oft arm an Nährstoffen. Da Nährstoffe die Grundlage für alle Stoffwechselprozesse darstellen, bestimmt deren extrazelluläre Abundanz und Zusammensetzung die Immunfunktion entscheidend mit. Funktionale und metabolische Anpassungen an Umweltbedingungen sind daher essentiell für eine effektive Immunantwort. Vor allem in humanen T-Zellen sind diese Anpassungen und deren Mechanismen weitestgehend unbekannt.

Ziel meiner Doktorarbeit war die Untersuchung der Stoffwechselprozesse in aktivierten humanen $CD4^+$ T-Zellen, sowie deren funktionale und metabolische Anpassungsfähigkeit an bestimmte Umweltbedingungen. Dabei waren besonders das Zusammenspiel und die Regulierung von Glykolyse und oxydativer Phosphorylierung während einer Immunantwort von Interesse. Hierzu wurde ein *in vitro* Verfahren entwickelt, um unterschiedliche T-Zellantworten in Gegenwart von verschiedenen Umweltbedingungen zu analysieren. Untersucht wurden Nährstoffmangel, in Form von sukzessivem Glukosemangel, und mitochondrialer Stress. Letzterer wurde durch spezifische Inhibitoren des respiratorischen Atmungskomplex I der Elektronentransportkette, sowie der ATP Synthase graduell induziert. Die funktionalen Änderungen der $CD4^+$ T-Zell Immunantwort konnten somit präzise mit Veränderungen der oxydativen Phosphorylierung und der Glykolyse verknüpft werden. Als funktionale Readouts dienten die T-Zell Aktivierung, Proliferation sowie die T-Zell Effektorfunktion in Form von Zytokinproduktion. Veränderungen im T-Zell Stoffwechsel wurden durch extrazelluläre Flux Analysen ermittelt. Darüber hinaus erlaubte eine Bestimmung der Glukoseaufnahme in die Zelle sowie eine Ermittlung der Produktion von reaktiven Sauerstoffspezies (ROS) eine zusätzliche Charakterisierung des Stoffwechsels. Mittels RNA Sequenzierung verschiedener $CD4^+$ T-Zell Subtypen in Gegenwart von Glukosemangel und mitochondrialem Stress wurden die funktionalen Veränderungen und die Umprogrammierung des Stoffwechsels auch auf transkriptioneller Ebene charakterisiert.

Im Rahmen dieser Arbeit wurde gezeigt, dass die T-Zell Aktivierung sowie die T-Zell Proliferation stark von mitochondrialer Energieproduktion abhängt. Die Produktion von Zytokinen hingegen wies ein hohes Maß an Robustheit und metabolischer Unabhängigkeit auf. Mitochondrialer Stress und mitochondriale Dysfunktion führten allerdings in den $CD4^+$ T-Zell Subtypen zu einer verringerten Expression von IFN-induzierten Genen. Darüber hinaus wurde deutlich, dass T-Zellen, im Gegensatz zu vielen anderen Zelltypen, mitochondriale Dysfunktionen nicht mit einer erhöhten glykolytischen Aktivität kompensieren. Diese Beobachtung wurde durch die unveränderte Expression glykolytischer Gene bestätigt. Dies deutet darauf hin, dass metabolische Anpassungen vor allem auf post-transkriptioneller Ebene stattfinden. Naive T-Zellen zeigten im Vergleich zu regulatorischen T-Zellen und T-Gedächtniszellen eine erhöhte Sensitivität gegenüber mitochondrialem Stress. Dies wurde durch eine gesteigerte Produktion von ROS, eine geringere Aktivierung, sowie durch einen Anstieg der Expression von Stress-induzierten Hitzeschockproteinen deutlich. Glukosemangel hatte keinen großen Einfluss auf T-Zell Funktionen, zeigten allerdings einen synergistischen Effekt mit mitochondrialem Stress. Zusätzlich zu den verwendeten, genau charakterisierten Inhibitoren, wurde das natürlich vorkommende Polyphenol Resveratrol getestet. Es wird vermutet, dass Resveratrol direkt oder indirekt mit dem mitochondrialem Stoffwechsel interferiert, der zugrundeliegende Wirkungsmechanismus ist allerdings noch weitestgehend unbekannt. Die im Rahmen dieser Doktorarbeit unternommenen Untersuchungen, deuten auf einen Wirkungsmechanismus hin, der den mitochondrialen Funktionswegen vorgeschaltet ist, da kein direkter Einfluss von Resveratrol auf die Zellatmung festgestellt wurde. In dieser Arbeit wurde erstmals gezeigt, dass Resveratrol die T-Zellfunktion dosisabhängig supprimiert. Vor allem die Produktion von Zytokinen, sowie die T-Zell Proliferation wurde maßgeblich eingeschränkt. Darüber hinaus konnte eine Reduzierung der ROS Produktion festgestellt werden. Transkriptionelle Analysen unterstützten diese Beobachtungen. Die Expression von Zytokinen, sowie die Expression bekannter Aktivatoren von NFκB wurden deutlich reduziert.

Meine Doktorarbeit stellt eine detaillierte Beschreibung des komplexen Zusammenspiels von T-Zell Funktion und Stoffwechsel dar. Die vorliegenden Ergebnisse zeigen, in welchem Ausmaß drei wesentliche Aspekte der T-Zell Funktionen, Aktivierung, Proliferation und Zytokinproduktion, durch Nährstoffknappheit und mitochondriale Aktivität beeinflusst werden. Insbesondere die Aktivierung der Immunzellen sowie die sich daran anschließende T-Zell Proliferation zeigten eine direkte Abhängigkeit von mitochondrialer Energieproduktion, wohingegen die Zytokinproduktion eine deutlich höhere Plastizität und metabolische Unabhängigkeit aufwies. Die hier gewonnenen Erkenntnisse ermöglichen neue Einblicke in die Wechselwirkung von Umweltbedingungen und adaptive Immunantwort.

1 INTRODUCTION

Immunity must respond to challenge. Response requires rapid changes in cells that are fueled by a large amount of energy, the ability of cells to perform functions in diverse environments, and the need to defend both acutely and chronically. The quality and regulation (fitness) of immune responses are in part genetically determined and in part determined by environmental factors. This gene-environment modification of immune fitness is an important determinant of susceptibility to multiple diseases including autoimmune diseases and cancer. I lean toward the notion that immune fitness requires an ability of cells to acquire and produce energy under conditions of stress. Under this hypothesis, knowing the metabolism that governs immune function will be critical to determining causes and therapy of immune-mediated disease. My thesis addresses this in human $CD4^+$ T lymphocytes, which are the directors of adaptive immunity and are cells affected by genetic susceptibility in disease such as type 1 diabetes. I have identified critical steps in the production of energy and used inhibitors that interfere with these steps leading to metabolic stress, sought to combine these with variation in nutrient ability and examined how $CD4^+$ T cell metabolism is altered by these conditions and related these changes to how key functions in the $CD4^+$ T cell response are affected. My findings have led to new knowledge regarding the essential metabolic pathways for $CD4^+$ T cell function and I hope and that these findings will eventually contribute to new therapies for immune mediated disease such as type 1 diabetes.

1.1 Cell metabolism in a nutshell

Immune cells with different functions use several different metabolic pathways to meet their energy demand and support cell growth and function. The diversity of these pathways is large. Nutrient composition of the local environment additionally shapes the coupling of metabolism and immune cell function and raises a need of metabolic flexibility for adaption mechanisms. This chapter provides an overview of the most important metabolic pathways in order to understand the complex interplay between the various pathways (Figure 1; Table 1).

Table 1: Overview of main metabolic pathways for T cell function. The location within the cell, their main process as well as the needed energy sources and energy outputs are described.

Metabolic Pathway	Location	Process	Energy Source	Energy Output
Glycolysis	Cytoplasm	Conversion of glucose into pyruvate	D-Glucose; NAD^+; ADP; P_i	Pyruvate; NADH; ATP
Tricarboxylic acid (TCA) cycle	Mitochondria	Oxidation of Acetyl-CoA to release stored energy	Acetyl-CoA; NAD^+; FAD^+; GDP;	CoA; NADH; $FADH_2$; GTP
Oxidative Phosphorylation (OXPHOS)	Mitochondria	Redox reactions carried out in the ETC, leading to a release of energy to produce ATP	NADH; $FADH_2$; ADP; O_2	NAD^+; FAD^+; H_2O; ATP
Fatty Acid Oxidation (FAO)	Mitochondria	Catabolic break down of fatty acids to generate Acetyl-CoA	Cn-acyl-CoA; FAD^+; NAD^+; CoA	Cn-2-acyl-CoA; $FADH_2$; NADH; Acetyl-CoA
Fatty Acid Synthesis (FAS)	Cytoplasm	Generation of FA derived from Acetyl-CoA	Acetyl-CoA; NADPH	Fatty acids; NADP
Pentose Phosphate Pathway (PPP)	Cytoplasm	Generation of reducing equivalent NADPH; precursor for nucleotides and amino acids	$NADP^+$; Glucose-6-phosphate	NADPH; ribose-5-phosphate

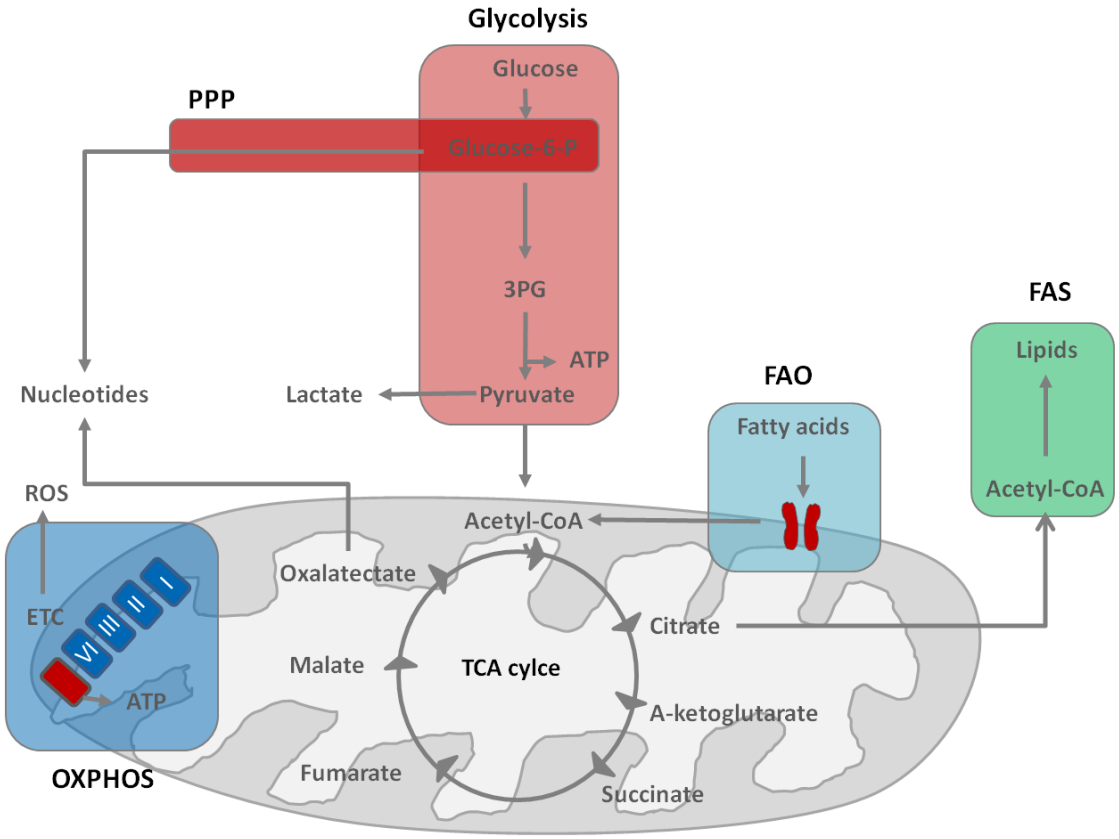

Figure 1: An overview of important metabolic pathways for T cell function. Glycolysis (red) breaks down glucose into two molecules of pyruvate in the cytoplasm. Pyruvate enters the mitochondria and fuels the TCA cycle. TCA cycle produces reducing equivalents and Acetyl-CoA. Fatty acid oxidation (blue) is a branching point of the TCA cycle. Furthermore the TCA cycle produces biosynthetic precursors. Intermediate pathway from glycolysis is the pentose phosphate pathway (PPP), (dark red) and fuels the production of nucleotides and amino acids. Oxalacetate from the TCA cycle can be used for production of aspartate nucleotide synthesis. Citrate can further be converted into Acetyl-CoA in the cytoplasm to fuel fatty acid synthesis (green). Reducing equivalents (NADH and $FADH_2$) from the TCA cycle are consumed in the ETC to produce ATP. ROS is further generated at the ETC and can serve as important signaling molecule (modified from Buck et al., 2015).

1.1.1 Glycolysis

Glucose uptake of cells is mediated by specific glucose transporters. Different tissues use different transporters, specifically adapted to their metabolic signature. Glucose transporter 1 (Glut1) is the favored glucose transporter in lymphocytes (Frauwirth et al., 2002; Macintvre et al., 2012). When glucose enters the cell, it is metabolized in a series of anaerobic steps in the cytosol into two molecules of pyruvate and two molecules of ATP in a process termed glycolysis. Moreover, glycolysis produces NADH from NAD^+, thereby providing an important cofactor for downstream metabolic processes. Glycolysis supports anabolic growth by rapidly providing energy and biosynthetic intermediates to support cell growth and proliferation. Cells are able to maintain a constant glycolytic flux without oxygen supply by lactate dehydrogenase (LDH) conversion of pyruvate to lactate. It was previously shown that T cells engage this pathway despite sufficient oxygen supply. This effect is known as aerobic glycolysis or the “Warburg effect” (Berg et al., 2010, chap. 16; O’Neill et al., 2016). The process of glycolysis can be broken down into two phases.

The first energy requiring phase includes the enclosure of glucose in the cell and its destabilization by attaching two molecules of phosphate, derived from ATP to the glucose molecule to yield the modified sugar D-Fructose-1,6-bisphosphate (FBP). The phosphorylation reactions destabilize the molecule so that it can be subsequently split into two three-carbon sugars.

The second energy releasing phase of glycolysis involves the cleavage of FBP into two 3 carbon molecules: Dihydroxyacetone phosphate (DHA) and D-Glyceraldehyde-3-phosphate (G3P). DHA is converted into G3P in the later step. Each three-carbon sugar is converted in a series of reactions into two molecules of pyruvate. During these steps, four molecules of ATP and two molecules of NADH are produced. Due to the investment of ATP in the first phase, glycolysis has a total net gain of two molecules of ATP. Each of the reactions requires its own glycolytic enzyme. The distinct steps of glycolysis are shown in detailed in Figure 2. The end products of glycolysis are:

Glucose + 2ADP + 2NAD^+ → 2x pyruvate + 2ATP + 2NADH + 2H^+ + 2H_2O (Berg et al., 2010, chap. 16).

1.1.2 TCA Cycle

The TCA cycle takes place in the mitochondrial cytosol and is the central metabolic hub within a cell. It is fueled by molecules which can be transformed into acetyl groups or dicarboxylic acids. The most common representatives are pyruvate and fatty acids. The TCA cycle is of major importance for the generation of various biosynthetic precursors, supporting the synthesis of amino acids, nucleotide bases, cholesterol and porphyrins. Furthermore, in combination with oxidative phosphorylation, it is considered as the most efficient way of generating energy in form of ATP.

The TCA cycle consists of many oxidation – reduction reactions by which glucose derivates are oxidized into carbon dioxide and the reducing equivalents NADH and $FADH_2$. They serve as high energy electron carriers that support the electron transport chain to build up the mitochondrial membrane potential and support oxidative phosphorylation. Prior to entering the TCA cycle, pyruvate is converted into Acetyl-CoA in the mitochondria via pyruvate dehydrogenase (PDC). Acetyl-CoA is combined with oxaloacetate to form citrate, which is converted into isocitrate and then into alpha-ketoglutarate and NADH. In the next step, succinyl CoA is converted into succinate in a process that also forms GTP. Subsequently fumarate is formed by succinate dehydrogenase (SDH) and $FADH_2$ is generated from FAD. SDH is furthermore the only enzyme of the TCA cycle which is also engaged in the electron transport chain carrier as complex II. Fumarate is transformed into malate. Malate is converted back again into oxaloacetate with NADH as a byproduct. A major function of the TCA cycle is the generation of high electron carrier NADH and $FADH_2$ to fuel the electron transport chain. The TCA cycle does not produce large amounts of energy. The electrons from NADH and $FADH_2$ are released in oxidative phosphorylation by flow through of several mitochondrial membrane carrier to generate a proton motive force across the inner mitochondrial membrane, which is used to drive the ATP synthase and

hence the production of ATP. The TCA cycle is considered as aerobic, even though oxygen is only needed indirectly. The final electron acceptor in the ETC is molecular oxygen. This is necessary to refill the NAD^+ FAD pool within a cell (Figure 2)(Berg et al., 2010, chap. 17; O'Neill et al., 2016).

1.1.3 Oxidative Phosphorylation

The NADH and $FADH_2$ generated during TCA cycle activity, together with fatty acid oxidation and glycolysis are used during oxidative phosphorylation to transfer their electrons to molecular oxygen and release a large amount of energy in form of ATP. The electron transfer is performed stepwise in a series of electron carriers embedded in the mitochondrial inner membrane (Table 2; Figure 2). This process generates 36 molecules of ATP. The electron flux through the membrane results in proton transfer (H^+) mediated by complex I, III and IV across the inner membrane into the intermembrane space. The emerging electrochemical proton gradient ($\Delta\phi m$) drives the function of the ATP synthase (complex V). An additional function of the electron transport chain beyond the production of ATP is the generation of ROS at complex I and III (Mehta et al., 2017; Sena and Chandel, 2012). The electron transport chain consists of five multi-subunit complexes. The main driving force of the ETC is borne from the fact that each membrane complex has a higher standard reduction potential compared to the electron donors. Oxygen has the highest standard reduction potential and is therefore located at the end of the ETC. Complex I and II accept electrons derived from NADH and $FADH_2$, respectively. The released electrons are subsequently transferred to coenzyme Q and complex III. The electron flux continues via complex IV to finally end in a delivery to molecular oxygen to form water. This process is responsible for the regeneration of NAD^+ and FAD. The proton motive force describes the energy derived from the proton transport across the inner mitochondrial membrane. Solely complex I, III and IV are able to transport protons from the inner to the outer membrane as electrons flow through the various complexes. The coupling of electron flow and proton motive force is referred as chemiosmotic coupling and a driver of ATP synthesis (Berg et al., 2010, chap. 18)

Table 2: Characterization of electron transport chain complexes embedded in the inner mitochondrial membrane.

ETC Complex	Protein name	Mechanism
Complex I	NADH-ubiquinone oxidoreductase	Integral protein, accepts electrons from NADH
Complex III	Succinate-ubiquinone oxidoreductase	Succinate dehydrogenase from the TCA cycle. Receives electron from FADH2 which are generated in the TCA cycle by the conversion of succinate to fumarate
Q	Ubiquinone/ ubiquinol	Ubiquinone is the oxidized form of ubiquinol. It receives electrons from various carriers.
Complex III	Ubiquinol-cytochrome c oxidoreductase	Integral protein, receives the electrons from ubiquinol and passes them further to cytochrome c
Complex IV	Cytochrom C oxidase	Integral protein accepts electrons form cytochorm c and further transports them to oxygen.
Complex V	ATP Synthase	Integral protein consists of several subunits and drives the production of ATP via chemiosmotic phophorylation. The proton gradient is used to drive the molecular rotor and phosphorylates ADP to ATP

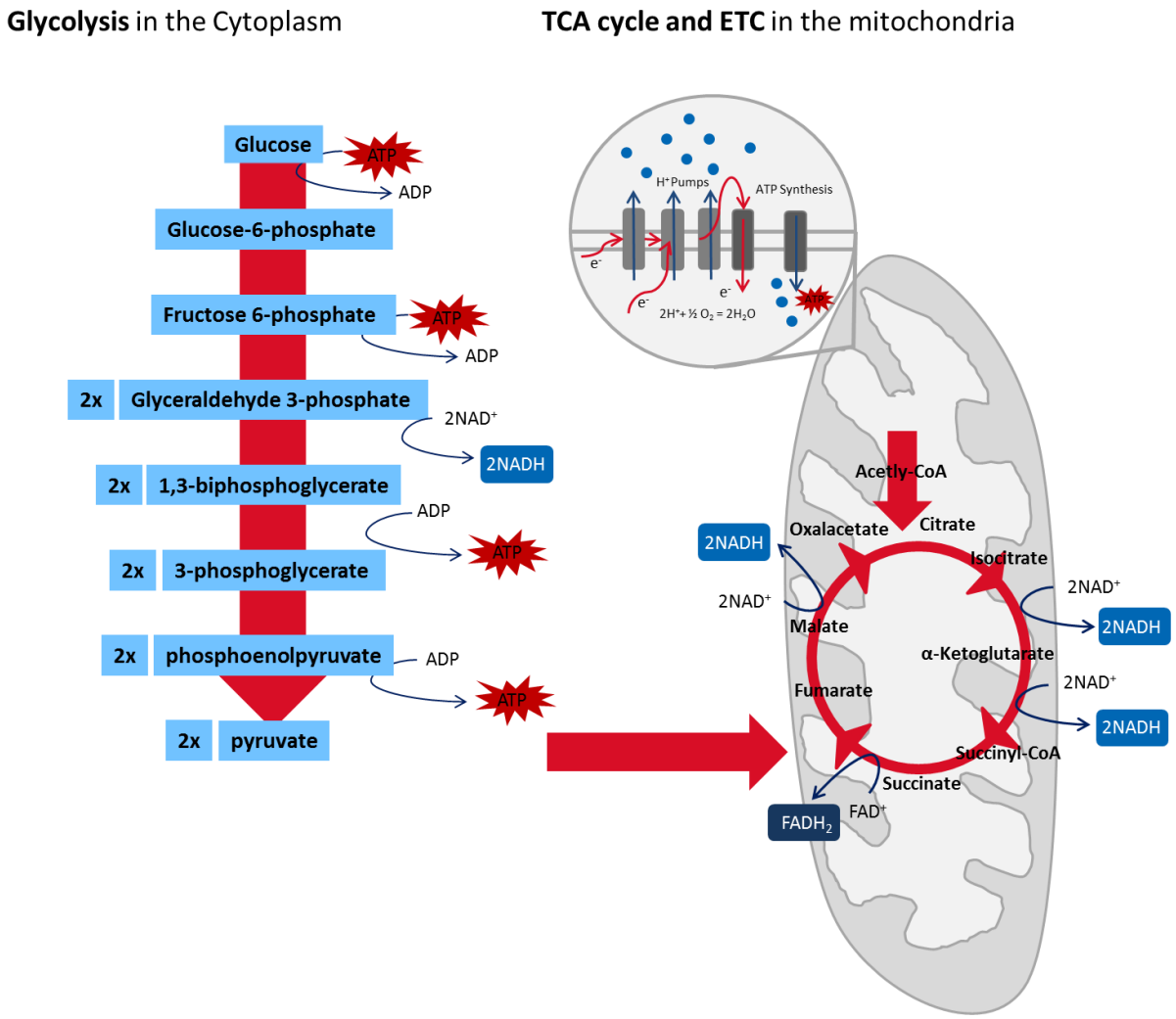

Figure 2: Model of cellular respiration. The process of glycolysis takes place in the cytoplasm of the cell. Tricarboxic acid cycle and OXPHOS are located in the mitochondria. Reducing equivalents NADH and $FADH_2$ are produced during Glycolysis and TCA cycle and are consumed in the ETC. ATP production takes place during glycolysis and OXPHOS.

1.1.4 Pentose Phosphate Pathway

The pentose phosphate pathway (PPP) is an alternative glucose shunt directed from glycolysis in order to generate NADPH and 5-carbon sugars (Figure 1). It is an important source for the production of nucleotides and amino acid precursors. The 5-carbon units are bound in DNA and RNA synthesis as well as in the generation of ATP, NADH, $FADH_2$ and coenzyme A synthesis. Most important, the PPP is designed to provide the cell's need for NADPH for reductive biosynthesis and hence mainly supports cell growth and survival. NADPH is required for fatty acid, cholesterol and nucleotide synthesis as well as for detoxification as it is engaged in the reduction of oxidized glutathione and cytochrome P450 monooxygenases.

The PPP consists of two phases. *The oxidative branch* leads to the production of NADPH. It is generated during the oxidation of glucose 6-phosphate to ribose 5-phosphate. *The non-oxidative branch* of the PPP catalyzes the interconversion of three to seven carbon sugars and results in the formation of 5-

carbon sugars for nucleotide synthesis or into the intermediates of the glycolytic pathway glyceraldehyde 3-phosphate (G3P). Both branches of the PPP take place in the cytosol (Berg et al., 2010, chap. 20.3; O'Neill et al., 2016).

1.1.5 Fatty acid oxidation

Fatty acids are high energy molecules and the breakdown of fatty acids forms an additional efficient way for ATP production (potentially over 100 ATP molecules). Fatty acid oxidation is a multi-step process and primarily takes place in the mitochondria. Fatty acids first enter the cytosol of a cell via fatty acid transporters such as the fatty acid translocase (CD36). In the cytosol, FAs are activated by conjugation with the coenzyme A (CoA), a step requiring ATP to produce acyl-CoA. Short chain fatty acids can enter the mitochondria by diffusion. Medium- and long-chain fatty acids instead need to be conjugated to carnitine via carnitine palmitoyl transferase I (CPT1) prior to mitochondrial entry. CPT1 sits on the inner surface of the outer mitochondrial membrane and represents a key regulatory checkpoint in fatty acid metabolism. Inside the mitochondria, the carnitine-tail is again removed to eventually yield acyl-CoA again. During β-oxidation, the fatty acid chains are degraded in a series of enzymatic reactions down to acetyl-CoA. NADH and $FADH_2$ are additionally generated. These products are further used in the TCA cycle and the electron transport chain (Almeida et al., 2016; Berg et al., 2010, chap. 22; O'Neill et al., 2016; Ward, 2015).

1.1.6 Fatty acid synthesis

Fatty acids can be synthesized *de novo* within the cell using mitochondrial citrate. Citrate from the TCA cycle is transported into the cytosol and converted into acetyl CoA. The carboxylation of acetyl-CoA by acetyl-CoA Carboxylase I (ACC1) generates malonyl-CoA. This is an irreversible reaction which requires ATP. The fatty acid chain is elongated by the multienzyme complex FASN (fatty acid synthase). In a series of NADPH-dependent reactions, acetyl molecules are added to the nascent acyl-chain. Palmitate is the produced precursor fatty acid and can be transformed into other fatty acids (Lochner et al., 2015; O'Neill and Pearce, 2015)

1.2 Human T cell activation, proliferation and differentiation

T cell activation is thought to start when the T cell receptor (TCR) binds to a cognate MHC:peptide complex. The ligation initiates an intracellular signaling cascade finally resulting in proliferation, differentiation and effector function. The rapid and clonal expansion following the activation of T cells must be accompanied by a change in nutrient and energy needs. This chapter reviews the classical T cell activation model and furthermore presents the state of the art of the role of T cell energetics on the initiation of the T cell immune response.

1.2.1 The classical model of T cell activation

Quiescent T cells are activated upon antigen binding to their T cell receptor. The antigen is presented to $CD4^+$ T cells via the Major Histocompatibility Complex II (MHCII) on specific antigen-presenting cells such as dendritic cells or macrophages. The TCR consists of α and β chains that have only a short intracellular tail without enzymatic activity and hence incapable of intrinsic signal transduction. Additional accessory proteins are needed to transmit the stimulatory signal. Upon TCR binding, the immunoreceptor tyrosin-based activation motifs (ITAM) of the TCR:CD3 complexes (10 in total) become phosphorylated and bind Zeta-chain-associated protein kinase 70 (Zap-70,) which phosphorylates the scaffold proteins linker of activation of T cells (LAT) and lymphocyte cytosolic protein 2 (SLP-76). These proteins bind to phospholipase C-γ (PLC), which upon phosphorylation cleaves Phosphatidylinositol 4,5-bisphosphate (PIP_2) into diacylglycerol (DAG) and inositol triphosphate (IP_3). This process initiates three different major pathways in T cells.

Within the first pathway, IP_3 diffuses into the cytosol and binds to receptor localized on the endoplasmic reticulum (ER) membrane. These receptors are calcium (Ca^{2+}) channels and release calcium within the ER, and eventually the cytosol where it binds to calmodulin leading to the activation of calcineurin. Calcineurin is responsible for activating the transcription factor nuclear factor of activated T cells (NFAT) by dephosphorylation. NFAT is subsequently able to enter the nucleus and initiate gene transcription necessary for cell proliferation and differentiation.

Second, DAG activates RasGRP (guanine-nucleotide exchange factor) by binding to its internal interaction module C1, and recruits RasGRP to the membrane, activating Ras. The activation of Ras initiates the mitogen-associated protein kinases (MAPK) cascade. This cascades ends with the activation of the transcription factor ETS domain-containing protein (Elk-1). Elk-1 cooperates with the serum response factor to initiate *FOS* gene transcription. FOS protein associates with Jun and forms the activator protein 1 (AP-1) heterodimer, which is activated by Jun kinase (JNK) activity.

In addition to Ras activation, DAG recruits an isoform of the protein kinase C, the protein kinase C-θ (PKC-θ) to the membrane. PKC-θ leads to the phosphorylation of CARMA1 and subsequently signal transduction via TNF receptor associated factor 6 (TRAF-6) recruitment to activate the nuclear factor-kappa-light-chain-enhancer of activated B cells (NFκB) by degradation of the Inhibitor of κB (IκB) by IκB kinase (IKK) (Figure 3).

TCR stimulation alone is insufficient for complete T cell activation. Co-stimulation plays a crucial role for the transition of a quiescent to an activated T cell. CD28 and the inducible co-stimulator (ICOS) are co-stimulatory molecules. CD28 interacts with its designated ligands B7.1 (CD80) and B7.2 (CD86) on the antigen-presenting cell. CD28 signaling supports T cell activation mainly by promoting T cell proliferation, cytokine production and cell survival. These events are mediated by signaling motifs present in the cytoplasmic domain of CD28. PIP_3 is subsequently activated and recruits Itk to the

membrane where Lck can phosphorylate Itk. PIP_3 furthermore recruits activated protein kinase B (Akt) to the membrane. Akt is responsible for stimulating T cell metabolism by increasing glucose uptake (reviewed in Murphy, 2011a; Smith-Garvin and Koretzky, 2009).

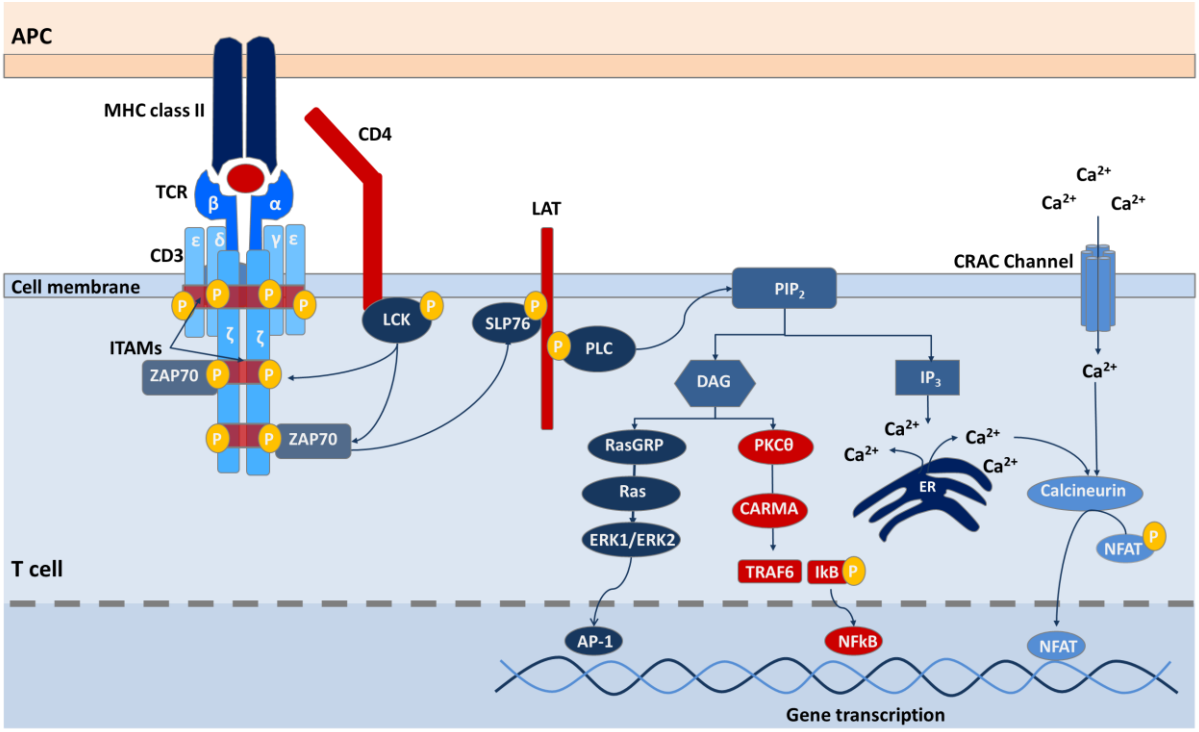

Figure 3: The TCR signaling cascades. The TCR complex is composed of α and β TCR heterodimers as well as the CD3 chains (ε, δ, γ, ζ) Each CD3 chain is associated with an ITAM-motive. After TCR ligation, LCK binds to the CD4 co-receptor, resulting in phosphorylation of the ITAMs. ZAP-70 binds to the phosphorylated ITAMs to become phosphorylated itself. Phosphorylated ZAP-70 activates SLP-76 and LAT. This activation process results in the activation of PLC, which cleaves the membrane located PIP_2 into DAG and IP_3. IP_3 initiates a Ca^{2+} efflux out of the ER. The depletion of calcium in the ER leads to an opening of CRAC channels and Ca^{2+} enters the cytosol. The additional calcium activates calcineurin, which dephosphorylates NFAT, allowing its entry into the nucleus. DAG recruits PKCθ and RasGRP. RasGRP activates Ras and ERK via phophorylation, initiating the formation of the transcription factor AP-1. PKCθ activates CARMA which recruits TRAF6. TRAF6 initiates the destruction of IκB and subsequently activates NFκB. These transcription factors induce a transcriptional program resulting in proliferation and differentiantion of T cells. (modified after Gaud et al., 2018; Murphy, 2012, chap. 7).

1.2.2 A metabolic extension of the T cell activation model

T cell stimulation not only leads to an initiation of signaling cascade to arouse T cells from the resting state but also stimulates a switch in metabolic programs and corresponding metabolic signaling pathways to adapt to the change in energetic needs of proliferating cells (Buck et al., 2015). It was also shown that metabolic signaling emanating from mitochondria seems to be crucial for the activating process itself (Chandel, 2015; L. Sena et al., 2013). Within the next section the classical T cell activation model will be extended with findings on the role of cell metabolism in the activation and proliferation process.

A crucial role of metabolic rewiring during the activation process was noticed decades ago with the engagement of the co-stimulatory molecule CD28 upon TCR ligation. TCR/CD28 signaling induces

phosphatidylinositol 3-kinase (P13K)-Akt signaling, resulting in a distinct increase in the expression of the glucose transporter, Glut1 and the subsequent increase in glucose uptake (Frauwirth et al., 2002; Jacobs et al., 2008). Furthermore, it was shown that the MAPK cascade downstream of TCR/CD28 signaling upregulates glycolysis. TCR stimulation also promotes metabolic reprogramming via c-Myc and hypoxia-inducible factor 1-alpha (HIFα) (Wang et al., 2012). Both are controlled by the mammalian target of rapamycin (mTOR) complex. mTOR is a protein kinase which acts as a regulator of environmental cues. This is particularly interesting because it links T cell activation to the microenvironment of the T cell (Pollizzi and Powell, 2015).

1.2.2.1 The metabolic transition from resting to activated T cells

Naive and resting T cells are thought to have low metabolic needs. Their quiescent state is maintained by IL-7. It sustains homeostatic proliferation and survival (Klein Geltink et al., 2018). Proliferation processes and cytokine production is not present and hence anabolic processes are negligible. An increased energetic requirement during transition from resting to activating state is mainly supported by engaging OXPHOS (Almeida et al., 2016; Buck et al., 2015). Glucose and fatty acids are entirely consumed for maximal energy production with the highest yield of ATP. The activation process induces a change in energy demand as well as raising a need for anabolic processes increasing macromolecule synthesis such as fatty acids and amino acids (Dimeloe et al., 2017).

1.2.2.2 T cell activation and the different fates of glucose

1.2.2.2.1 Aerobic glycolysis

The increased Glut1 expression on the cell surface leads to a high glucose flux into the cell. Glycolytic and glutaminolytic genes are upregulated and an augmented glycolytic flux is observed. Lactate levels drastically increase indicating an increased conversion of the glycolytic end product pyruvate to lactate (Klein Geltink et al., 2018). This seems paradox. A switch to a metabolic pathway which is usually engaged upon low oxygen conditions and only produces 2 molecules of ATP instead of 30 molecules using OXPHOS activity, glycolysis seems counterproductive (Berg et al., 2010, chap. 18.6). Initially it was thought that aerobic glycolysis allows T cells to produce ATP much faster as compared to mitochondrial derived ATP. However, an increased ATP:ADP ratio would result in an inhibition of glycolysis via AMP-activated protein kinase (AMPK) (Lunt and Vander Heiden, 2011). Another hypothesis is that aerobic glycolysis is used for the production of biosynthetic precursors. Aerobic glycolysis maintains a high glycolytic flux by producing NAD^+ which is needed for the glycolytic enzymes such as Glyceraldehyde 3-phosphate dehydrogenase (GAPDH) (Dimeloe et al. 2017). Byproducts resulting from high rates of glycolysis are linked to the diverted PPP, serine biosynthesis pathway and de novo FAS. Nevertheless also this theory is controversial (Olenchock et al., 2017).

1.2.2.2.2 The TCA cycle

Mitochondrial respiration was also shown to be increased upon T cell activation. Pyruvate production still takes place and enters the mitochondria to fuel the TCA cycle as well as the electron transport chain. The increased glycolytic flux upon activation produces higher levels of pyruvate. Even though the majority might be transformed into lactate, it is still sufficient to increase mitochondrial function (Klein Geltink et al., 2018). Pyruvate enters the mitochondria via mitochondrial pyruvate carrier and is subsequently converted into Acetyl-CoA and fuels the TCA cycle. Acetyl-CoA is converted into carbon dioxide and water together with Guanosine triphosphate (GTP) and the co-factors NADH and $FADH_2$ needed for the electron transport chain. Beyond that, the TCA cycle is important for the production of precursors to cover the increased need for biosynthesis. Crucial branching points are citrate, needed for de novo fatty acid synthesis, α-Ketoglutarate which is a primary source for purines, proline, arginine and glutamine. Succinyl-CoA can fuel the production of porphyrins and hemes. Oxalacetate can be used for the production of many amino acids such as aspartate, serine, glycine, and tryptophan as well as pyrimidines. It furthermore serves as a branching point for gluconeogenesis. Upon activation, main benefit of TCA cycle engagement is rather the production of those intermediates than the production of co-factors needed for OXPHOS (Lunt and Vander Heiden, 2011; Maciolek et al., 2014).

1.2.2.2.3 Fatty acid metabolism

Upon TCR stimulation, there is not only a switch from OXPHOS towards glycolytic pathways, but also fatty acid synthesis is upregulated (Kidani et al., 2013; Michalek et al., 2011; Yang et al., 2013). This engagement of FAS further implicates a down regulation of FAO (Wang et al., 2011). The engagement of FAS is mediated via mTOR dependent pathways. Specifically mTORC1 seems to be essential for lipid biosynthesis and is mediated via the induction of sterol regulatory element binding protein (SREBP) (Yang et al., 2013). The mTOR-SREBP pathway results in an increased expression of ACC1, FASN and hydroxymethylglutaryl-CoA reductase (HMGRCR), the rate limiting enzyme in cholesterol synthesis (Kidani et al., 2013; Wang et al., 2011). The concrete necessity of upregulating FAS is still under investigation. Knock-out and loss of function experiments of ACC1 or the SREBP chaperone SCAP revealed a role of FAS specifically during T cell activation and differentiation by affecting mTOR-mediated metabolic reprogramming (Berod et al., 2014; Kidani et al., 2013; Lochner et al., 2015). Homeostatic T cell proliferation instead remained largely unaffected (Kidani et al., 2013; Lochner et al., 2015). Furthermore, fatty acid (FA) mediated post-translational protein modification are crucial for the activation process. Protein palmitoylation of important proteins involved in T cell activation ensure sustained signal processing (Arcaro et al., 2000; Crise and Rose, 1992; Koegl et al., 1994). This protein palmitoylation is needed for the recruitment of signaling molecules to the immunological synapsis (Ladygina et al., 2011). Hence FA-mediated protein modification profoundly shapes the activation process upon TCR ligation (Lochner et al., 2015).

1.2.2.2.4 OXPHOS and mitochondrial dynamics

In contrast to macrophages and dendritic cells (DCs), cells of the adaptive immune system do not shut down OXPHOS upon activation and proliferation (Kelly and Neill, 2015). Inhibition of mitochondrial ATP production leads to an impaired T cell activation indicating that ETC function is necessary for T cell effector function. Furthermore, in glucose-free medium the addition of pyruvate to bypass glycolytic flux, T cell activation and proliferation is maintained. Hence activated T cells are highly glycolytic, but mitochondrial function is sufficient to achieve activation and proliferation (L. Sena et al., 2013).

Recently mitochondria gained a lot of interest as signaling organelles upon TCR ligation. The production of mitochondrial ROS (mtROS) at complex I and III of the ETC seems to be important for the activation process. Some models propose that mtROS is involved in Ca^{2+} uptake and subsequently NFAT entry into the nucleus. Mitochondria localize close to the immune synapse upon TCR stimulation and act as a local Ca^{2+} buffer system. They take up Ca^{2+} and locally release ATP into the cytoplasm (Ledderose et al., 2014). Other mitochondrial pathways were reported to increase upon activation. Newly synthesized mitochondria in activated T cells depict a different equilibrium of active pathways. The folate-mediated one-carbon metabolism is significantly upregulated in activated T cells supporting an increase in purine and pyrimidine synthesis. It is also important to provide precursor for NADPH and glutathione synthesis (Ron-Harel et al., 2016). TCR stimulation furthermore results in a change of mitochondrial mass, size, shape and location. This mitochondrial remodeling is termed as mitochondrial dynamics (Rambold and Pearce, 2018; Ron-Harel et al., 2016). Interestingly the morphological changes such as shape and cristae architecture is linked to the different activation states of immune cells and influence the metabolic programming. Mitochondrial dynamics also depict a high sensitivity towards environmental cues such as nutrient availability and hypoxia (Rambold and Pearce, 2018).

1.3 The effect of microenvironment on T cell function

Immune cells migrate through the body with only few residential types and experience changing environmental conditions. Upon activation they migrate to their destinations such as the site of inflammation, infection, tumor sides or to secondary lymphoid tissues. Spare glucose, amino acid and lipid concentrations influence the dynamic metabolic program and hence also immune cell function (Walls et al., 2016). Complex nutrient-sensing systems have to monitor, transduce and initiate adaptive mechanisms to guarantee an adequate adapted immune response. The interplay of T cells with their local microenvironment is highly investigated (Efeyan et al., 2015; Walls et al., 2016; Wei et al., 2017). Here, the state of the art of nutrient-sensing, signal processing and adaptation programs to changing environmental conditions is summarized.

1.3.1 Nutrient restriction impairs T cell function

Sites of tumor, infection and inflammation are potentially hostile environments characterized by a scarcity of glucose and oxygen and other essential nutrients. Cancer- and activated immune cells are highly glycolytic and compete for glucose and amino acids such as glutamine. Due to the high glycolytic flux, lactate levels massively increases at tumor sites. Lactate was shown to dampen T effector cell function and stabilize T_{reg} differentiation (Angelin et al., 2017). T cells at tumor sites must also function in the presence of hypoxia (Chang et al., 2015; Hirayama et al., 2009). Inflammation induces an invasion of immune cells that quickly deplete local nutrients. Again glucose competition takes place. Neutrophils, in particular, have low mitochondrial respiration and subsequently maintain their energy supply with increased glycolytic flux. During bacterial infection, the pathogen itself also consumes the surrounding nutrients. Virus are known to reprogram the infected cells towards higher glycolytic rates to support their own replication machinery (Khan et al., 2015; Walls et al., 2016). Certain diseases such as diabetes have fluctuating glucose availability due to insufficient insulin or to insulin resistance, the effect of which is unknown for T cell function.

This short overview of the impact of various environmental conditions underline the importance of nutrients as highly relevant modulators of T cell function and underpins the importance of nutrient-sensing in T cells and the need for metabolic adaptation mechanisms, which have only started to be explored.

1.3.2 Glucose and glutamine sensing

T cells meet their energy demand and biosynthetic production capacity mainly by glucose and glutamine uptake. Glucose fuels glycolysis, the TCA cycle and the oxidative phosphorylation and supports a variety of biosynthetic pathways. Glucose-sensing is highly investigated in many cell types but in T cells a direct glucose sensor is yet not identified.

AMPK and mTORC1 are important metabolic sensors but they do not specifically sense glucose levels. AMPK is activated upon increasing AMP:ATP ratios and subsequently inhibits glycolytic activity and promotes the switch from anabolic to catabolic metabolism to restore ATP levels. Hence AMPK senses nutrient levels indirectly by responding to energy stress and nutrient restriction in general. It was shown that AMPK initiates a metabolic checkpoint in T cells upon glucose limitation. It is characterized by dampened activation and proliferation capacity as well as a reduction in IFNγ secretion (Blagih et al., 2015). AMPK seems to be particularly sensitive towards glucose and glutamine alterations. It was reported that glucose starvation sensed by AMPK leads to an inhibition of mTOR activity and mediates the switch to glutamine metabolism to fuel the TCA cycle (Blagih et al., 2015). Engagement of glutaminolysis was able to maintain murine T cell energetics and survival but did not rescue T effector cell function upon glucose starvation. Hence glutamine pathway engagement upon glucose starvation

sensed by AMPK is insufficient to explain T cell adaptation towards nutrient fluctuation in order to maintain their function. AMPK is also an agonist of mTOR. mTOR is the main activator of glycolytic flux but mTOR also does not respond specifically to glucose concentration. Instead, mTOR is a sensor of amino acid levels, and the mTOR subunit mTORC1 is highly responsive to amino acids. Therefore, glucose and glutamine levels indirectly affect the AMPK/mTOR signaling axis, leading to large-scale metabolic rewiring (Blagih et al., 2015; Rolf et al., 2013; Walls et al., 2016).

In the following section I will summarize some important investigations in glucose-sensing beyond immune cells that are relevant for the aim of this thesis. Although a distinct glucose-sensor in T cell has not yet been identified, some glucose-sensing mechanisms are elucidated in other cell types. Glucokinase (GCK) for instance catalyzes the first step in glycolysis and phosphorylates glucose to glucose-6-phosphate (G6P). Hexokinases usually have K_m values (an inverse measure of affinity) to glucose below physiological levels. GCK instead has a much higher K_m (around 7mM glucose or above) and consequently is only active upon sufficient glucose abundance (physiological glucose concentration range around 5mM). This glucose sensing function of GCK has not be shown in T cells (Efeyan et al., 2015; Nordlie et al., 1999; Printz et al., 1993).

Glut1 is the main glucose transporter in T cells and upregulated upon T cell activation and often mentioned in the context of glucose sensing. Instead Glut1 is not a glucose sensor. Glut2 in contrast senses extracellular glucose levels. The mechanism is similar to that of GCK. Glut2 compared to Glut1 or Glut4 has a high K_m (20mM). The K_m for Glut4 instead is about 5mM and the K_m for Glut1 is even lower with 1mM glucose. Glut2 allows efficient glucose transport only under high glucose concentration. Glut4 and Glut1 instead are always saturated when transported to the membrane and hence do not have regulatory roles (Thorens and Mueckler, 2010). Interestingly, Glut1 on a whole organism level is favorably expressed in fetal tissue to support rapid organism growth (Efeyan et al., 2015). The dominant expression of Glut1 in T cells is not surprising, given that T cells rapidly respond to activation and undergo proliferation. It remains to be understood how T cells sense glucose depletion or abundance, how this is transduced within the cell, and which mechanisms compensate the lack of glucose availability to maintain effector T cell function.

1.3.3 Amino acid sensing

Activated T cells require amino acids for biosynthetic production and increase their uptake accordingly. Moreover, amino acids act as an additional source for metabolites that fuel the TCA cycle or other metabolic processes. The most prominent amino acid sensor is mTORC1 and hence mTOR represents a central regulator of immune cell function. mTOR also plays a major role in lineage commitment of naive T cells into T_H1 and T_H17 cells (Delgoffe et al., 2011, 2009). mTOR is activated by growth factors as well as by amino acids and switched off by AMPK. mTOR is activated downstream of specific amino

acid sensors such as the cytosolic sensors for leucine and arginine Sestrin2 and Castor or the lysosomal arginine sensor Slc38a9. These sensors activate Rag GTPases which in turn facilitate mTORC1 activity (Bar-Peled and Sabatini, 2014). Glutamine deprivation inhibits mTOR activity in lymphocytes. Most likely, glutamine is needed for a sufficient leucine uptake through the Slc7a5 amino acid transporter. In addition to mTOR, c-Myc is a key regulator of metabolic reprogramming. c-Myc assures the sustained transporter expression for glucose and amino acids and transferrin (CD71). C-Myc becomes activated upon high amino acid availability and is otherwise rapidly degraded to ensure a tight control of glycolytic pathways (Walls et al., 2016). Its expression depends on O-GlcNAcelyation which is fueled mainly by glutamine and hence shows a strong dependence on local nutrient availability (Swamy et al., 2016).

GCN2 is a serine/threonine kinase and is able to sense low amino acid levels. Uncharged transfer RNAs (tRNAs) are a consequence of amino acid depletion. GCN2 binds to those uncharged tRNAs and becomes activated. Upon activation, the eukaryotic initiation factor 2a (elF2a) is deactivated and reduces general translation (Walls et al., 2016; Wei et al., 2017).

Different amino acids are specifically important for T cell function. Arginine is important for T cell proliferation and is directly metabolized in T cells. Activated T cells increase their arginine metabolism mediated by arginase 2 and is furthermore important for T cell survival. Arginine sensing is still elusive. Potential arginine sensors are BAZ1B, PSIP1 and Translin (Wei et al., 2017). Serine was shown to be specifically important during T cell activation by providing intracellular glycine and one-carbon units for purine nucleotide biosynthesis (Ron-Harel et al., 2016; Wei et al., 2017).

1.3.4 Fatty acid sensing

Free fatty acids (FFA) are taken up from diet and are also produced by the gut microbiome as well as by breakdown of triacylglycerides in the liver and adipose tissue. FFAs are aliphatic carbon chains, which occur in different lengths. They can be found in saturated and unsaturated forms. Short chain fatty acids (SFA), middle chain fatty acids (MCFA) and long chain fatty acids (LCFA) are distinguished and sensed by immune cells, and affect different aspects of immune function. Each type of FFA has its own G protein coupled receptor (GPCR). Particularly important for T cell function are SCFA. Acetate, propionate and butyrate impact differentiation of $CD4^+$ and promoting T_{reg} cell and $CD8^+$ memory cell formation. Within the intestines, SFCAs bind to the GPCR43 receptor located on T_{reg} cells promoting their differentiation and function. Butyrate inhibits the histone deacetylase (HDAC) resulting in the acetylation of the Forkhead box P3 (FoxP3) promotor to assuring its stable expression (Arpaia et al., 2013; Smith et al., 2013; Wei et al., 2017). During acute infection, serum levels of acetate increase. These are required for optimal $CD8^+$ memory formation. Mechanistically, acetate promotes the

acetylation of GAPDH resulting in increased glycolytic flux (Balmer et al., 2016). The inhibition of HDAC further increases the acetylation of S6K, promoting T_H1 and T_H17 differentiation (Wei et al., 2017).

1.3.5 Oxygen sensing

The main sensors of oxygen in T cells are the prolyl hydroxylase domain proteins (PHD) (Clever et al., 2016). The use oxygen and alpha-ketoglutarate to hydroxylate HIF1α. Upon hydroxylation, HIFα is recognized by the Hippel-Lindau tumor suppressor protein (pVHL) for degradation. Upon decreasing oxygen, PHD loses oxygen as a co-factor and becomes inactivated. HIFα is stabilized under hypoxic conditions and operates as a transcription factor for glycolytic genes to support oxygen independent energy yielding pathways (Jaakkola et al., 2001; Wei et al., 2017). In T cells, it was shown that HIFα is important for the metabolic switch to aerobic glycolysis and that this HIFα-dependent remodeling is crucial for T_H17 development. Furthermore HIF1α equips the cell with metabolic plasticity to adapt to cellular stress (Shi et al., 2011; Wei et al., 2017), including an inhibition of T_{reg} development mediated by HIFα interaction with RORγt and Foxp3 (Dang et al., 2011).

1.3.6 Redox balance

The delicate balance of NAD^+/NADH ratio is crucial for T cell homeostasis. A dysregulation of ETC function likely leads to an unbalanced redox system with increased levels of NAD^+. Infections are a common source of increasing concentrations of NAD^+. Accumulation of NAD^+ increases ADP-ribosylation. The purinergic receptor P2X7 becomes ADP-ribosylated and activates NAD^+-induced cell death (NCID) (Seman et al., 2003). It was shown *in vivo* that increasing levels of NAD^+ decreases $CD4^+$ and $CD8^+$ T cell numbers (Adriouch et al., 2007). T_{reg} cells are more sensitive to NCID as compared to effector T cells (Hubert et al., 2010). Intact ETC function is a crucial regulator of NAD^+/NADH redox balance. An unbalanced NAD^+/NADH ratio due to ETC dysregulation affects mitochondrial aspartate synthesis and subsequently negatively influences purine and pyrimidine biosynthesis and hence cell proliferation. The addition of pyruvate rescues cell proliferation upon mitochondrial dysfunction via reduction by lactate deyhdrogenase (Harris, 1980; King and Attardi, 1989). The underlying mechanism remained elusive until recently, when it was shown that pyruvate restores the NAD^+ levels by activating the cytosolic branch of the aspartate synthesis via aspartate aminotransferase GOT1. This compensates for the loss of mitochondrial aspartate synthesis by activating cytosolic MDH1 via pyruvate derived NAD^+, which in turn leads to the production of oxalacetate, a precursor of aspartate (Birsoy et al., 2015; Wei et al., 2017).

1.4 Metabolic checkpoints and pathways shape T cell lineage commitments

In this section, I provide further insights into the distinct metabolic programs engaged by various T cell subsets. A brief overview of the current concepts of lineage $CD4^+$ T cell differentiation will be provided and the influence of mTOR and AMPK as well as FA metabolism will be discussed.

1.4.1 $CD4^+$ and $CD8^+$ T cell differentiation - the classical model

$CD4^+$ T cells initiate the adaptive immune response upon efficient antigen:MHC ligation. T cells are activated, clonally expand and subdivide into highly specified effector cell subsets.

$CD4^+$ T cells provide help to B cells for antibody production, class switching and somatic hypermutation of immunoglobulin genes. Furthermore they enhance, maintain and regulate responses of the T cell immune response, control and activate macrophage function and protect from autoimmunity. To cover these wide spectra of function, naive T cells differentiate into different effector T cell subsets with distinct functions. T_H1, T_H2, T_H17, T_{FH} and regulatory T cells represent some of these subsets. T_H1 cells protect against bacterial and viral infections. T_H2 cells combat parasites, especially helminths. They are responsible for the class switching of B cells to produce IgE antibody involved in allergies. T_H17 cells protect against extracellular bacteria and fungi by stimulation of the neutrophil response. T_{FH} cells are responsible for the T cell help to B cells. Finally regulatory T cells dampen the active immune response and prevent T cell responses against self-antigens. The induction of the distinct pathways for lineage commitment may be achieved by environmental determinants. The current model suggests an involvement of the local cytokine milieu during T cell receptor stimulation by inducing distinct transcription factors driving the various differentiation programs. Briefly, a defined cytokine composition activates distinct signal transducer and activator of transcription (STAT). They, in turn activate the expression of the master transcription factor of each subset in order to induce in collaboration the production of signature cytokines.

Each subset has its particular induction pathway panning out from a distinct set of cytokines defining their identity and specific cytokine secretion. T_H1 T cells were shown to rely on IFNγ and IL-12 for induction. Activated STAT1 and STAT4 upregulate the key transcription factor T-bet, leading to the production of IFNγ and IL-2. T_H2 favorably develop in the presence of IL-4, which promotes STAT6 phosphorylation and subsequently resulting in GATA3 expression, the transcription factor specific for T_H2 function. The key cytokines of T_H2 cells are IL-4, IL-5 and IL-13. T_H17 rely on IL-6 and TGF-β for induction. STAT3 activation and the transcription factor RORγt (orphan nuclear hormone receptor) inducing the secretion of IL-17, IL-22 as well as IL-21. T_{reg} cells are distinguished by the expression of FoxP3, the master transcription factor of regulatory T cells as well as the surface marker expression of CD25. Culture conditions containing TGF-β and IL-2 as well as the absence of proinfammatory cytokines such as IL-6 are required for in vitro T_{reg} induction. Differentiated T_{reg} cells produce IL-10 as well as TGF-

β. IL-6 seems to be required for T_{FH} development. It leads to the induction of the main transcription factor B-cell lymphoma 6 protein (Bcl-6). Bcl-6 is also responsible for the expression of CXCR5, the receptor for the chemokine CXCL13 which is produced by stromal cells of the B cell follicle. T_{FH} cells are characterized by the production of IL-4 and L-21. An overview of the lineage inducing signals, the master transcription factors as well as the signature cytokines are shown in Figure 4 (Murphy, 2011b; Zhu et al., 2010).

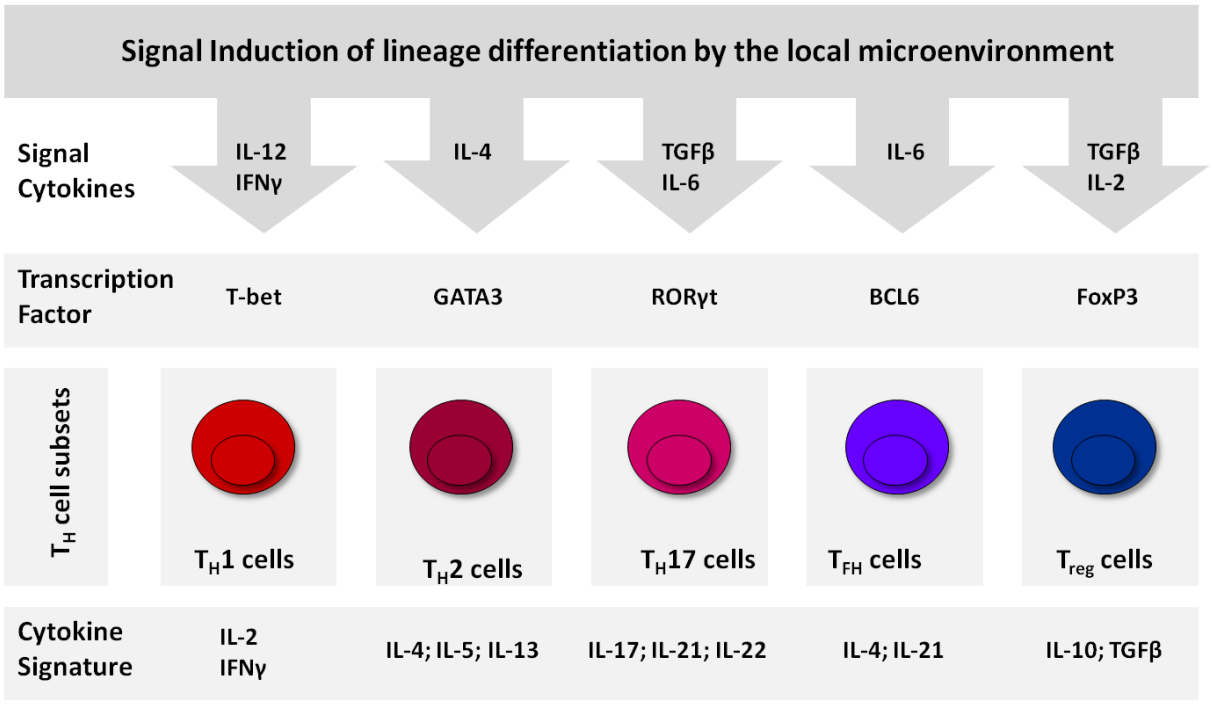

Figure 4: The local cytokines causes naive T cells to differentiate into distinct effector subsets. Antigen presenting cells activate naive T cells. The cytokine composition surrounding the naive T cells shape the development of the various $CD4^+$ T cell subsets (modified after Murphy, 2012, chap. 9; Zhu et al., 2010)

1.4.2 Metabolic influence on T cell differentiation

While a major focus of research has been on the local environment conditions that influence T cell subset differentiation, there is a growing body of evidence linking lineage commitment to T cell metabolism. The following section reviews this evidence.

1.4.2.1.1 Memory T cells

Memory T cells are long-lasting antigen-experienced T cells. At the end of an immune response the majority of effector CD8 and CD4 T cells die, leaving a minority that constitute the immunological memory of the response. A second exposure to the agent engages a faster and enhanced response from the memory T cells as compared to the initial response from naive T cells. Recent efforts investigating the metabolic profile of memory T cells discovered profound differences in their metabolic equipment. It seems that specific metabolic advantages in memory T cells are responsible for their rapid recall ability. Memory T cells remain in a quiescent state engaging preferentially catabolic pathways such as FAO and glucose oxidation (Fox et al., 2005; Yusuf and Fruman, 2003).

Apparently, a memory intrinsic feature constitutes a higher spare respiratory capacity (SRC) together with increased mitochondrial biogenesis and augmented expression of ETC-affiliated proteins (Buck et al., 2016; Dimeloe et al., 2016). Not much is known about memory $CD4^+$ T cells or human memory T cells in general. The majority of studies concentrate on murine $CD8^+$ T cells which will be presented in more detail.

$CD8^+$ memory T cells were shown to have a higher metabolic fitness for fast intervention upon second immune challenges (van der Windt et al., 2013). Mitochondrial morphology of memory T cells showed intriguing differences and can be directly linked to distinct metabolic features. Their inner mitochondrial membrane (IMM) is tightly packed and creates a large surface area for ETC supercomplex formation, allowing for highly efficient OXPHOS. The mitochondria furthermore possess an elongated phenotype due to increased fusion events. These were shown to facilitate the production of NADH as well as electron transfer through the ETC. Mitochondrial fusion events are crucial during the switch from effector to memory phenotype. *Buck et al.* highlighted the critical impact of mitochondrial dynamics for the different metabolic programs of T cell subsets as well as for their formation (Buck et al., 2016).

In addition to mitochondrial morphology and OXPHOS rates, FA metabolism was shown to tip the balance in fate decision of memory and effector T cells. Upon memory formation, effector T cells switch from FAS to FAO. mTOR inhibition by rapamycin further impedes anabolic metabolism and promotes memory T cell formation (Araki et al., 2009; Pearce et al., 2009; Rao et al., 2010). *Pearce and colleagues* investigated memory formation in murine TRAF6 deficient $CD8^+$ T cells, which show dysfunctional FAO followed by impaired memory formation that could be linked to a decrease in AMPK expression. Convincingly, treatment with the AMPK inhibitor metformin restored FAO capability (Pearce et al., 2009). Another study confirmed this observation by using AMPKα-deficient mice (Rolf et al., 2013). The mechanism of action of AMPK-regulated FA metabolism is not entirely understood. Studies showed that AMPK inactivates FAS and activates FAO by interfering with both ACC isoenzymes ACC1 and ACC2 (Wakil and Abu-Elheiga, 2009). Also, an indirect upregulation of FAO via mTOR inhibition and subsequent AMPK activation has been discussed (DeBerardinis et al., 2006). Interestingly, and compared to other FAO engaging subsets, memory CD8 T cells were shown to have a futile cycle of FAS and FAO (O'Sullivan et al., 2014). The fatty acids for energy production are solely derived through de novo FAS and are not taken up externally. Indeed inhibition of FAS impaired $CD8^+$ memory formation and it is suggested that this coupling of FAS and FAO is a reason for their long term survival and rapid recall capacity (Lochner et al., 2015)

1.4.2.1.2 T effector cells and T regulatory cells

mTOR was first discovered as cellular target of rapamycin and is a serine/threonine kinase consisting of two different complexes mTORC1 and mTORC2 and their associated proteins (Brown et al., 1994;

Pollizzi and Powell, 2015). Due to the distinct complexes, mTOR has the ability to respond to different stimuli leading to different pathway activation and function. I already introduced mTORC1 as a nutrient sensor. mTORC2, in contrast, is activated by certain cytokines and growth factors (Chantranupong et al., 2016; Kim et al., 2013; Laplante and Sabatini, 2012; Pollizzi and Powell, 2015; Waickman and Powell, 2012). Until now, no study confirms the involvement of both complexes in T cell differentiation. mTORC1 dysfunction was shown to inhibit the differentiation of T_H1, T_H2 and T_H17 cells (Battaglia et al., 2006, 2005; Delgoffe et al., 2009). A T cell specific deletion of mTORC1 upstream of Rheb specifically diminished T_H1 and T_H17 development but not T_H2 (Delgoffe et al., 2011). Deleting the scaffolding protein of mTORC1 Raptor specifically in T cells only resulted in diminished T_H17 differentiation (Kurebayashi et al., 2012). However another publication described restricted T_H2 development in this context (Yang et al., 2013). So far most studies could only agree on the impact of mTORC1 on T_H17 development and the concrete influence on other subsets requires further analysis. mTORC2 involvement in T cell differentiation processes is even less clear. Deletion of Rictor, the scaffolding protein of mTORC2 restricted T_H2 differentiation as well as T_H1. The latter though with contradictory results (Delgoffe et al., 2011; Lee et al., 2010). Not only T helper cell differentiation is affected by mTOR. Regulatory T cell differentiation is promoted upon mTOR inhibition (Delgoffe et al., 2011). Moreover, $FoxP3^{cre}$ $Raptor^{fl/fl}$ mice developed autoimmune responses pointing to a requirement of mTORC1 for T_{reg} suppressive function (Zeng et al., 2013).

In view of the importance of mTOR for T cell lineage differentiation, it seems likely that its agonist AMPK also influences T cell differentiation. Indeed, experiments with the AMPK activator metformin leads to impaired T_H1 and T_H17 development (Kang et al., 2013; Zhao et al., 2015). Furthermore, AICAR, another activator of AMPK, was shown to be beneficial in competing inflammatory disease models (Bai et al., 2010; Nath et al., 2005). Metformin treatment decreases T_H17/T_{reg} ratios in experimental arthritis or colitis models (Son et al., 2014). AICAR, but not metformin was shown to favor T_{reg} development *in vitro* (Gualdoni et al., 2016). A potential reason may be that metformin also has been described to be an inhibitor of respiratory complex I and might point towards a mechanism of action downstream of respiratory chain inhibition (Andrzejewski et al., 2014; Wheaton et al., 2014). Interestingly, some studies highlighted the fact that a lack of AMPK still allows effector T cell differentiation under appropriate metabolic conditions but results in impaired metabolic adaptation upon nutrient starvation (Blagih et al., 2015; Mayer et al., 2008).

Fatty acid metabolism was shown to alter T effector cell differentiation. In particular, the balance between effector and regulatory T cell decision appears highly sensitive to FA metabolic alterations. Apparently, their need for FAS differs (Berod et al., 2014; Endo et al., 2015). It was shown that inhibiting ACC1 and subsequently de novo FAS restrained T_H1 and T_H17 differentiation and consequently enhances the differentiation into T_{reg} cells (Berod et al., 2014). Treatments with ACC-specific inhibitors

protected mice from experimental autoimmune encephalomyelitis (EAE) (Berod et al., 2014; Endo et al., 2015). It is proposed that FAS inhibition shifts T_H17 differentiation towards T_{reg} induction. ACC1 inhibition was shown to change the nuclear localization of RORγt and decrease its binding to the il17a enhancer region (Endo et al., 2015). Furthermore, T_{reg} cells have a higher capacity for external FA uptake and hence may compensate for FAS inhibition more efficiently as compared to their effector counterparts (Gerriets and Kishton, 2014; Michalek et al., 2011). Naive T cells cultured under T_{reg} conditions *in vitro* have high rates of FA uptake and low rates of glycolysis. This suggests that T_{reg} cells preferentially engage OXPHOS and FAO. Indeed, blocking CPT1 with etamoxir inhibited T_{reg} cell development (Michalek et al., 2011).

It is clear that the metabolic phenotypes of the various T cell subsets are still poorly understood and highly controversial. T cell metabolic needs for suppressive functions, homeostatic proliferation as well as the metabolic changes during an immune response of the distinct T cell subsets are only beginning to be understood. Moreover, connecting T cell function to environmental conditions and understanding their metabolic flexibility on a molecular level and the consequents for their function might allow specific manipulation of T cell subsets and function.

1.5 Aim of the Thesis

The link between a T cell's microenvironment and their function is poorly understood. In the scope of this thesis I aim to describe human $CD4^+$ T cell flexibility to different environmental factors such as nutrient availability and cellular stress. As my tools, I will use *in vitro* models of human $CD4^+$ T cell function under different nutrient availability and in the presence of cellular stress, and examine metabolic, T cell function, and genetic changes under these conditions. My overall objective is to determine how cell environment perturbations that alter T cell metabolism will affect the adaptive $CD4^+$ T cell response. In doing so, I expect to provide novel findings and insight into how immune responses in inflammatory conditions may be modulated for improved health.

2 MATERIALS AND METHODS

2.1 Material

2.1.1 Chemicals and reagents

The used chemicals in this PhD thesis are listed in Table 3.

Table 3: Chemicals and reagents

Chemical Name	Manufacturer
1x PBS	Gibco, Invitrogen Ltd., Paisley, UK
2-Deoxy-D-Glucose (2-DG)	Sigma-Aldrich, Inc., St. Louis, MO, USA
Antimycin A	Sigma-Aldrich, Inc., St. Louis, MO, USA
BD FACS™ Clean Soluation	BD Bioscience; San Jose, CA, USA
BD FACS™ Rinse Solution	BD Bioscience; San Jose, CA, USA
BD FACS™ Sheath Solution	BD Bioscience; San Jose, CA, USA
Bovine serum albumin (BSA)	Sigma-Aldrich, Inc., St. Louis, MO, USA
Dimethyl sulfoxide (DMSO)	Sigma-Aldrich, Inc., St. Louis, MO, USA
DNA*Zap*™ Solutions	Life Technologies, Carlsbad, CA, USA
Ethylendiaminetetraacetic acid (EDTA)	Sigma-Aldrich, Inc., St. Louis, MO, USA
Ethanol	Carl Roth GmbH + Co.KG Karlsruhe, Germany
Ethanol absolute	Carl Roth GmbH + Co.KG Karlsruhe, Germany
FCCP	Sigma-Aldrich, Inc., St. Louis, MO, USA
Ficoll®-Paque PREMIUM	GE Healthcare; Chicago, IL, USA
Formalin (10%, neutral buffered)	Sigma-Aldrich, Inc., St. Louis, MO, USA
Muse Guava Instrument Cleaning (ICF) solution	Merck Millipore, Darmstadt, Germany
Oligomycin	Sigma-Aldrich, Inc., St. Louis, MO, USA
Rotenone	Sigma-Aldrich, Inc., St. Louis, MO, USA
Trypan blue stain	Gibco, Invitrogen Ltd., Paisley, UK

2.1.2 Cell culture media and supplements

Cell culture media and the supplements are listed in Table 4. Serum used for cell culture was heat inactivated at 56°C for 30 minutes and filtered through a 0.45µm steritop filter (Millipore) and aliquots were stored at -20°C. Culture media was additionally filtered through a 0.22µm steritop filter (Millipore) and stored at -4°C not longer than 4 weeks.

Table 4: Cell culture media and supplements

Name	Manufacturer
RPMI 1640 medium, no glutamine	Life Technologies, Carlsbad, CA, USA
RPMI 1640 medium, no glucose,	Life Technologies, Carlsbad, CA, USA
XF Assay Medium, Modified DMEM (0mM glucose)	Agilent technologies; Santa Clara, CA, USA
Human Serum AB (HS)	PAA Laboratories GmbH; Pasching, Austria
Penicillin-Streptomycin (P/S)	Lonza; Verviers, Belgium
Recombinant human IL-7 (25µg)	R&D Systems; Minneapolis, MN, USA
D-Glucose	Sigma-Aldrich, Inc., St. Louis, MO, USA
Insulin, human recombinant (yeast)	Roche; Basel, Switzerland
Resveratrol	Abcam; Cambridge, UK

2.1.3 Commercial Kits

Commercial kits used for cell separation, stimulation, flow cytometry staining and RNA isolation are listed in Table 5.

Table 5: Commercial kits

Name	Catalogue number	Manufacturer
Cell stimulation		
Dynabeads® Human T-Activator CD3/CD28	111-31D	Invitrogen; Oslo, Norway
Tetanus Toxoid zur Injektion	02/232	Andreae Noris Zahn AG; Ottendorf-Okrilla, Germany
Cell Separation		
CD4 MicroBeads, human	130-045-101	Miltenyi; Bergisch-Gladbach, Germany
CD25 MicroBeads II, human	130-092-983	Miltenyi; Bergisch-Gladbach, Germany
Flow cytometry staining		
2-NBDG	Thermo Fisher Scientific; Waltham, MA, USA	
BD Cytofix/Cytoperm Fixation/Permeabilization Solution	554714	BD Bioscience; San Jose, CA, USA
BD^{TM}CompBeads Anti-Mouse Ig,κ/Negative Control Compensation Particles Set	552843	BD Bioscience; San Jose, CA, USA
CS&T Research Beads	650621	BD Bioscience; San Jose, CA, USA
Protein Transport Inhibitor (Containing Brefeldin A)	555029	BD Bioscience; San Jose, CA, USA

Quant-iT™ Pico Green™ dsDNA Reagent	Thermo Fisher Scientific; Waltham, MA, USA	
RNAseq		
miRNeasy Micro Kit	217084	Quiagen; Hilden, Germany
RNasin Plus Rnase Inhibitor	N2611	Promega Corporation; Madison WI, USA
Agilent RNA 600 Pico Kit	5067-1513	Agilent technologies; Santa Clara, CA, USA

2.1.4 Buffers

Prepared buffers for cell culture and flow cytometry are listed in Table 6.

Table 6: Prepared buffers

Buffer name	Composition
FACS buffer	0.1% BSA in 1x PBS
MACS buffer	0.5% BSA; 2mM EDTA in 1x PBS
FACS sort buffer	1% human serum in 1x PBS

2.1.5 Consumables

Cell culture material used in this PhD thesis is listed in Table 7.

Table 7: Cell culture materials

Name	Specification	Manufacturer
Cell culture plates	Cellstar® 69 well suspension culture plate, sterile, U-bottom with lid	Greiner bio-one GmbH; Frickenhausen, Germany
Heparin blood collection tubes	BD Vacutainer® Glass Sodium Heparin Plasma tube 10ml	BD Bioscience; San Jose, CA, USA
FACS tubes	BD Falcon™ Polystyrene round bottom tubes 5ml Tube 4.5ml, 75x12mm, conical base, PS	BD Bioscience Discovery; Labware, Bedford MA USA Sarstedt, Wedel, Germany
FACS tubes filter caps	Cell strainer cap	BD Bioscience Discovery; Labware, Bedford MA USA
Falcon tubes	15, 50ml	Greiner bio-one GmbH; Frickenhausen, Germany or BD Bioscience Discovery; Labware, Bedford MA USA
Injekt® Solo	Injekt® Solo 10mL	Braun;Melsungen, Hessen, Germany

MACS column filters	Pre-separation filters, 30µM	Miltenyi Biotech; Bergisch-Gladbach, Germany
MACS columns	LD columns LS columns MS columns	Miltenyi Biotech; Bergisch-Gladbach, Germany
Neubauer improved	C-Chip Neubauer improved	NanoEnTek Inc.; Waltham, MA, USA
Pasteur pipettes	3ml	VWR; Darmstadt, Germany
Pipette tips	Without filter, 0.1-10µl, and 50-1000µl Without filter, 10-200µl	Eppendorf AG; Hamburg, Germany Greiner bio-one GmbH; Frickenhausen, Germany
Reagent reservoir	50ml reagent reservoir polystyrene	Corning Incorporated; New York, USA
Serological pipettes	Cellstar®, 5ml, 2.0ml	Greiner bio-one GmbH; Frickenhausen, Germany
Stericup and Steritop	Vacuum filter bottles, PES Membrane 0.22µm	Merck Millipore; Darmstadt, Germany
Syringe filters	Syringe filter units with 0.22µm	Corning Inc., Corning NY USA
Tips for Multipipette	2.5ml, 5ml Combitips plus	Eppendorf AG, Hamburg, Germany

2.1.6 Technical equipment

Used technical equipment for this PhD thesis is listed in Table 8.

Table 8: Technical equipment

Device	Name	Manufacturer
Bioanalyzer	Agilent 2100 Bioanalyzer System	Agilent technologies; Santa Clara, CA, USA
Cell counter	MUSE Cell Analyzer	Merck Millipore; Darmstadt, Germany
Cell sorter	Aria III	BD Bioscience; San Jose, CA, USA
Centrifuge (molecular biology, fixed angle rotor)	Centrifuge 5424R	Eppendorf AG; Hamburg, Germany
Centrifuge (cell culture, swing-out rotor)	Haereus Multifuge X3R	Thermo Fisher Scientific; Hudson, NH, USA
Extracellular flux analyzer	Seahorse Xfe96 Analyzer	Agilent technologies; Santa Clara, CA, USA
Flow Cytometer	LSR Fortessa	BD Bioscience; San Jose, CA, USA
Incubator	BBD 6220 CO_2 – Incubator	Thermo Fischer Scientific, Hudson, NH, USA

Inverted microscope	Leica DM IL LED	Leica Microsystems GmbH; Wetzlar, Germany
MACS magnets and stands	QuadroMACS™ Seperator	Miltenyi Biotech, Bergisch-Gladbach, Germany
Microcentrifuge	Eppendorf® minispin®	Eppendorf AG; Hamburg, Germany
Plate Reader	PHERAStar FS	BMG Labtech
Sterile work bench	ScanLaf Mars Safety Class 2	LaboGene ApS, Allerød, Denmark
Waterbath	Incubation/Inactivation Water Bath 1008	GFL Gesellschaft für Labortechnik mbH, Burgwedel, Germany

2.2 Methods

2.2.1 Study Population

This PhD thesis concentrates on metabolic characterization of human peripheral blood $CD4^+$ T cell populations as well as on their designated T cell function such as activation, proliferation capacity and cytokine secretion. Non-diabetic donors are recruited from the Munich Diabetes Bioresource study. Children and young adults between two and 40 years are included for the study. Only adult samples were used in the thesis. All gave informed consent for blood draws. The study was approved by the ethical committee (Ethical approval number 5049/11)

2.2.2 Isolation of Peripheral blood mononuclear cells

Peripheral blood mononuclear cells (PBMC) were isolated from freshly collected heparinized blood and processed. Mononuclear cells were isolated by density gradient centrifugation over Ficoll-Paque (GE Healthcare) according to the manufacturer's protocol. Cell number and viability was determined with a hemocytometer and staining with trypan blue in a 1:2 or 1:10 ratio. Alternatively a standardized Muse count and viability solution on the Muse cell analyzer (Merck Millipore) was used.

2.2.3 Magnetic activated cell sorting for purification of immune cell subsets

Magnetic activated cell sorting (MACS) of the isolated PBMC's was used to either purify $CD4^+$ T cells for the majority of performed T cell assays or to deplete $CD25^+$ T cells prior to fluorescence activated cell sorting of regulatory T cells. Two different kits were used; the human $CD4^+$ MicroBeads and human $CD25^+$ MicroBeads II (Miltenyi Biotec). The kits were used on whole mononuclear cells fraction according to manufacturer's protocols and adjusted to the cell numbers. $1x10^7$ or $1x10^8$ labelled cells were passed through LS columns ($CD4^+$ purification) or through LD columns ($CD25^+$ depletion). The purity of the isolated cell subsets were validated by flow cytometry by staining $0.5x10^5$ cell with either

anti-CD4-PerCP (clone: SK3; BD Pharmingen) or CD25-PE (clone: M-A251; BD Pharmingen) for 20 minutes at 4°C in the dark in FACS buffer (PBS $^{-/-}$ containing 0.5% BSA).

2.2.4 Xf extracellular flux analysis

The Agilent Seahorse XF technology is a live-cell metabolic assay platform which measures oxygen consumption rates (OCR) and extracellular acidification rates (ECAR) in real time in a multi-well plate. The real-time measurements are conducted by isolating a small volume (about 2µl) above a monolayer of cells within a microplate. The oxygen consumption of cells (respiration) and proton secretion (glycolysis) is measured in intervals of a few minutes by solid state sensor probes (200 micron above the cell monolayer). OCR and ECAR ratios are calculated after each measurement (Figure 5). After each round of recording, probes rise and the medium is allowed to mix and return to baseline values. An integrated drug delivery system allows the addition of up to four compounds per well in adjustable intervals (Figure 5A). Seahorse XF Assay was performed using the XF96 extracellular flux analyzer (Agilent Seahorse). $2x10^5$ $CD4^+$ T cells per well were cultured and stimulated with anti CD3/CD28 Dynabeads (Thermofisher) in 96 cell culture plates (Costar) for 48h in growth medium (RPMI 1640). The Seahorse sensor cartridge was hydrated in a non-CO_2 incubator overnight prior measurement (Agilent Seahorse XF Calibrant). The day of the assay, culture medium was replaced stepwise with non-buffered XF assay medium (Agilent Seahorse) up to 180µL and the designated assay conditions were added. The cells were subsequently transferred into the XF cell culture plate. To ameliorate cell adhesion and distribution within a well, culture plates were spun down at 180 RCF, brakes were set to 5 (acceleration and deceleration). The cell microplate was placed in a 37°C incubator without CO_2 for 45 minutes. The various assay compounds were loaded into the injector ports within the cartridge. 2µM oligomycin (ATP synthase inhibitor), 1.5µM carbonyl cyanide 4(trifluoromethoxy)phenylhydrazone (FCCP; depolarizes the mitochondrial membrane by transporting protons across its inner membrane), 2.5µM rotenone (complex I inhibitor) and antimycin A (complex III inhibitor) were injected. Glycolysis was monitored in the presence of the glycolytic inhibitor 2-desoxyglucose (2-DG) at 1mM (Figure 5B). The injection volume was 20µL. Baseline OCR and ECAR were measured four times before the first injection. OCR is reported as pmol/min and ECAR in mpH/min. For comparability, ECAR rates are indicated as PPR [pmol/min].

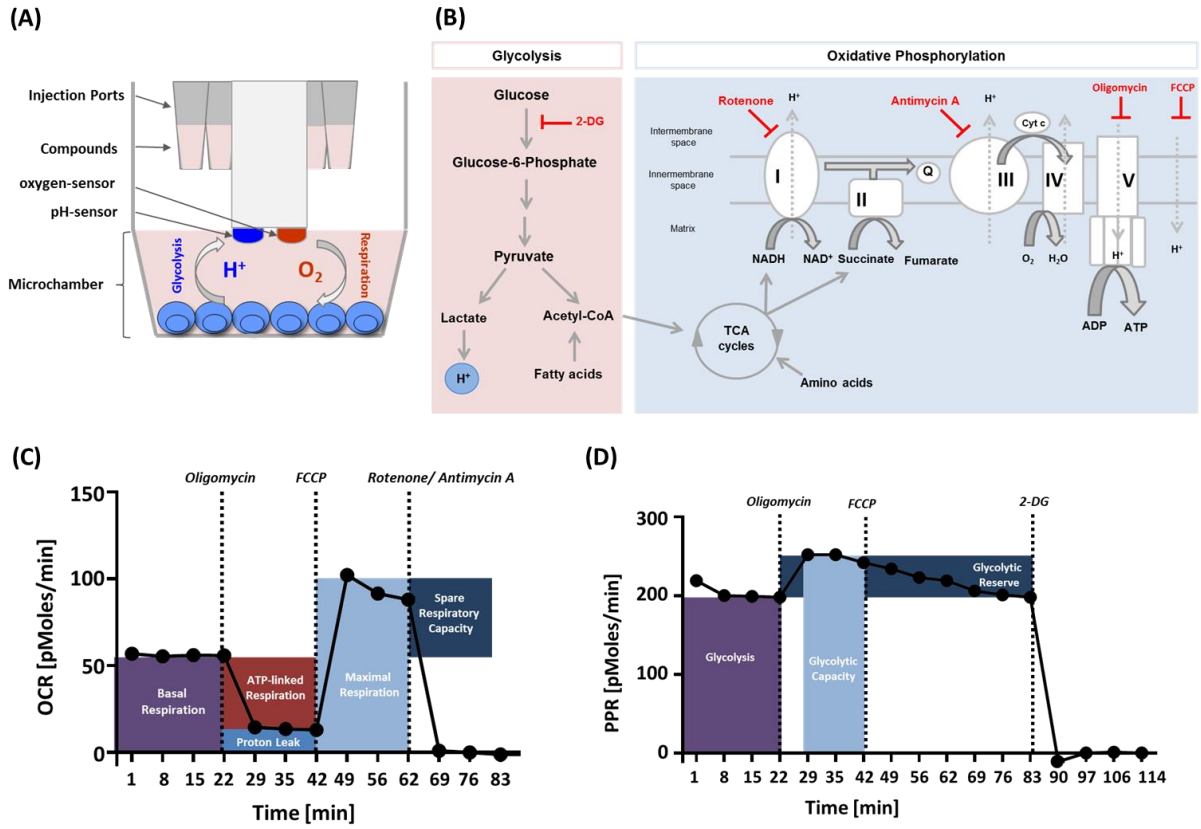

Figure 5: Measuring cell metabolism with xf96 extracellular flux analyzer (A) The Agilent seahorse technology uses a transient microchamber which allows nondestructive metabolic measurements in real time. Sensors integrated in the cartridge contain two fluorophores that measure oxygen (O_2) and the pH. The sensors lower to 200 microns above the cell layer. The emerging microchamber monitors changes in oxygen concentration and pH during each measurement cycle and calculates oxygen consumption (OCR) and extracellular acidification rate (ECAR). (B) The assay reveals fundamental parameters of mitochondrial and glycolytic function by injecting different inhibitors; Oligomycin, FCCP, Rotenone together with Antimycin A as well as 2-DG. (C) The mitochondrial respiration signature consisting of basal respiration, ATP-linked Respiration, proton leak, maximal respiration and spare respiratory capacity. (D) Glycolytic parameters are measured due to the injection of oligomycin, FCCP and 2-DG. Glycolytic rate, glycolytic capacity and glycolytic reserve are calculated.

The standard parameters defining the respiration signature of cells are shown in Figure 5C and D. The calculation of each respiration module for a given dataset is listed in Table 9.

Basal respiration is the respiration that meets the cell's endogenous ATP demand. The rate is defined by ATP utilization, substrate supply and oxidation or proton leak. It is composed of two processes: respiration that drives ATP synthesis and respiration associated with proton-leak pathways.

ATP-linked respiration is the respiration sensitive to oligomycin. It defines the amount of respiration utilized for ATP production. The ATP demand of the cells dictates this respiration parameter. The ATP respiration is controlled by ATP utilization, ATP synthesis and substrate supply and oxidation. The ATP demand of a cell mainly changes based on the energy-requiring processes such as macromolecule synthesis, cell motility or proteasome activity.

Proton-leak linked respiration describes the leak of protons though the inner mitochondrial membrane independently of ATP synthase activity and thereby consuming the membrane potential. Incomplete coupling of electron transport and ATP synthase activity causes the leak of protons. Respiration

insensitive to oligomycin defines proton leak. The molecular nature of the proton leak is not entirely understood.

Maximal respiration is determined by uncoupling the ATP synthase function and the electron transport using an uncoupler such as FCCP. In response of the protonophor, substrate oxidation as well as the ETC function increases in order to maintain the mitochondrial membrane potential. FCCP shuttles protons across the inner membrane and thereby dissipates the proton motive force, causing maximal activity of the electron transport chain. Maximal respiration is dictated by substrate availability and its oxidation. Changes in maximal respiration may indicate changes in mitochondrial biogenesis or cristae structure.

The *spare respiratory capacity* (SRC) is defined as the difference between basal and protonophore-stimulated respiration. Broadly, this indicates the ability of a cell to meet an increased energy demand and respond to oxidative stress. A decrease in SRC function might be associated with mitochondrial dysfunction or indicate an increased ATP demand. The lack of SRC does not *per se* indicate malfunction. Cells with higher SRC values may be characterized by increased mitochondrial biogenesis during terminal respiration and this might imply the capacity to execute energetically demanding, cell-specific functions or substantiate in increased substrate provision (Divakaruni; et al., 2014).

Table 9: Mitochondrial respiration and glycolytic parameters were conducted by the mitochondrial stress test (Agilent Seahorse). The calculation of the parameters is presented.

Respiration Rate	Calculation
Non-mitochondrial respiration	MIN(measurement after Rotenone/Ant A injection)
Basal Respiration	(measurement prior to injection)-(non. Mitochondrial respiration)
Proton leak-linked respiration	MIN(measurement after Oligomycin addition but prior to FCCP injection)-(non. Mitochondrial respiration)
ATP-linked respiration	(basal respiration)-(proton leak)
Maximal respiration	MAX(measurement after FCCP injection)-(non. Mitochondrial respiration)
Spare respiratory capacity	(maximal respiration)-(basal respiration)
Glycolysis	MEAN(measurement prior to first injection)
Glycolytic capacity	MEAN(measurement after Oligomycin injection and prior FCCP injection)
Glycolytic reserve	(Glycolytic Capacity)-(Glycolysis)

2.2.5 Normalization of the extracellular flux data to DNA content

Long-term incubation with inhibitors or drugs for 48 hours or longer can lead to variation in T cell number. Different T cell numbers per well influence the extracellular flux data. Normalization of the

data to the DNA content is required. Quant-iT™ PicoGreen ® dsDNA reagent was used to determine the cell number for each well. After completing the xf extracellular flux measurement, the seahorse plate containing the measured cells and the media was frozen and stored at -80°C for at least 3 days. Prior to PicoGreen measurement, the plate was carefully thaw in a water bath at room temperature for approximately 30 minutes. Protein kinase K was added (3µL per well of the stock solution) to each well and carefully mixed. Cells were incubated for 1 hour at 37°C. Subsequently cells were mixed again and centrifuged at 400g for 10 minutes to bring down the cell debris. 100µl of the upper layer of each well was taken and diluted in 1x TE buffer (diluted in distilled H_2O). Λ-DNA standards were used to calculate the DNA content of each well. Depending on the actual cell number per well, 10µL of each sample and DNA standards was transferred into a fluorescent plate. Quant-iT Picogreen reagent was diluted 1:200 in 1x TE buffer and 100µL added to each well, mixed and incubated for 5 minutes in the dark at room temperature and mixed again prior measurement. Fluorescence was measured on a PheraStar Platereader (Excitation; 480, Emission: 520). Gain and focal adjustment was performed using the highest standard DNA sample. The focus should be approximately 6.5 and gain set to 400. The plate was measured after 10 and 15 minutes again to confirm value consistency.

2.2.6 Flow cytometry

2.2.6.1 Sample optimization using instrumental set up

Multicolor flow cytometry was performed on an LSR Fortessa (BD Biosciences) equipped with a violet (405nM), blue (488nm), yellow-green (561nm) and red (633nm) laser. Particle size and granularity was measured by the forward scatter (FSC) and side scatter (SSC) detectors. Area, height and width parameters of the FSC and SSC detectors were utilized for lymphocyte discrimination and doublet exclusion. Stable performance of the flow cytometer was maintained by cytometer setup and tracking using CS&T (CS&T beads; BD Bioscience) prior to measurement or at least twice per week. The instrumental setup is described in Table 10.

Table 10: Instrumental setup LSR Fortessa (BD Bioscience)

Laser	Longpass filter	Bandpass filter	Detected fluorochromes by PMT
405nm	600LP	610/29	Brilliant Violet 605, Qdot605
	505LP	525/50	Brilliant Violet 510, AmCyan
		450/50	eFluor450, Pacific Blue
488nm	685LP	710/50	PerCP, PerCP-Cy5.5
	505LP	530/30	Alexa Fluor488, CFSE, FITC
		488/10	SSC
561nm	750LP	780/60	PE-Cy7
	685LP	710/50	PE-Cy5.5

	635LP	670/30	PE-Cy5
	600LP	610/20	PE-Texas Red
		585/15	PE
640nm	750LP	780/60	APC-Cy7
	690LP	730/45	APC-Alexa 700
		670/14	eFluor670, APC

The spectral overlap of the used fluorochromes in multicolor panels were compensated using polystyrene microbeads coated with anti-mouse immunoglobulin κ (CompBeads, BD Bioscience), which non-specifically binds any mouse κ light chain-bearing antibody. The beads were stained with one antibody each and the PMT voltages were set using unstained CompBeads and subsequently single staining was acquired and recorded. CompBeads were used for surface and intra-cellular markers as well as 1:1 mixture of labeled and unlabeled cells. Dead/alive staining was compensated using alive and heat-shocked cells (10min at 65°C). Compensation of spectral overlap was calculated using an automatic tool within the BD FACSDiva software. Raw data was exported as 3.0 fcs-files and analyzed using FlowJo software (Version 10; TreeStar Inc.).

2.2.6.2 Fluorescence activated cell sorting (FACS) on a single cell level

$CD4^+$ T cell subsets were sorted for RNAseq experiments. $CD4^+$ naive, memory and T_{reg} cells were sorted at high purity on a FACSAria III (BD Biosciences). The cytometer was equipped with a violet (405nm), blue (488nm) and red laser (633nm). Cells were sorted into tubes (15ml Falcon tubes; Greiner) at a speed of 5000 events/second for T_{reg} sorting and 10000 to 15000 events/seconds for naive and memory T cell sort. For T_{reg} cell isolation, $CD25^+$ PBMCs were first depleted by MACS separation. T_{reg} cells were sorted by FACS as $CD4^+$ (CD4-AmCyan/BV510; clone: SK3; BD Pharmingen) $CD25^+$ (CD25-PE; clone: M-A251); $CD127^-$ (CD127-PE-Cy7; clone: A019D5; Biolegend) and 7AAD (7AAD-PerCp) for live/dead discrimination. CD4 MACS separation was performed on the $CD25^-$ cell fraction. Subsequently naive and memory T cells were sorted as $CD4^+$ (CD4-AmCyan/BV510; clone: SK3), $CD25^-$ (CD25-PE; clone: M-A251; BD Bioscience) and $CD45RA^+$ and $CD45RO^-$ for naive and $CD45RA^-$ and $CD45RO^+$ for memory (CD45RA-FITC; clone: HI100; Biolegend; CD45RO-APC; clone: UCHL1; BD Pharmingen). The cells were stained in sorting buffer and sorted into RPMI 1640 supplemented with 5mM glucose, 10% HS and 0.1ng/mL IL-7.

2.2.7 T cell functional assays

2.2.7.1 T cell activation

Early activation of $CD4^+$ T cells was investigated by analyzing the surface expression of CD69 (anti-CD69-FITC; clone: FN50 BD Bioscience) CD25 (anti-CD25-PE; clone: M-A251; BD Bioscience) and CD154

(anti-CD154-Brilliant Violet 605; clone:24-31; Biolegend) using flow cytometry. 2 x10^5 T cells/well were seeded in 96 well-plates and stimulated under the designated conditions for 16h and stained using the following monoclonal antibodies: anti CD4-PerCP (clone: SK3; BD Pharmingen), anti CD69-FITC (clone: FN50; BD Pharmingen), anti CD25-PE (clone: M-A251; BD Pharmingen) and anti CD154-Brilliant Violet 605 (clone:24-31; Biolegend). The cells were stained for 20 min at 4°C in phosphate-buffered saline without Ca^{2+} and Mg^{2+} (PBS $^{-/-}$; Gibco) containing 0.5% BSA. Subsequently, cells were washed with PBS$^{-/-}$ and stained for 15 min at room temperature with Zombie NIR (Biolegend) for discriminating dead and living cells. T cells were fixed with 1.5% Formalin in PBS$^{-/-}$ and samples were acquired within 24h using the Becton Dickinson LSR Fortessa flow cytometer and analyzed with FlowJo software (Version 10; Treestar Inc.). Representative FACS plots and the gaiting strategy is shown in Figure 6.

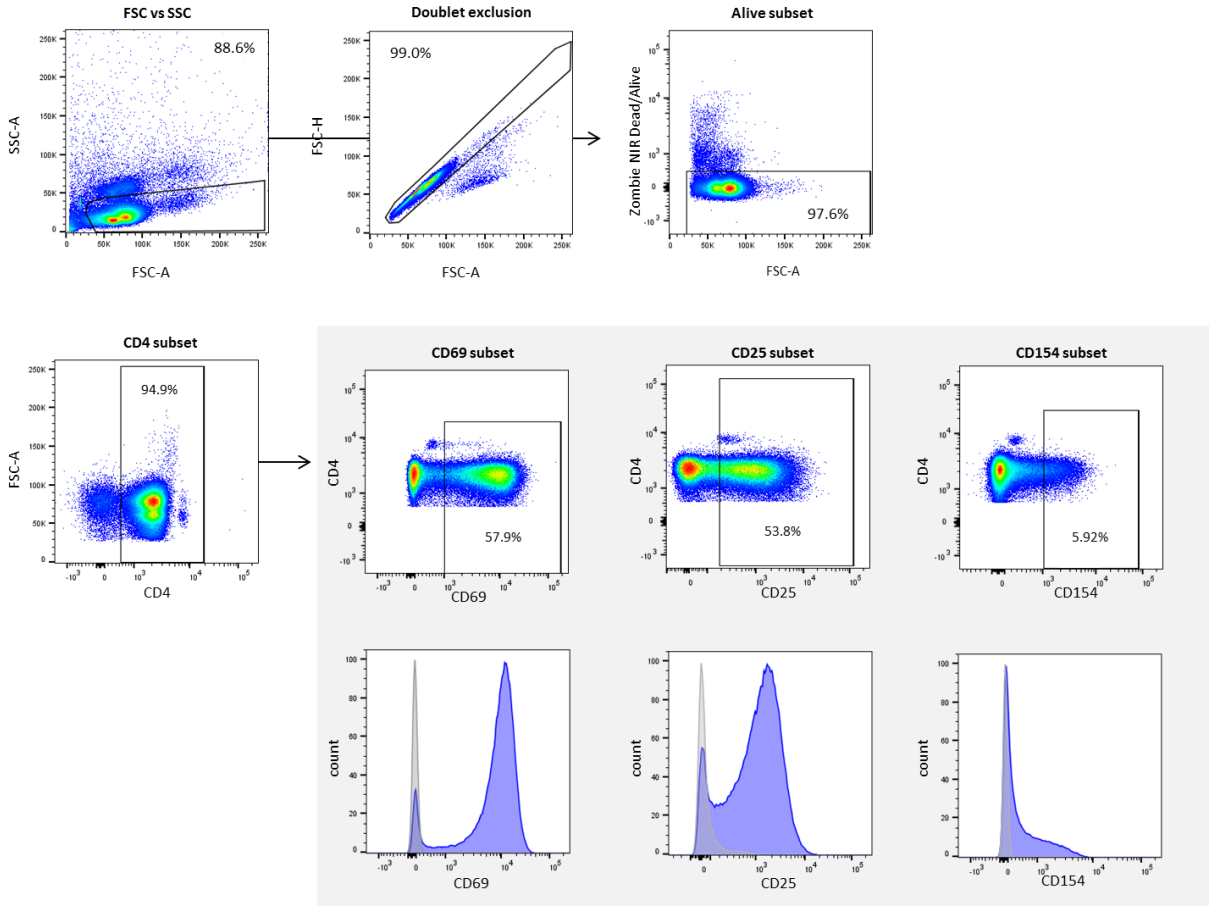

Figure 6: Representative FACS plots and gating strategy of human CD4$^+$ T cell activation status following polyclonal stimulation. Single lymphocytes were identified by forward and side scatter, live cells gated as Zombie/NIR negative. CD4$^+$ gated T cells were analyzed for the expression of the activation markers CD69, CD25 and CD154. Gating strategy was adjusted according to unstimulated T cell control subsets (Grey histograms in the lower lanes).

2.2.7.2 T cell proliferation assay

The T cell proliferation assay analyzed the frequency of cells that had undergone proliferation by using the cell proliferation dye eFluor450 (eBioscience). The long term expression of the activation markers CD69 (anti-CD69-FITC; BD Bioscience), CD25 (anti-CD25-PE; BD Bioscience) and CD154 (anti CD154-Brilliant Violet 605; Biolegend) was also monitored. $CD4^+$ T cell were incubated with eFluor450 (1:1000 for $10x10^6$) in PBS according to manufacturer's protocol for 20 min at room temperature. The reaction was stopped by adding RPMI 1650 medium supplemented with 10% HS. The cells were incubated on ice for 5 additional minutes and washed twice with culture medium. 2 $x10^5$ labeled T cells were cultured per well in 200µL RPMI in the presence of anti CD3/CD28 Dynabeads and the tested culture conditions for 72h in 96 round bottom culture plates additionally supplemented with 0.1ng/µL IL-7. Subsequently, the cells were stained using the following monoclonal antibodies: anti CD4-PerCP (clone: SK3; BD Pharmingen), anti CD69-FITC (clone: FN50; BD Pharmingen), anti CD25-PE (clone: M-A251; BD Pharmingen) and anti CD154-Brilliant Violet 605 (clone: 24-31; Biolegend). The cells were stained for 20 min at 4°C in phosphate-buffered saline without Ca^{2+} and Mg^{2+} ($PBS^{-/-}$; Gibco) containing 0.5% BSA. Cells were washed with $PBS^{-/-}$ and stained for 15 min at room temperature with Zombie NIR (Biolegend). T cells were fixed with 1.5% Formalin in $PBS^{-/-}$ and samples were acquired within 24hrs using the Becton Dickinson LSR Fortessa flow cytometer and analyzed with FlowJo software (Version 10; Treestar Inc.). Representative FACS plots and the gaiting strategy is shown in Figure 7.

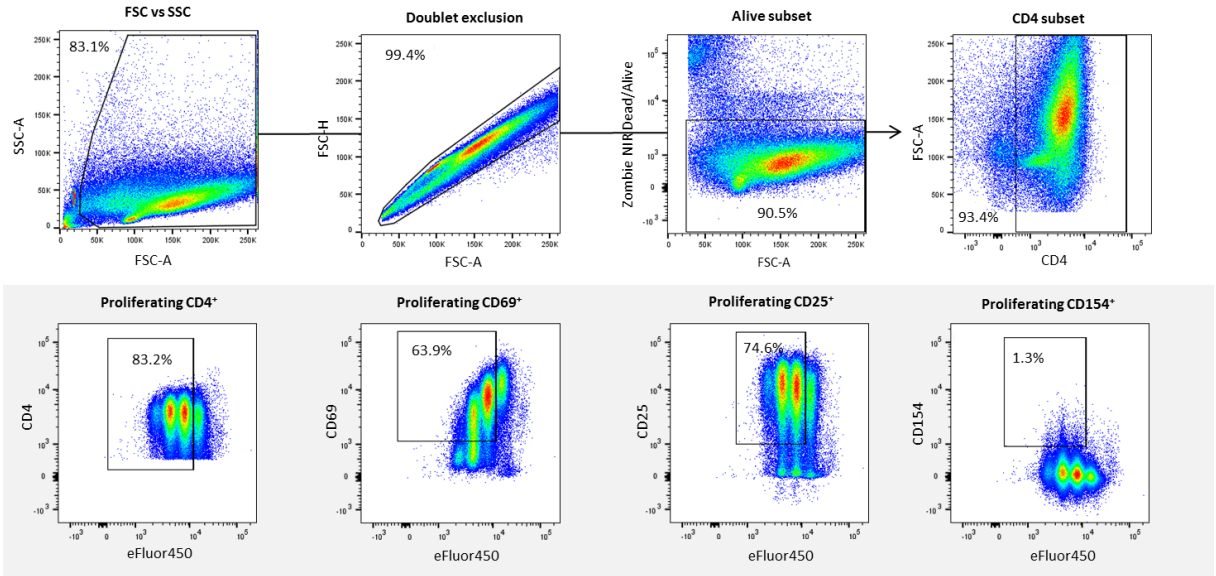

Figure 7: Representative FACS plots of the proliferation of freshly isolated human $CD4^+$ T cells after 72 hours of polyclonal stimulation. Single lymphocytes were identified by forward and side scatter, live cells were distinguished as negative subsets of the viability dye Zombie/NIR. $CD4^+$ T cells were monitored for their proliferation capacity with the cell cycle tracker eFluor450.The frequency of activation marker positive proliferated cells was also calculated.

2.2.7.3 T cell cytokine secretion

CD4⁺ T cells were stimulated with anti CD3/CD28 Dynabeads (Thermofisher) for 6h. Brefeldin A was added for the last 4h (10µg/mL, Sigma-Aldrich). A non-stimulated sample served as a negative background control. Cells were fixed and permeabilized using Cytofix/Cytoperm solution (BD Bioscience) according to the manufacture's protocol. Subsequently, cells were stained with pre-titrated concentrations of antibodies. Surface staining was performed with CD4-FITC (Biolegend). Intracellular staining was performed with anti-IL-4-Brilliant Violet 605 (Biolegend), anti-IL-17A-Brilliant Violet 510 (Biolegend), anti-IL-22-eFluor450 (eBioscience), anti-IFNγ-PE-Cy7 (BD Bioscience) and anti-IL-21 PE (eBioscience).

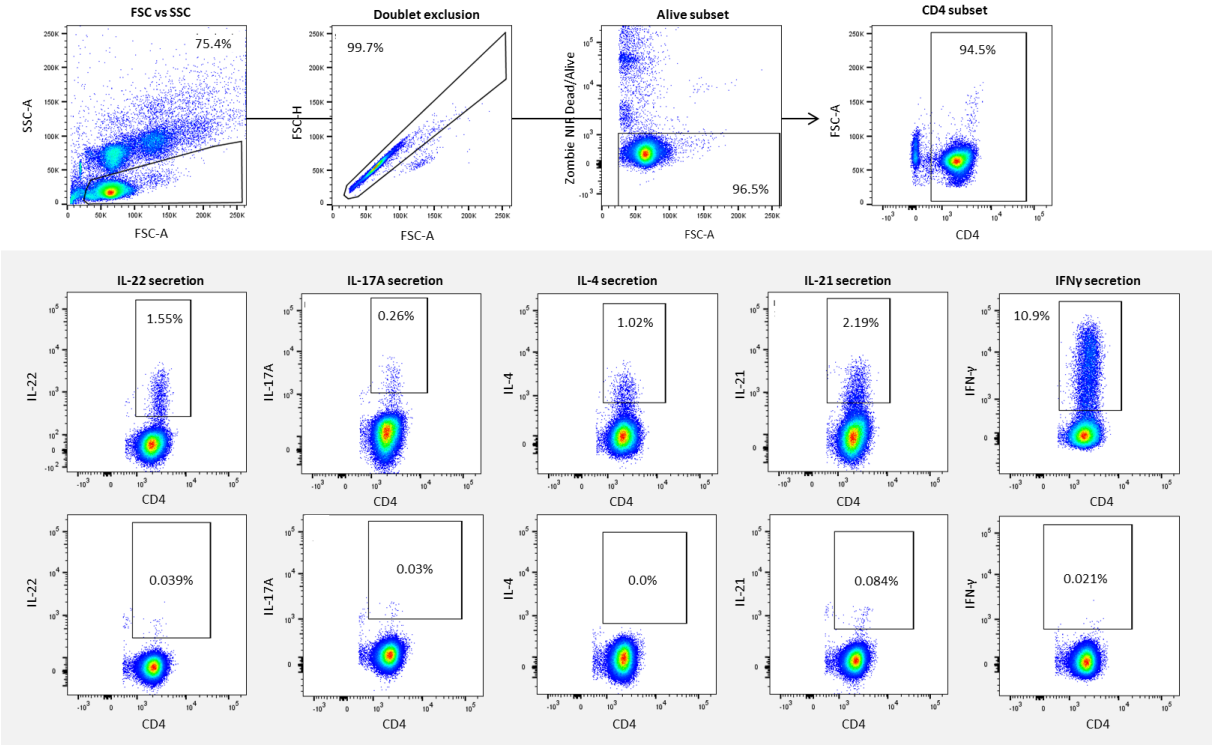

Figure 8: Representative FACS plots and gating strategy of intracellular cytokine staining in human CD4⁺ T cells following 6 hours of polyclonal stimulation and 4hrs of incubation with the transport inhibitor Brefeldin A. Single lymphocytes were identified by forward and side scatter. Living cells were gated as negative subsets of the viability dye Zombie/NIR. CD4⁺ gated cells were analyzed for IL-22, IL-17A, IL-4, IL-21 and IFNγ.

2.2.8 Glucose uptake assay

Glucose uptake was monitored using the labeled glucose 2NBDG (Thermo Fisher). CD4⁺ T cells were cultured for 16h in RPMI 1640 growth medium supplemented with 5% human serum, 1% Penicillin/Streptamycin and 2mM L-Glutamine (already included in the RPMI) as well as 0.1ng/mL IL-7. Anti CD3/CD28 Dynabeads [1:4] was used for stimulation. The cells were starved in glucose-free culture medium (RPMI 1640) for the last 2h prior to measurement. 50µM of 2NBDG was added to the cells and subsequently incubated for additional 10min at 37°C. T cells without αCD3/CD28 Dynabeads stimuation with and without 2NBDG as well as αCD3/CD28 Dynabeads stimulated cells without 2NBDG

served as negative controls. The cells were washed twice with PBS $^{-/-}$ and once with FACS buffer. The cells were stained for CD4 at 4°C for 10min and washed again twice with FACS-buffer. Samples were immediately acquired using the LSR Fortessa flow cytometer (Becton Dickinson) and analyzed with the FlowJo software (Version 10; Treestar Inc.). Figure 9 shows a representative FACS plot and the gating strategy.

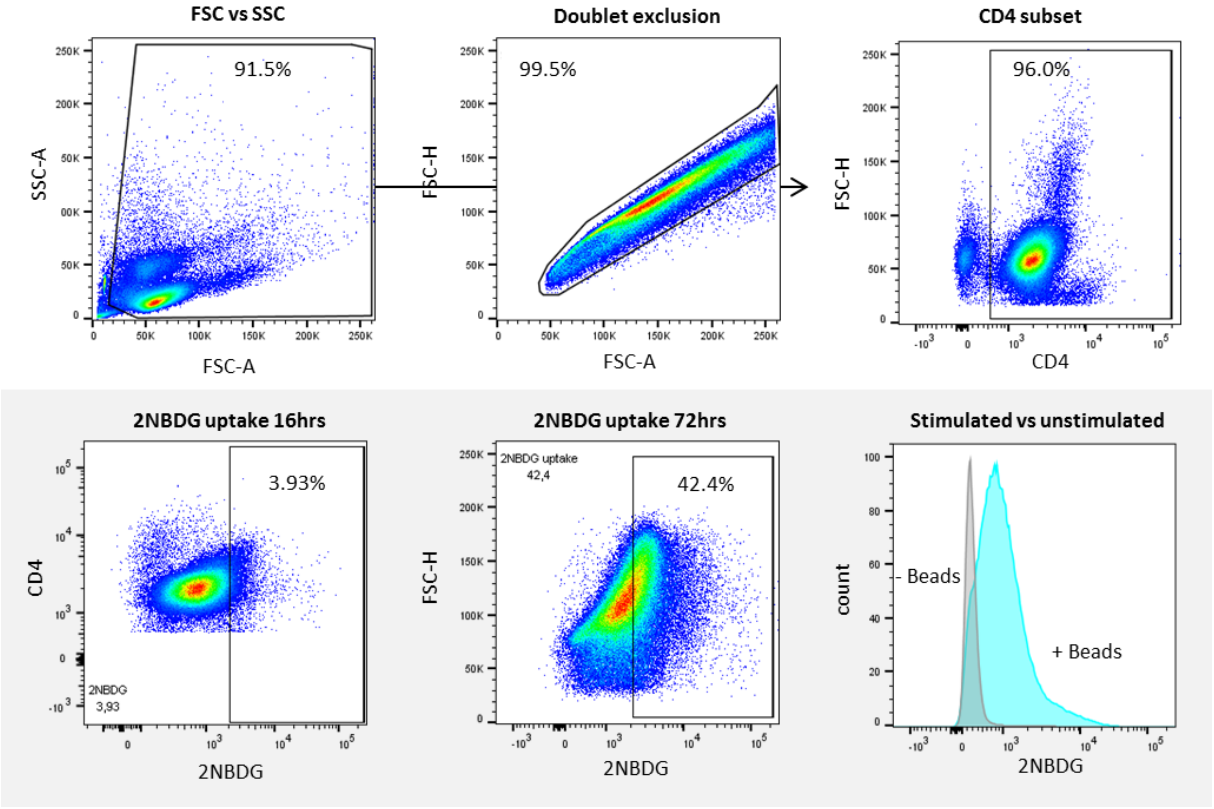

Figure 9: Representative FACS plots and gating strategy of glucose uptake measured by 2NBDG after 16 hours of polyclonal stimulation. Single lymphocytes were identified by forward and side scatter. $CD4^+$ cells were analyzed for the labeled glucose signal, 2NBDG-FITC. The histogram shows the glucose uptake in stimulated (blue) and unstimulated (grey) $CD4^+$ T cells.

2.2.9 Live cell superoxide indicator

MitoSOX™ Red Mitochondrial Superoxide indicator (Thermo Fisher) for live-cell imaging was used to detect cellular ROS production. Reactive oxygen species are produced mainly at the mitochondrial transport chain in activated T cells. The electron transport is tightly coupled to the ATP production. 1-3% of the mitochondrial oxygen (the final electron acceptor at the ETC) is incompletely reduced leading to an electron leakage. Those electrons interact with molecular oxygen and create reactive oxygen species. In low abundance, ROS is an important in initiating T cell activation. High ROS concentrations cause DNA damage and cell death. MitoSOX™ red mitochondrial superoxide indicator enters the mitochondria and is oxidized by superoxide resulting in red fluorescence. The oxidation only takes place in the presence of superoxides and not by other ROS species or reactive nitrogen species. Superoxide dismutase present in the cells can prevent the oxidation process. MitoSOX™ red has an

excitation/emission maxima of approximately 510/580 nm. After a stimulation time of 16 h using anti CD3/CD28 Dynabeads [1:4 ratio], the cells were incubated with 5µM MitoSOX™ directly added to the assay medium (L. A. Sena et al., 2013). Cells were washed twice with FACS buffer followed by anti-CD4 staining (CD4-Brilliant Violet 510) for 10 min at 4°C and dead/ alive discrimination (Zombie/NIR - APC-Cy7 - Biolegend). After two washing steps in FACS buffer, the samples were immediately acquired on the ARIA III.

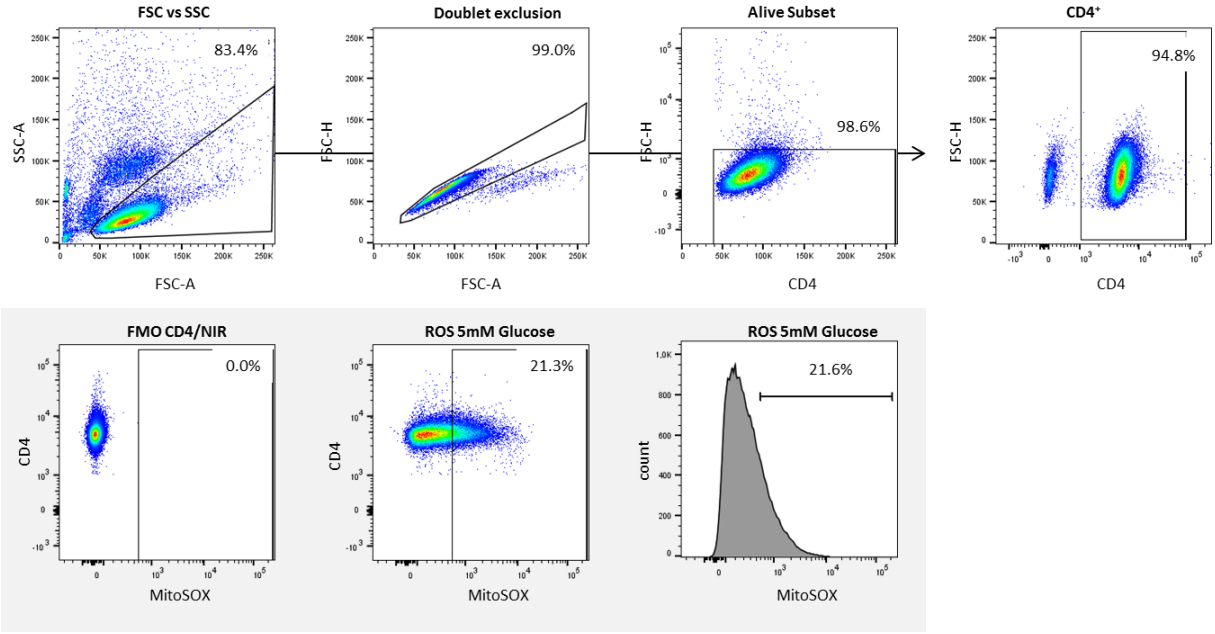

Figure 10: Representative FACS plots and gating strategy of superoxide production in CD4⁺ T cells after 16 hours of polyclonal stimulation. Single lymphocytes were identified by forward and side scatter. Living cells were identified by negative Zombie/NIR signal. CD4⁺ T cells were analyzed for MitoSOX signal, indicating superoxide production. Representative FACS plots are shown for FMO (- MitoSOX) and ROS production at 5mM glucose.

2.2.10 RNA isolation

RNA was isolated from stimulated CD4⁺ T cell subset. The miRNeasy micro Kit was used according to the manufacturer's protocol. The stimulated cells were harvest and centrifuged for 5 min at 500 x g. The supernatant was removed and 700µL of QIAzol Lysis Reagent was added. Cells were homogenized by vortexing for 1 min and stored at -80°C until further processing. Cell lysates were thawed on the benchtop at RT for 5 min. 140µL chloroform was added to each tube and shaken for 15 s. The homogenate was incubated for 3 min at RT and centrifuged for 15 min at 12 000 x g at 4°C. The upper aqueous phase was carefully transferred to a new collection tube. 1.5 volumes of 100% ethanol was added and mixed by pipetting. 700µL of the sample were pipetted into a RNeasy MinElute spin column and centrifuged at 8000 x g for 15 s at room temperature, the flow-through discarded and the centrifugation step was repeated with the remaining sample. The column was washed by addition of respective buffers (700µL RWT buffer; 500µL RPE buffer) by centrifugation (15 s at 8000 x g). The RNeasy MinElute spin column was transferred into a new 2ml collection tube and centrifuged at full

speed for 5 min to dry the membrane of the column. The RNeasy MinElute spin column was placed into a new collection tube and 14µL of RNase-free water was added to the membrane and centrifuged at full speed for 1min. Eluted RNA was stored at -80°C until further processing.

2.2.11 RNA quality control

The RNA concentration and integrity number (RIN) of the isolated RNA was measured. The isolated RNA was diluted 1:20 in RNase-free water and denatured for 2 min at 72°C. 1µL of RNasin Plus RNase Inhibitor (Promega) was added to each sample. 1µl of denatured sample was loaded onto an Agilent RNA 6000 Pico Chip. The chip was prepared according to the manufacturer's protocol and measured using the Agilent 2100 Bioanalyzer.

2.2.12 RNA sequencing

50ng of each RNA sample was submitted to the Deep Sequencing Facility of Dr. Andreas Dahl (CRTD) for RNA sequencing. mRNA was isolated by poly-dT pull down by strand specific RNA-Seq library preparation. Next generation sequencing (NGS) was performed using the Illumina platform with 30 Mio reads per sample (single end 75bp). Generated raw data was processed by Dr. Virag Sharma (CRTD). Fastq files corresponding to each sample was aligned to the human transcriptome (Ensembl ver 91) using STAR (version 2.5.4a). Reads that mapped to more than one location in the transcriptome were discarded. The resulting bam files were used to generate a count matrix using featureCounts. Differentially expressed genes were identified using DESEQ2 by first merging technical replicates from the same samples and then filtering genes where the p-value (after correction for multiple testing) was less than 0.05.

2.2.13 Data analysis and statistics

Statistical analysis was performed using Graph Pad Prism 7 software (GraphPad Software, San Diego, CA, USA). Data are presented as mean. Multiple Comparisons were conducted using one-way analysis of variance (ANOVA) with the Greenhouse-Geisser correction and Dunnett's multiple comparison test, with individual variances computed for each comparison. Alternatively, a paired t-test was performed, where paired samples were compared. Differences were considered as significant when *P ≤ 0.05; ** P≤0.01; *** P≤0.001; **** P≤0.0001. Identification of differentially expressed genes was done via the R package – DESeq2. Briefly, DESeq2 uses a negative binomial distribution to model the read counts and obtain an estimate of the fold change between a test condition and a control condition between different samples and treatments. The resulting p-value was then corrected for multiple testing using the Benjamini and Hochberg procedure. To ascertain if the differentially expressed genes were

enriched for a particular GO term/KEGG pathway/Mammalian phenotype (also known as a library) terms, the package Enrichr was used. Briefly, Enrichr uses a hypergeometric test to compute a p-value which reflects if the genes in an input list are enriched for a particular library term then compared to the background set of all genes. This p-value is corrected for multiple testing using the standard Benjamini and Hochberg procedure.

3 RESULTS

In the scope of my thesis I explored T cell flexibility and revealed adaptation mechanism of human $CD4^+$ T cells that allow maintained function in changing environments. Here, T cell flexibility is composed of metabolic flexibility and functional flexibility. The first describes the capacity to adapt fuel oxidation to its availability and energy needs. Functional flexibility means that activation and proliferation are not strictly linked to effector function even though they are usually bound upon immune stimulation. T cell might engage or bypass clonal expansion or effector function depending on the surrounding environmental conditions.

The metabolic signature of human $CD4^+$ T cells is insufficiently investigated and determining their ability of acclimatize to changing microenvironments is still unknown. Autoimmune and metabolic disease-related conditions of type I and type II diabetes were of specific interest. The effects of cellular stress, represented by mitochondrial dysfunction, varying glucose concentration and different insulin levels were investigated. Mitochondrial function was already shown to control T cell activity. Not only the mitochondrial energy production, but also its signaling capability constitutes a fundamental component of controlling adaptive immunity. Hence mitochondrial dysfunction might cause immune deregulation and autoimmunity. Fluctuating glucose and insulin levels are common and well-known phenomena in diabetic patients. Instead their effect on T cell metabolism and function and subsequently the impact on disease progression still lack completeness. The cell's flexibility was further analyzed by investigating the influence of these conditions alone and in combination with mitochondrial stress.

I developed an experimental set up which allows the alignment of T cell metabolic features to its function. A metabolic characterization of the T cells was performed by using extracellular flux analysis, glucose uptake assays and ROS production. T cell functional assays including activation status, proliferation capacity and cytokine secretion were determined by flow cytometric analysis. Gene enrichment and pathway analysis for adaption mechanisms was performed by RNA sequencing.

3.1 The human $CD4^+$ T cell immune response has distinct phases

The analysis of the various T cell function parameters depends on the time window after T cell stimulation. Therefore, an accurate description of the different immune response phases post-activation was needed. I identified distinct time points for the activation and proliferation phases as well as their transition phase. Metabolic activities were analyzed at three distinct time points by investigating the glucose uptake using flow cytometry.

3.1.1 A precise phase determination of stimulated human CD4⁺ T cells

Human CD4⁺ T cells were analyzed for the expression of CD69 as a marker of activation and for their proliferation rate using flow cytometry after polyclonal stimulation over a period of 96h. I used anti-CD3/CD28 Dynabeads as a stimulation model. CD69 is a transmembrane C-type lectin protein and one of the earliest inducible cell surface proteins on activated T cells. T cells were also labelled with the cell proliferation dye eFluor450. A time course of activation and proliferation allowed the identification of the optimal timing for investigating activation and proliferation and to identify a time window for potential metabolic rewiring during the transition from activated cells to proliferating cells. The results are shown in Figure 11.

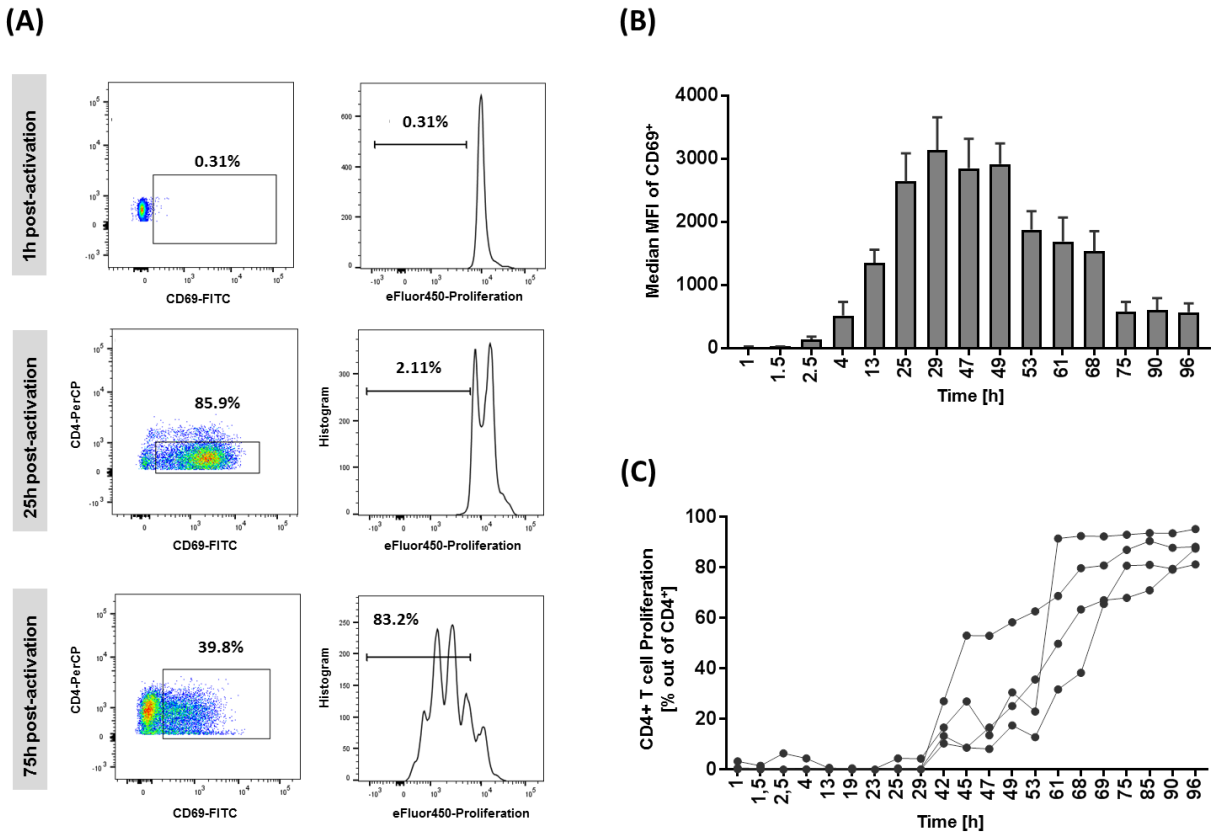

Figure 11: A time course of human CD4⁺ T cell activation and proliferation status. Human CD4⁺ T cells were cultured in 5mM glucose and stimulated using anti-CD3/CD28 human T cell activation Dynabeads. The representative FACS plots (A) show CD69 expression (left) and cell proliferation (right) at 1h, 25h and 75h post-stimulation as a percentage of CD4⁺ cells. The graph in (B) shows the median fluorescence intensity (MFI) +SEM of the expression of the cell surface marker CD69⁺ at distinct time points over a period of 96h (n=5). Graph (C) depicts the cumulative number of proliferated cells as % out of CD4⁺ T cells by flow cytometry over time. Proliferation was tracked using the cell proliferation dye eFluor450. Four independent experiments performed in technical duplicates are shown.

Representative FACS plots of CD69⁺ T cells and proliferation are shown in (A) after 1h, 25h and 75h post-activation. CD69⁺ cells and proliferation was not detected after 1h (0.31%). 25h of stimulation increased CD69 expression to 86%. After 75h post-stimulation, the activation marker decreased to 40% and 83% of the CD4⁺ T cells had proliferated. A more complete time course for CD69 expression and proliferation was performed over 96h (Figure 11B, C). Up-regulation of CD69 was first observed at 2.5

h post-stimulation. The first obvious differences was observed after 13h of stimulation (2.5h: MFI: 137 ± 45.2; vs 1h MFI: 21 ± 5.417; Figure 11B). A sharp rise was detected after 13h post-stimulation compared to 4h post stimulation (MFI: 13h 1352 ± 207.8 vs MFI: 4h 515.5 ± 217.2) and again after 25h post stimulation (MFI: 25h MFI: 2852 ± 465.9 vs MFI 13h 1352 ± 207.8). The intensity of CD69 expression reached its maximum at 25h (MFI: 2852 ± 465.9) and 29h (MFI: 2919 ± 323.9) and subsequently declined at 53h and after 75h post-stimulation (MFI 53h: 1535 ± 316.3; MFI 75h: 569 ± 140.1) (Figure 11A). Figure 11C shows the cumulative number of proliferated cells as percentage out of $CD4^+$ T cells. Proliferation initiated around 42h (16.9% of $CD4^+$ T cells) and reached its maximum at 68h to 85h with the present stimulation model (85h: 84% proliferating $CD4^+$ T cell). A high rate of proliferation was associated with a decline of activation marker expression (mean number of proliferating cells 75h post stimulation: 82.2%; MFI of $CD69^+$ after 75h post stimulation: 570.6) (Figure 11B and C).

Based on this data, activation was chosen to be monitored after 16h. Here exclusively activation processes took place. 72h was chosen to monitor T cell proliferation. Proliferation was highly active and the activation phenotype was lost (Figure 11A and B). T cell metabolism is likely to be particularly interesting during the transition phase from activation to proliferation. Hence 48h post-activation was chosen for metabolic studies. At this point, activation marker expression was at its maximum and proliferation activity was in its earliest phase.

3.1.2 The activation and proliferation phase time points differ in their glucose uptake

Glucose uptake after TCR stimulation was investigated to further substantiate and characterize the metabolic signature and remodeling during activation and proliferation phases. The cells were stimulated by anti-CD3/CD28 Dynabeads and cultured in 5mM glucose for 0h, 16h or 72h.

Figure 12 shows the glucose uptake using labelled glucose (2NBDG). Representative FACS plots of the incorporated glucose signals are shown in (A). The glucose incorporation increased from 0h to 16h to approximately 10% (Figure 2A) and after 72h post-stimulation to 52%.

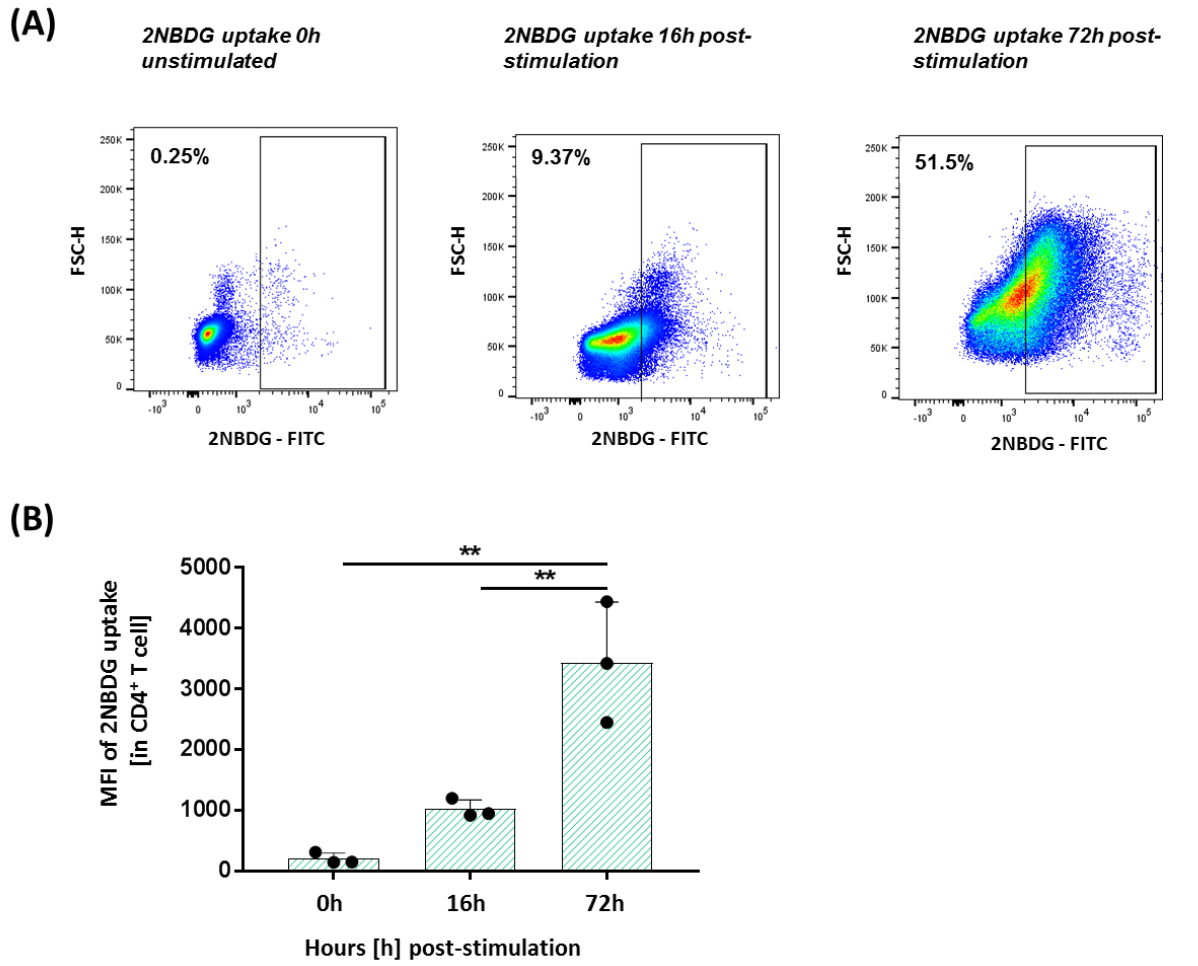

Figure 12: Glucose uptake during CD4⁺ activation (16h) and proliferation phase (72h) human CD4⁺ T cells were activated using anti-CD3/CD28 Beads in the presence of 5mM glucose for 0h, 16h and 72h. Representative FACS plots of incorporated labelled glucose (2NBDG) are shown in (A) for the three different time points. The Mean fluorescent intensity (MFI) of 2NBDG uptake into CD4⁺ T cells in the control (0h), activation phase (16h) and proliferation phase (72h) are shown (B). N=3; one point represents one independent experiment performed in technical duplicates; Ordinary one-way ANOVA with Turkey's multiple comparison test with a single pooled variance and 95% confidence interval was performed. (*P ≤ 0.05; ** P≤0.01; *** P≤0.001; **** P≤0.0001) (0h vs 72h; p=0.0012; 16h vs 72h; p=0.0055).

3.2 Mitochondrial derived ATP is indispensable for T cell activation and proliferation

I next asked whether mitochondrial energy production was relevant during activation and proliferation. The glucose assay suggested a different need for glucose at the intersections of the quiescent, activation and proliferation phases. These results mainly favored the notion of an importance for glucose consuming pathways such as glycolysis during proliferation. In order to investigate the reliance of mitochondrial derived ATP for activation and proliferation of human CD4⁺ T cells, the function of the ETC complex V and hence mitochondrial ATP production was blocked using the specific inhibitor oligomycin. In order to discriminate the importance of mitochondrial ATP production for activation and proliferation processes, two conditions were tested and are illustrated in Figure 3A and B. In both conditions, T cells were stimulated with anti-CD3/CD28 Dynabeads at time

point 0h. Oligomycin was either added at time point 0h post-stimulation (Figure 13A) and removed after 16h together with the anti-CD3/CD28 Dynabeads or added after 16h post-stimulation (Figure 13B) until the very end of the stimulation period (time point 72h). The cumulative number of proliferating $CD4^+$ T cells is shown in Figure 13 for both conditions. Proliferation of the T cells was nearly completely repressed when oligomycin was added during the activation phase (p=0.029) (Figure 13A). Proliferation was furthermore excessively inhibited when oligomycin was added during the proliferation phase (p=0.012) (Figure 13B). These experiments strongly suggest a necessity for mitochondrial function, especially mitochondrial ATP production for activation as well as proliferation processes.

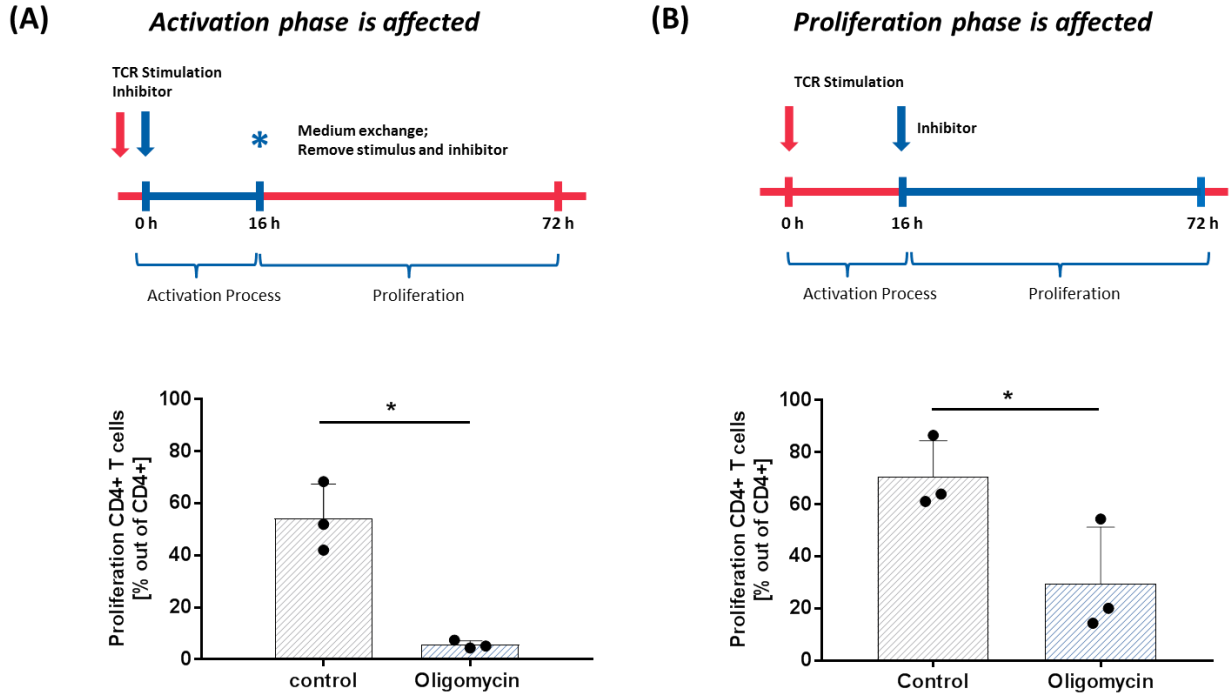

Figure 13: The importance for mitochondrial ATP production for human $CD4^+$ T cell activation and proliferation. The illustration in the upper panel describes the experimental set up. Human $CD4^+$ T cells were stimulated using anti-CD3/CD28 Dynabeads. Oligomycin was either added directly at time point 0h to the cell culture (A) or after 16h (B). ATP-dependent activation was investigated by removing stimulus and inhibitor again after 16h (A). ATP-dependent proliferation was investigated by continuous stimulation and inhibitor addition after 16h (B). Cell proliferation served as a read out and was monitored after 72h using the proliferation marker eFluor450. The graphs (lower panel) represents the percentage of proliferating cells out of $CD4^+$ T cells for both experimental set ups. One dot represents one independent experiments performed in technical duplicates (N=3). Paired t-test (*P ≤ 0.05; ** P≤0.01; *** P≤0.001; **** P≤0.0001) (A) * p=0.029 and (B) * p=0.012.

3.3 Mitochondrial impairment severely affects T cell function

I demonstrated that mitochondrial ATP production is crucial for T cell activation and proliferation (Figure 13). However, mitochondria are not only a source for ATP. They are also important generators of signaling molecules such ROS or Ca^{2+}. They furthermore play a role in maintaining the NAD/NADH redox balance, in pyrimidine and amino acid biosynthesis and others. In order to investigate the importance of mitochondrial function on T cell biology, different inhibitors that specifically target

distinct components of the ETC or related pathways were investigated and summarized in Table 11. The importance of the ATP synthase was tested using oligomycin. The importance of complex I was tested using rotenone. Resveratrol is a naturally occurring polyphenol and its mechanism of action still remains elusive. It is suggested to inhibit the ATP synthase, complex I or the mTOR pathway via Sirtuin 1 (SIRT1) and AMPK (Alayev et al., 2015; de Ligt et al., 2015; Gueguen et al., 2015; Price et al., 2012).

Table 11: Mitochondrial inhibitors with different targets to further investigate the importance of mitochondrial pathways for $CD4^+$ T cell function.

Mitochondrial Inhibitors	Mechanism of Action
Oligomycin	Inhibition of ATP Synthase
Rotenone	Inhibition of Complex I of the mitochondrial electron transport chain
Resveratrol	ATP synthase inhibitor; Complex I inhibitor or mTOR inhibition via SIRT1 and AMPK

3.4 The different inhibitors have diverse metabolic consequences

The dose-dependent effects on T cell metabolism and function of the various inhibitors were analyzed. T cell metabolism was monitored using the *xf* extracellular flux analyzer. Human $CD4^+$ T cells were cultured for 48h in 5mM glucose and the inhibitors were added in real time during the measurement after the 48h cultivation time.

Oligomycin and rotenone profoundly decreased ATP production at a concentration of 1 and 2.5µM (for oligomycin 1µM p=0.0015 and 2.5µM p=0.0015; for rotenone 1µM p=0.030 and 2.5µM p=0.027). Resveratrol did not affect mitochondrial ATP-linked respiration at any of the tested concentrations (Figure 14:).

Maximal respiration SRC were also analyzed (Figure 15). Oligomycin and rotenone injection differed in their effects on maximal respiration and SRC. Oligomycin had no effect on maximal respiration or on SRC. However, rotenone treatment decreased maximal capacity and SRC in a dose dependent manner (Maximal respiration, 2.5µM p=0.034; SRC: 1µM p=0.0090; 2.5µM p=0.0049) (Figure 15). Resveratrol did not affect maximal respiration or SRC.

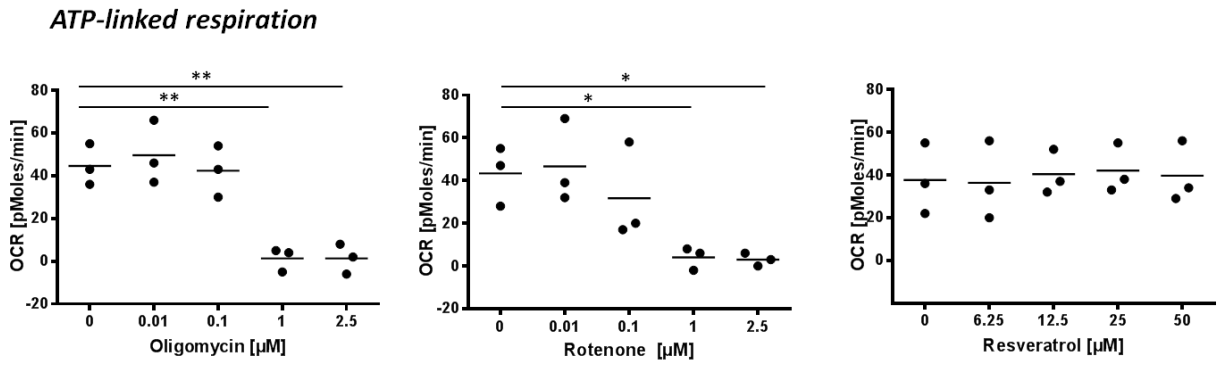

Figure 14: mitochondrial ATP-linked respiration of human CD4⁺ T cells in the presence of different concentration of mitochondrial inhibitors. Human CD4⁺ T cells were stimulated with anti-CD3/CD28 Dynabeads for 48h and T cell respiration signature was analyzed using the xf extracellular flux analyzer. Mitochondrial ATP-linked respiration of various concentrations of oligomycin, rotenone and resveratrol added in real time during the measurement is shown. (N=3) one point represents one independent experiment performed in technical duplicates; Ordinary one-way ANOVA; Dunnett's multiple comparisons test, with a single pooled variance. (*P≤0.05 ; ** P≤0.01; *** P≤0.001; **** P≤0.0001). Oligomycin: 1µM p=0.0015; 2.5µM p=0.0015; Rotenone: 1µM p=0.027; 2.5µM p=0.030.

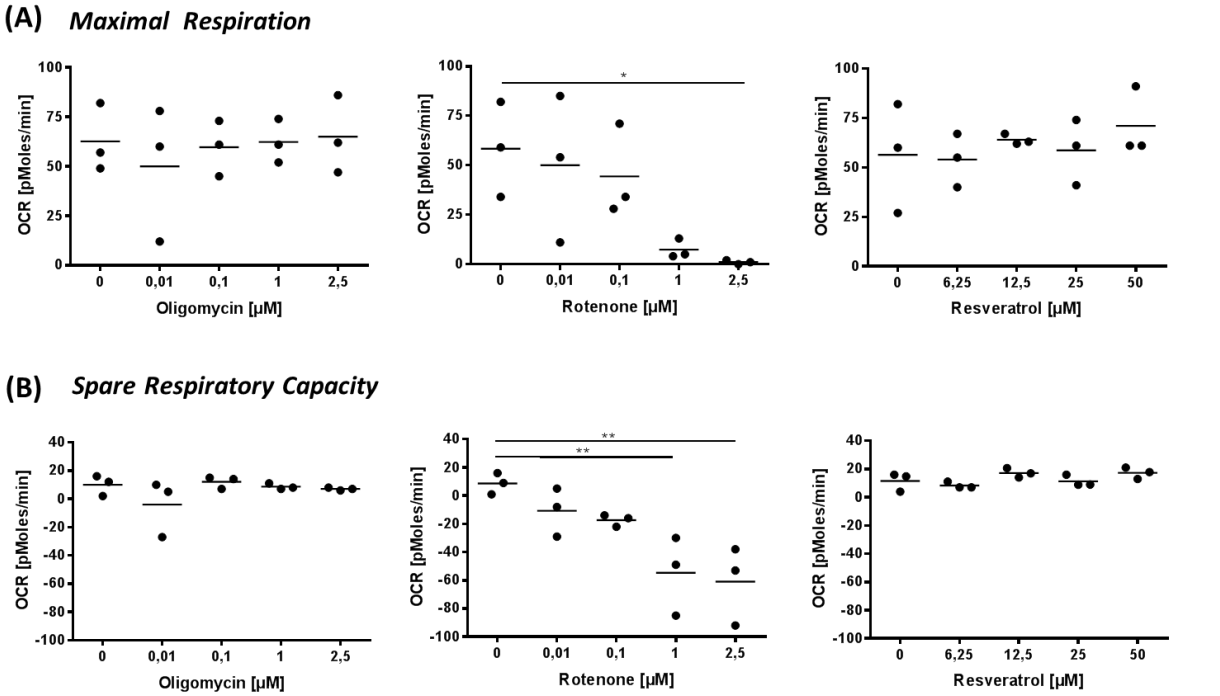

Figure 15: Spare respiratory capacity and maximal capacity of human CD4⁺ T cells in the presence of different concentrations of mitochondrial inhibitors. Human CD4⁺ T cells were stimulated with anti-CD3/CD28 Dynabeads for 48h and T cell respiration signature was analyzed using the xf extracellular flux analyzer. Spare respiratory capacity (SRC) and maximal respiration of various concentrations of oligomycin, rotenone and resveratrol added in real time during the measurement is shown. (N=3). Ordinary one-way ANOVA; Dunnett's multiple comparisons test, with a single pooled variance. (*P≤0.05; ** P≤0.01; *** P≤0.001; **** P≤0.0001). Rotenone: Spare respiratory capacity, 1µM p=0.0090; 2.5µM p=0.0049; Maximal respiration, 2.5µM p=0.034.

Many cell types compensate for impaired mitochondrial ATP production by increasing glycolytic rates (Gaude et al., 2018; Pavlova and Thompson, 2016). Here, T cells treated with oligomycin showed only a minor compensatory increase of the glycolytic rates at the corresponding concentration (2.5µM,

p=0.041) (Figure 16). The increase of glycolysis appeared insufficient to rebalance the ATP need. The Glycolytic rates were unaffected upon rotenone and resveratrol injection.

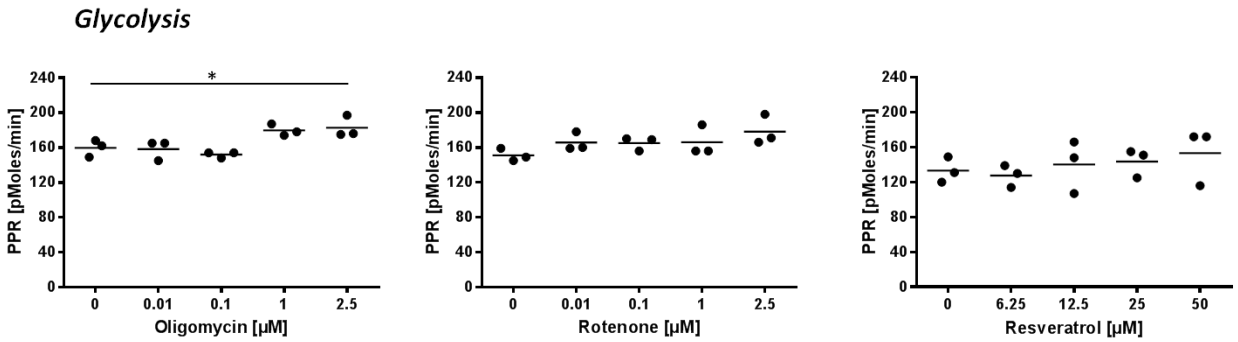

Figure 16: Glycolytic activity of human CD4⁺ T cells in the presence of different concentration of mitochondrial inhibitors. Human CD4⁺ T cells were stimulated with anti CD3/CD28 Dynabeads for 48h and T cell respiration signature was analyzed using the xf extracellular flux analyzer. Glycolytic activity at various concentrations of oligomycin, rotenone and resveratrol is shown. (N=3); (*P≤0.05; ** P≤0.01; *** P≤0.001; **** P≤0.0001) Ordinary one-way ANOVA; Dunnett's multiple comparisons test, with a single pooled variance. (Oligomycin: p=0.041).

Real-time injection of resveratrol did not alter T cell metabolism. This suggests a different mechanism of action compared to oligomycin and rotenone. I aimed to further investigate resveratrol's efficacy on T cell respiration. Cells were stimulated for 48h and increasing concentration of resveratrol were added for the last 16h to investigate long-term effects on T cell metabolism by extracellular flux measurement (Figure 17). The basal respiration and ATP-linked respiration decreased in a dose-dependent manner (Basal Respiration: 50µM p=0.024; ATP-linked Respiration: 100µM p=0.030). Instead maximal respiration and spare respiratory capacity significantly increased (Maximal Respiration: 50µM p=0.021; SRC 50µM p=0.0043). Glycolytic characteristics also significantly decreased at a concentration of 50µM of resveratrol (Glycolysis: 50µM p=0.0058; Glycolytic Capacity: 50µM p=0.0022).

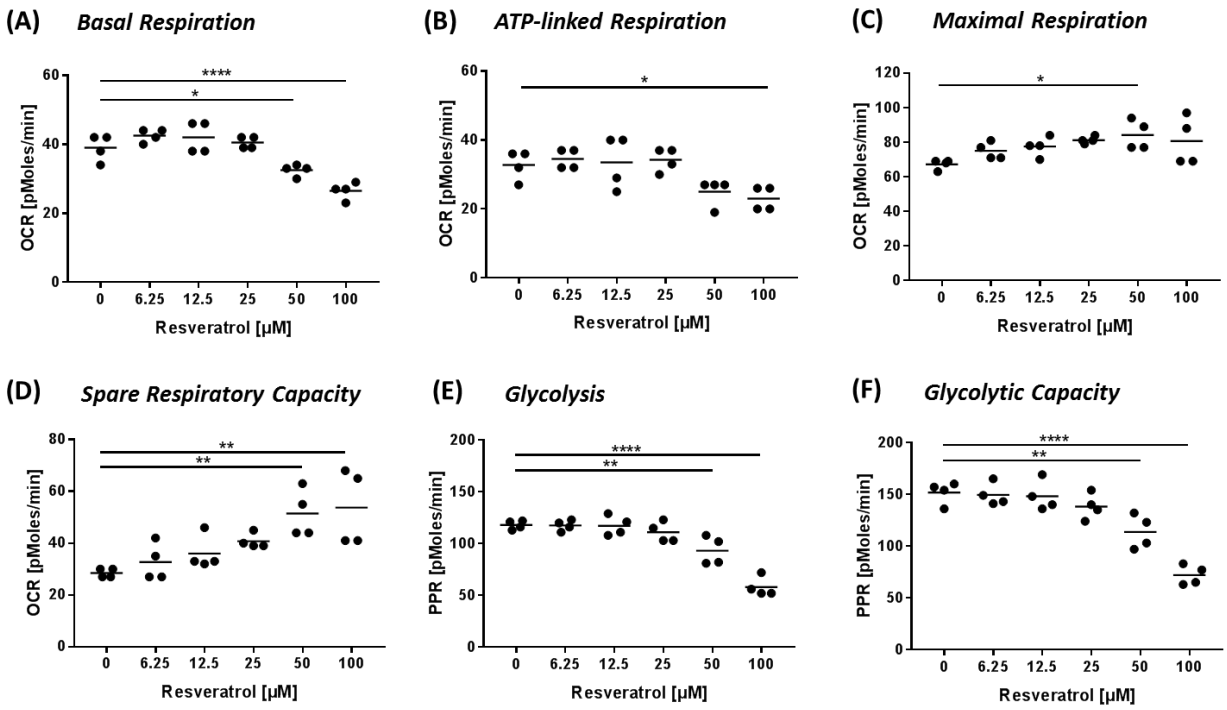

Figure 17: Respiratory signature of CD4⁺ T cells after resveratrol incubation. Human CD4⁺ T cells were stimulated with anti-CD3/CD28 Dynabeads for 48h and treated for the last 16h with resveratrol. T cell respiration signature was analyzed using the xf extracellular flux analyzer. Basal respiration, mitochondrial ATP-linked respiration, maximal respiration, spare respiratory capacity as well as glycolysis and glycolytic capacity are shown for various resveratrol concentrations (N=4). One point represents one donor. Experiments are performed in five technical replicates per condition; Ordinary one-way ANOVA; Dunnett's multiple comparisons test, with a single pooled variance. (*P≤ 0.05; ** P≤0.01; *** P≤0.001; **** P≤0.0001); Basal respiration: 50µM p=0.024; 100µM p=0.0001; ATP-linked respiration: 100µM p= 0.030; Maximal respiration 50 p=0.021; Spare respiratory capacity: 50µM p=0.0043; 100µM p=0.0019; Glycolysis: 50µM p=0.0058, 100µM p=0.0001; Glycolytic capacity 50µM p=0.0022, 100µM p=0.0001.

3.5 The metabolic inhibitors impede cellular glucose uptake

For further metabolic characterization of the inhibitor effect, a glucose uptake assay was performed using the labelled glucose 2NBDG. The cells were treated with the metabolic inhibitors for 16h and 72h. Each inhibitor led to a reduction in glucose uptake after short term (16h) and long term (72h) incubation (Figure 18). Glucose uptake was reduced using 50µM resveratrol (16h, mean=0.44, fold reduction p=0.0066; 72h, mean=0.42, fold reduction p=0.0003), 1µM oligomycin (16h, mean=0.56, fold reduction p=0.0224; 72h, mean=0.44, fold reduction p=0.0004) and 1µM rotenone (16h, mean=0.57, fold reduction p=0.026; 72h, mean=0.58, fold reduction p=0.0026).

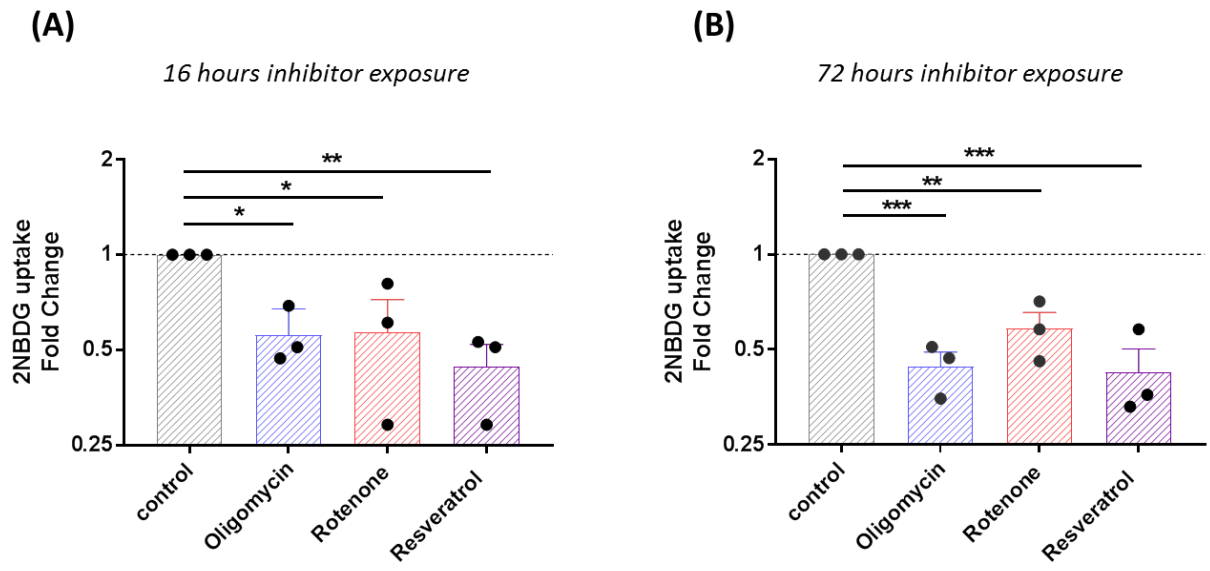

Figure 18: Glucose uptake of human CD4⁺ T cells after 16h and 72h of stimulation in the presence of mitochondrial inhibitors. CD4⁺ T cells were cultured and stimulated with anti-CD3/CD28 Dynabeads for 16h and 72h in the presence of 5mM glucose and starved for the last two hours. Labelled glucose (2NBDG) was added for 10min to the culture and glucose uptake was followed by flow cytometric analysis. Oligomycin and rotenone were tested at concentration of 1µM and resveratrol at 50µM. Data are shown as Fold change to control and mean + SEM (N=3). Ordinary one-way ANOVA; Dunnett's multiple comparisons test, with a single pooled variance was performed. (*P ≤ 0.05; ** P≤0.01; *** P≤0.001; **** P≤0.0001); 16h: Oligomycin p=0.022, rotenone p=0.026, resveratrol p=0.0066; 72h: Oligomycin p=0.0004, rotenone p=0.0026, resveratrol p=0.0003.

3.6 Reactive oxygen species production is affected by metabolic inhibitors

MitoSOX red was used to investigate ROS production after 16h of inhibitor incubation in stimulated and in unstimulated conditions (Figure 19). ROS production increased upon TCR stimulation in control conditions (stimulated CD4⁺ T cells: mean=176; unstimulated CD4⁺ T cells: mean=62.6; p=0.0054). This emphasizes the need of ROS for the activation process. ROS production was further analyzed as a potential consequence of mitochondrial inhibition. ROS production in unstimulated CD4⁺ T cells was markedly increased in the presence of 1µM.rotenone (MFI control = 62.64; mean 1µM rotenone = 223.2; p=0.0001) as well as with 1µM oligomycin (MFI control = 62.64; MFI = 204.0; p=0.0001) compared to the control condition (MFI = 62.64). 50µM of resveratrol did not alter ROS production (MFI control = 62.64; MFI resveratrol = 55.21. Upon polyclonal stimulation, 1µM of oligomycin (MFI = 272.2) and 1µM rotenone increased ROS production (MFI = 290.3; p=0.033) compared to control (MFI = 176). 50µM Resveratrol dampened the ROS production upon stimulation (MFI = 83.85, p=0.108).

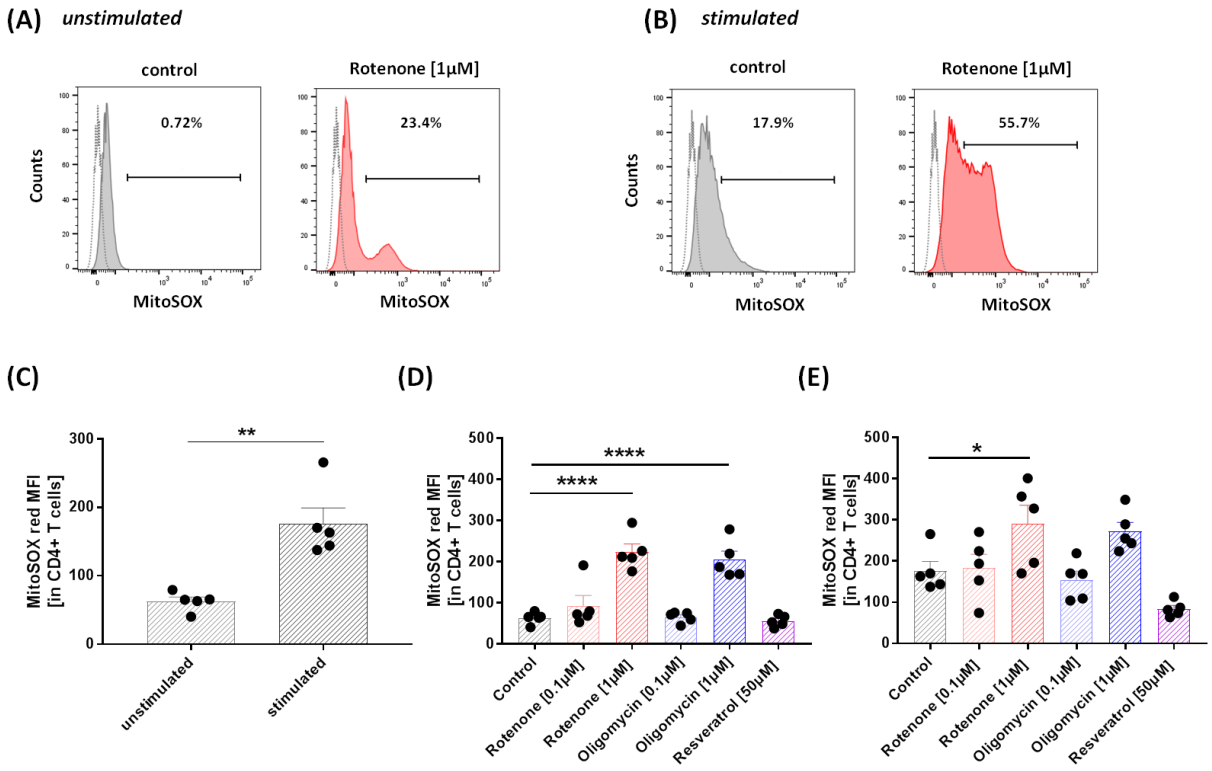

Figure 19: Production of reactive oxygen species in unstimulated and stimulated conditions and in the presence of mitochondrial stress. $CD4^+$ T cells were treated for 16h with different concentration of rotenone and oligomycin [0.1; 1µM] as well as one concentration of resveratrol [50µM]. ROS production was investigated by flow cytometry using MitoSOX red. (A) Representative FACS plots of unstimulated $CD4^+$ T cells of the control condition and in the presence of 1µM rotenone. (B) Representative FACS plots of anti CD3/CD28 beads stimulated $CD4^+$ T cell without inhibitor (control) and 1µM rotenone. (C) MFI of MitoSOX red in unstimulated and stimulated $CD4^+$ T cells without inhibitors. (D) Mean fluorescence Intensity (MFI) of MitoSOX red for the different conditions in unstimulated cells. (E) MFI of MitoSOX red for the different conditions in stimulated cells. Mean + SEM (N=5) are shown. A paired t-test was performed in (E) p=0.0054). Ordinary one-way ANOVA; Dunnett's multiple comparisons test, with a single pooled variance was performed for (D) and (E). (*P≤0.05; ** P≤0.01; *** P≤0.001; **** P≤0.0001). Unstimulated condition (D) with rotenone [1µM] p=0.0001 and oligomycin [1µM] p=0.0001; Stimulated condition (E) with rotenone p=0.033.

3.7 Oligomycin and rotenone severely impact T cell activation

The tested metabolic inhibitors varied in their modification of mitochondrial respiration, glycolysis and their effect on ROS production. I, therefore, continued to investigate the effects on T cell function. T cell activation was monitored by the expression of the early activation marker CD69, CD25 and CD154 using flow cytometric analysis. $CD4^+$ T cells were cultured in 5mM glucose and stimulated using anti-CD3/CD28 Dynabeads for 16 h (Figure 20). Representative FACS plots show inhibition of activation, manifested by fewer cells expressing the activation markers (Figure 20A). Oligomycin treatment resulted in a marked decrease in CD69, CD25 and CD154 expression, starting at 0.01µM of oligomycin (0.1µM oligomycin: CD69 p=0.022; CD25 p=0.040; Figure 10 B). Activation is affected at a lower concentration range as compared to mitochondrial ATP-linked respiration (compare Figure 14:). Also Rotenone substantially reduced the activation phenotype but from a concentration similar to what was observed for ATP-linked respiration (compare Figure 14:) (1µM rotenone: CD69 p= 0.0001; CD25

p=0.0006; 2.5µM rotenone: CD69 p=0.0003; CD25 p=0.0024). Resveratrol slightly decreased CD154 and CD25 expression at a concentration of 50µM (CD154 50µM p=0.019; CD25 50µM p=0.046).

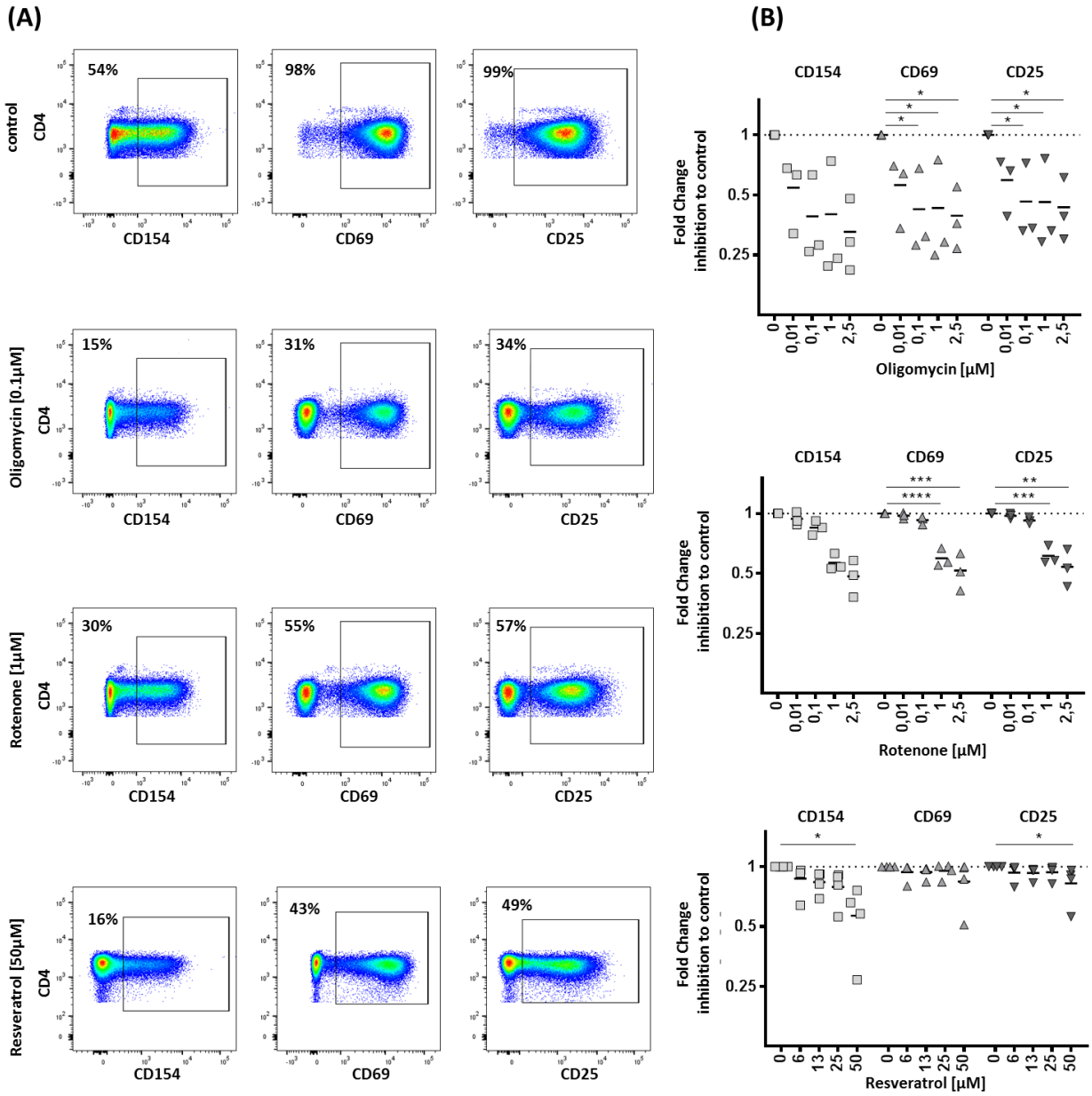

Figure 20: T cell activation in the presence of various concentrations of mitochondrial inhibitors. T cells were cultured in 5mM glucose and polyclonal stimulated for 16h in the presence of various concentrations of oligomycin, rotenone and resveratrol. T cell activation is represented by the proportion of cells expressing the activation markers CD154, CD69 and CD25 shown in representative FACS plots in (A). The data in (B) is shown as fold change to control. The experiments are performed in technical duplicates. One point represents one independent donor; oligomycin and rotenone (N=3) and resveratrol (N=4). Ordinary one-way ANOVA with Dunnett's multiple comparisons test and a single pooled variance was performed. (*P ≤ 0.05; ** P≤0.01; *** P≤0.001; **** P≤0.0001); Oligomycin: CD69 0.1µM p=0.022, 1µM p=0.024, 2.5µM p=0.017; CD25 0.1µM p=0.04; 1µM p=0.039; 2.5µM p=0.029. Rotenone: CD69 1µM p=0.0003, 2.5µM p=0.0001; CD25 1µM p=0.0024, 2.5µM p=0.0006. Resveratrol: CD154 50µM p=0.019; CD25 50µM p=0.046.

3.8 Metabolic interference impedes T cell proliferation

T cell function was further analyzed by investigating $CD4^+$ T cell proliferation by flow cytometry using the cell proliferation dye eFluor450. T cells were polyclonal stimulated for 72h and analyzed for proliferation and activation marker expression (Figure 21). Representative FACS plots of the control condition shows proliferation of approximately 80%. Each of the three inhibitors tested decreased T cell proliferation (Figure 21 B). Similar to what was observed for activation, oligomycin decreased proliferation at 0.01 µM (mean proliferation = 35.47% vs mean proliferation control = 81.36%; p=0.0022) and at higher concentrations. Substantial Inhibition of proliferation by 1µM rotenone was observed (mean proliferation = 6.33% vs mean proliferation control = 81.18%; p=0.0012). Resveratrol decreased proliferation capacity in a dose-dependent manner and significantly blocked proliferation from 25µM (mean proliferation = 51.38% vs mean proliferation = 93.86%; p=0.0004).

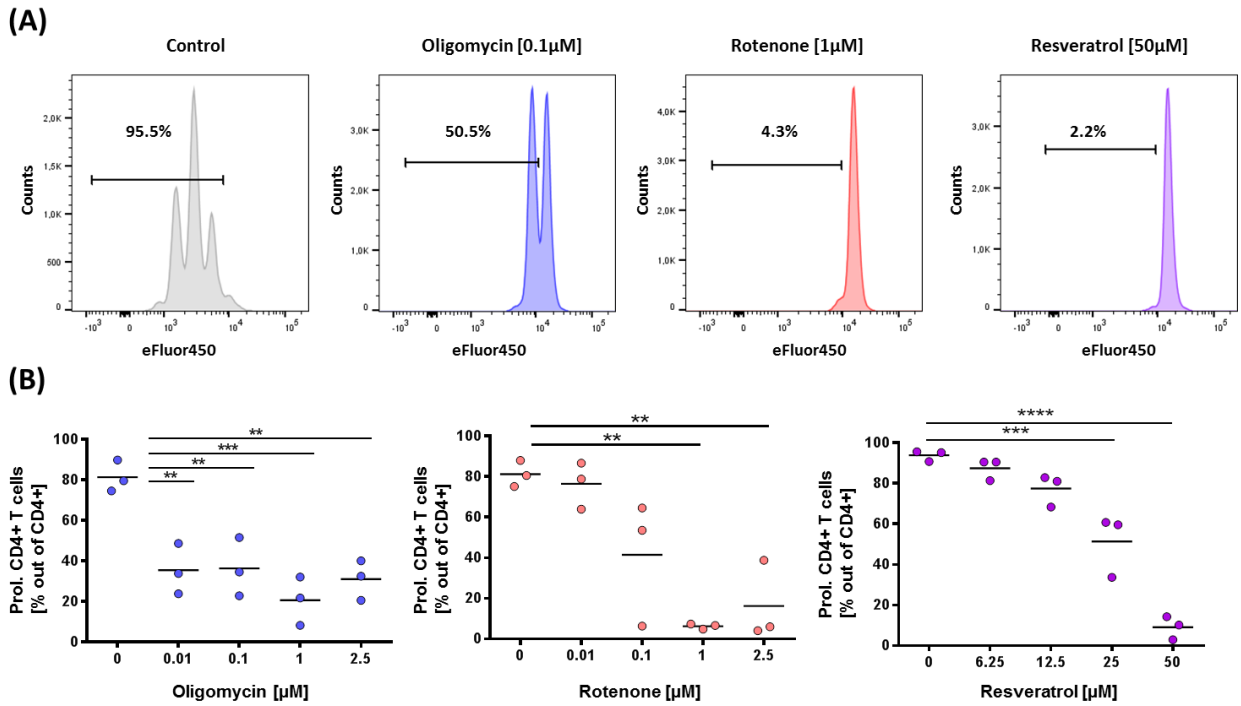

Figure 21: Proliferation of human $CD4^+$ T cells in the presence of mitochondrial inhibitors. Human $CD4^+$ T cells were cultured for 72h in 5mM glucose and stimulated using anti-CD3/CD28 Dynabeads. Proliferation was tracked using eFluor450. One point represents one independent experiment and data is shown with mean (N=3); (*P ≤ 0.05; ** P≤0.01; *** P≤0.001; **** P≤0.0001) Ordinary one-way ANOVA; Dunnett's multiple comparisons test, with a single pooled variance was performed. Oligomycin: 0.01µM p=0.0022, 0.1µM p=0.0025, 1µM p=0.0003, 2.5µM p=0.0011; Rotenone: 1µM p=0.0012, 2.5µM p=0.0034; Resveratrol 25µM p=0.0004, 50µM p=0.0001)

Long-term activation marker expression was investigated to determine whether effects on proliferation were paralleled with alterations in the expression of surface markers. The data in Figure 22 shows the fold change of expression marker of inhibitor to control. Whereas under control conditions, the number of cells positive for CD154 expression had declined after 72 h, it remained high when cells were stimulated in the presence of oligomycin or rotenone (oligomycin: 0.01µM p=0.023;

rotenone: 1µM p=0.015). CD69 and CD25 remained largely unaffected at 72 hours in the presence of these two inhibitors. In contrast, stimulation in the presence of resveratrol did not affect CD154 expression, but resulted in more cells positive for CD69 (6.25µM; p=0.0081).

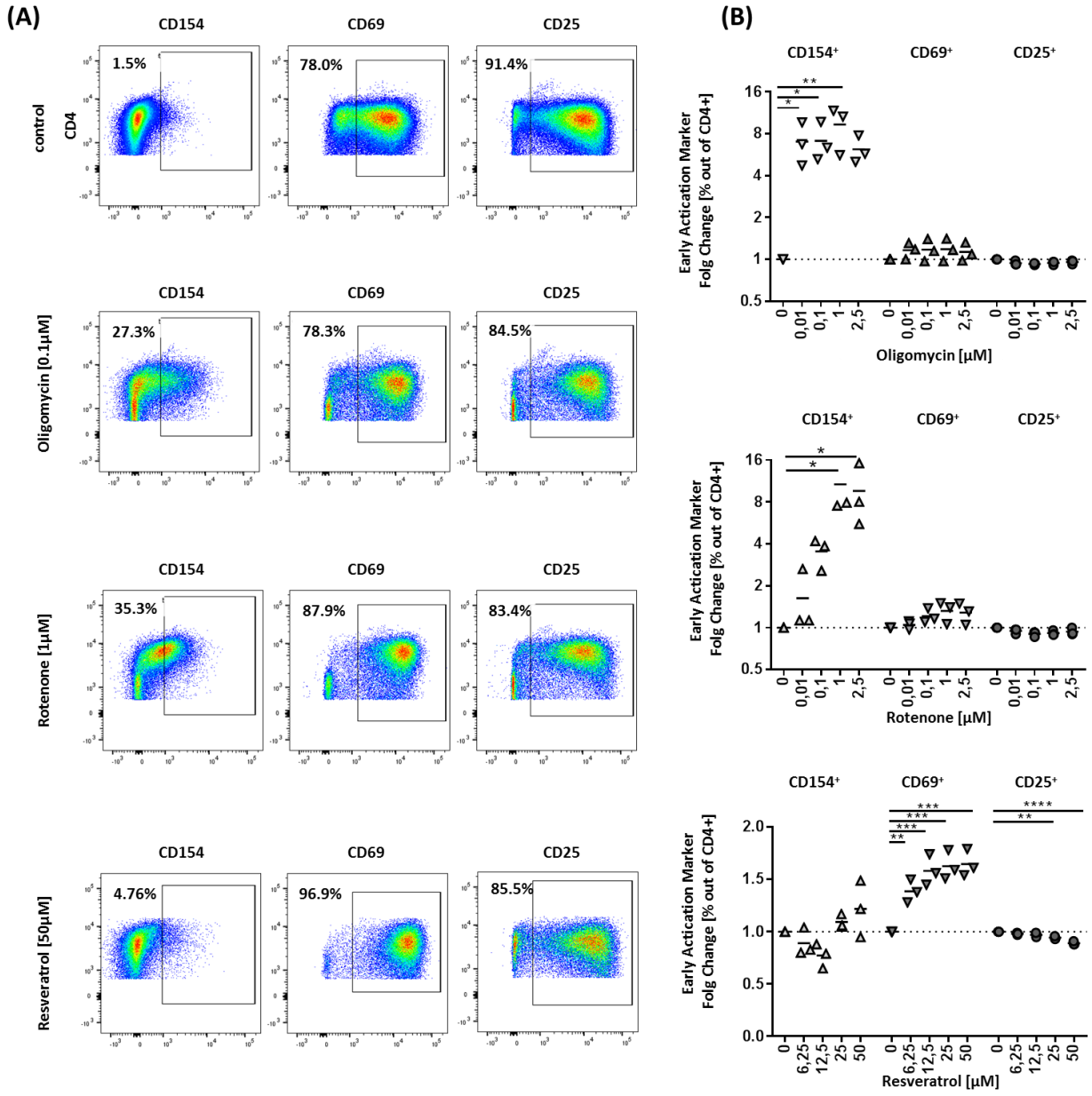

Figure 22: Activation marker expression after 72h. Human CD4⁺ T cells were cultured for 72h in 5mM glucose and stimulated using anti-CD3/CD28 Dynabeads. Different concentrations of oligomycin, rotenone and resveratrol were added for the entire culture period and activation marker expression was analyzed by flow cytometry. Representative FACS plots are shown in (A) and the corresponding graphs depicted as fold change to control in (B). One point represents one independent experiments and data is shown with mean (N=3). Ordinary one-way ANOVA; Dunnett's multiple comparisons test, with a single pooled variance was performed (*P ≤ 0.05; ** P≤0.01; *** P≤0.001; **** P≤0.0001). Oligomycin: CD154 0.01µM p=0.023, 0.1µM p=0.022, 1µM p=0.0032; Rotenone: CD154 1µM p=0.015, 2.5µM p=0.029; Resveratrol: CD69 6.25µM p=0.0081, 12.5µM p= 0.0004, 25µM p=0.0003, 50µM p=0.0002; CD25 25µM p=0.0024; 50µM p=0.0001)

3.9 T cell effector function is highly robust towards mitochondrial dysfunction

The effect of mitochondrial dysfunction on T cell immune response was further assessed by intracellular cytokine staining. $CD4^+$ T cells were stimulated in total for 6h and the transport inhibitor BFA was added for the remaining 4h of the cultivation time. This time point was chosen in order to achieve the highest diversity in cytokine secretion (Kaveh et al., 2012; Nomura et al., 2000). The expression of the signature cytokines for the main CD4 effector subsets IFNγ, IL-21, IL-4, IL-17A and IL-22 was analyzed via flow cytometry (Figure 24) in the presence of the metabolic inhibitors (Figure 24).

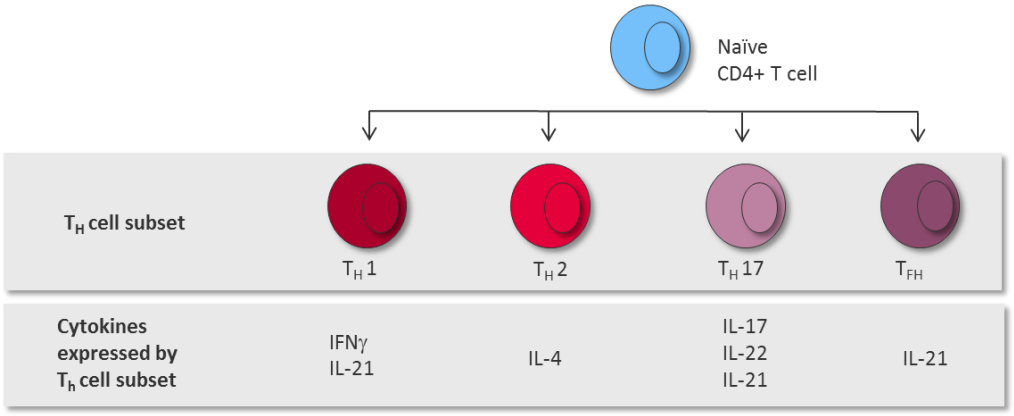

Figure 23: Representation of $CD4^+$ T cell subsets and their designated cytokines. Naive T cells differentiate into various T_H cell subsets. T_H1, T_H2, T_H17 and T_{FH} cells. Each subset can be distinguished by a specific set of signature cytokine expression, depicted in the lower row.

The mitochondrial inhibitors oligomycin and rotenone had only minor and inconsistent effects on T cell cytokine production. Rotenone slightly decreased cytokine production at concentration of 0.1µM rotenone but a general decrease upon mitochondrial inhibition was not evident (0.1µM Rotenone: IL-4 p=0.0074; IFNγ p=0.0007). In contrast, resveratrol significantly and consistently decreased production of IFNγ, IL-21, IL-4, and IL-17 in a dose-dependent manner starting at a concentration of 25µM of resveratrol (resveratrol: IL-22 25µM p=0.0025,; IL-4 25µM p=0.0223, 100µM p=0.0007; IL-21 25µM p=0.0005,; IFNγ 25µM p=0.0009).

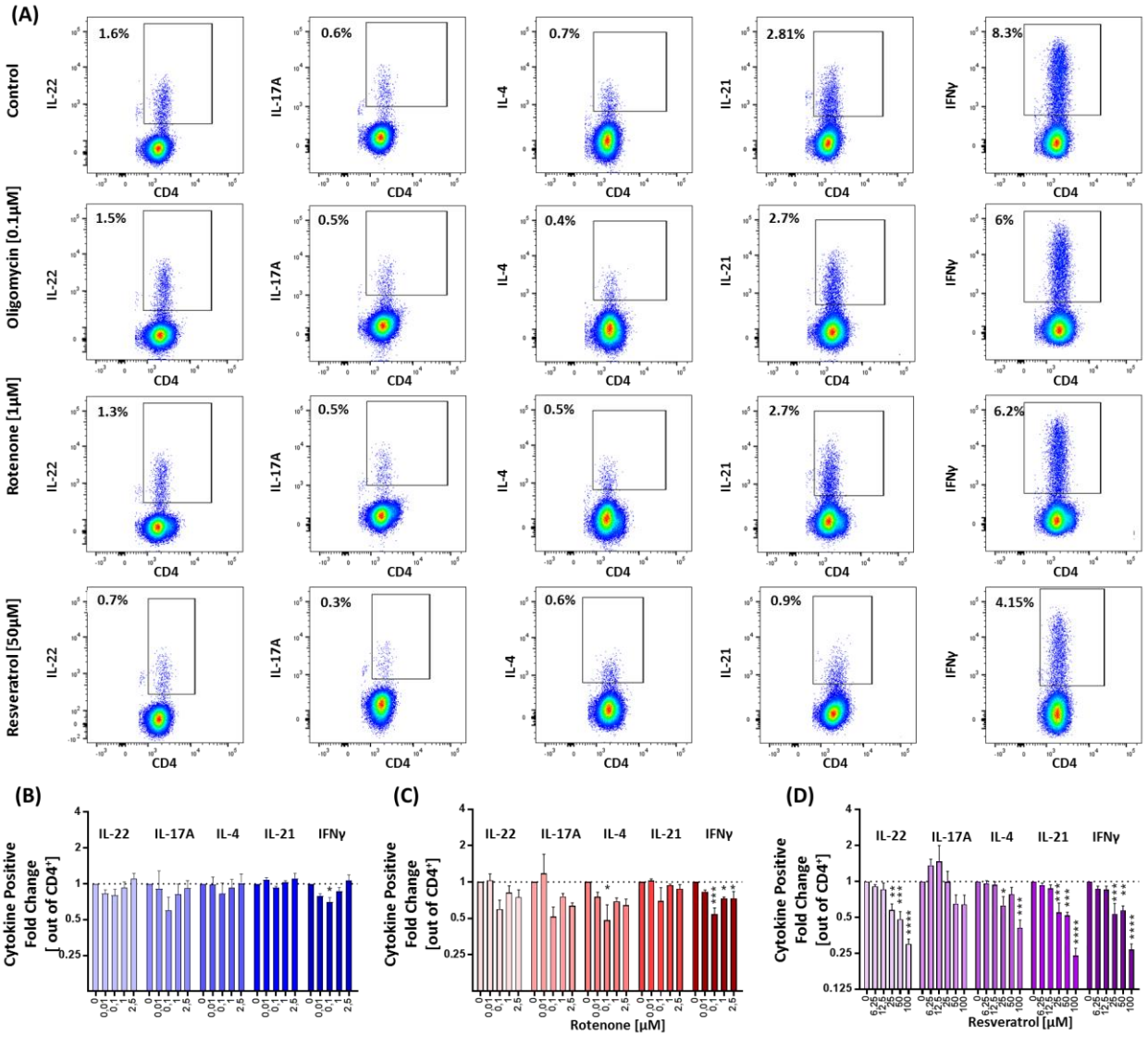

Figure 24: The effect of mitochondrial dysfunction on human CD4⁺ T cell cytokine production. T cells were stimulated with anti-CD3/CD28 Dynabeads for 6h and treated with oligomycin, rotenone and resveratrol. Secretion inhibitor Brefeldin A was added for the remaining 4h of the total stimulation time of 6h. Cytokine production of CD4⁺ T cells was investigated using flow cytometry. (A) Representative FACS plots of all measured cytokines are shown under control condition and in the presence of oligomycin [0.1µM], rotenone [1µM] and Resveratrol [50µM]. The frequency of cytokine positive cells was measured for each cytokine. The graphs in B, C, and D show the effect of oligomycin, rotenone, and resveratrol, respectively on cytokine positive cells (N=3). The data is shown as fold change to 0µM concentration of inhibitor. (*P≤0.05; ** P≤0.01; *** P≤0.001; **** P≤0.0001). Ordinary one-way ANOVA; Dunnett's multiple comparisons test with a single pooled variance was applied. Oligomycin: IFNγ 0.1µM p=0.039; Rotenone: IL-4 0.1µM p=0.0074, IFNγ 0.1µM p=0.0007, 1µM p=0.024, 2.5µM p=0.024; Resveratrol: IL-22 25µM p=0.0025, 50µM p=0.0005, 100µM p=0.0001; IL-4 25µM p=0.022, 100µM p=0.0007; IL-21 25µM p=0.0005, 50µM p=0.0003, 100µM p=0.0001; IFNγ 25µM p=0.0009, 50µM p=0.0018, 100µM p=0.0001).

3.10 Glucose availability affects T cell metabolism and T cell proliferation

3.10.1 T cell respiration decreases in low glucose conditions

OXPHOS was shown to be important for T cell activation and proliferation processes and less crucial for cytokine secretion (Figure 20; Figure 21; Figure 24). The following experiments aim to analyze the necessity for glycolysis for the various aspects of T cell functions. Glucose demand was shown to be increased upon activation and especially crucial during T cell proliferation (Figure 12). The experiments performed in this section investigate the effect of different glucose concentrations, ranging from hypo- to hyperglycemia, (0mM to 25mM) on T cell metabolism and function.

$CD4^+$ T cells were cultured for 48h and stimulated using anti-CD3/CD28 Dynabeads in the presence of varying glucose concentration and T cell respiration was examined (Figure 25)**.** Hypoglycemia (0 to 2mM glucose) decreased basal respiration (0mM p=0.0001; 1mM p=0.0032), mitochondrial ATP-linked respiration (1mM p=0.0001 2mM p=0.0063) and maximal respiration (0mM p=0.0006). Strikingly, 0mM glucose did not completely inhibit ATP production (p=0.0001) and hyperglycemia (15 to 25mM) did not further increase respiration rates (Figure 25A, B, C). Spare respiratory capacity increases in hypo and hyperglycemic conditions (1mM Glucose p= p=0.0010; 25mM glucose p=0.0042). Glycolytic rates were severely decreased in the presence of low glucose levels and entirely blocked by 0mM glucose (0mM p=0.0001; 1mM p=0.0001 2mM p=0.0005).

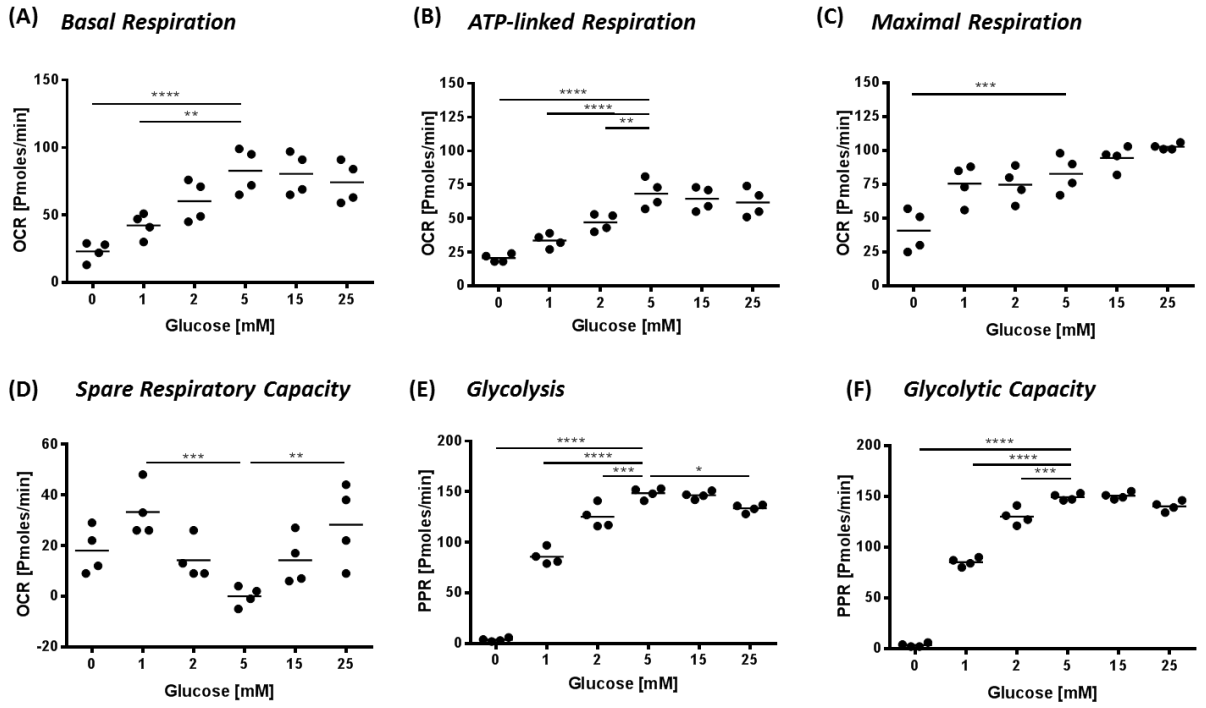

Figure 25: The effect of glucose availability on CD4⁺ T cell metabolism. Human CD4⁺ T cells were cultured for 48h in varying glucose concentration. Anti-CD3/CD28 Dynabeads were used for stimulation. T cell respiration signature and T cell glycolytic rates were monitored using *xf* extracellular flux analyzer. Hypoglycemia (<5mM glucose) decreased ATP linked respiration as well as glycolytic flux (*P ≤ 0.05; ** P≤0.01; *** P≤0.001; **** P≤0.0001) Ordinary one-way ANOVA; Dunnett's multiple comparisons test with a single pooled variance. Basal respiration: 0mM p<0.0001; 1mM p=0.0032; ATP-linked Respiration: 0mM p=0.0001; 1mM p=0.0001; 2mM p=0.0063; Maximal Respiration: 0mM p=0.0006; Spare Respiratory Capacity: 1mM p=0.0010; 25mM p=0.0042; Glycolysis: 0mM p=0.0001; 1mM p=0.0001; 2mM p=0.0005; 25mM p=0.02; Glycolytic Capacity: 0mM p=0.0001; 1mM p=0.0001; 2mM p=0.0001.

3.10.2 The production of reactive oxygen species is maintained upon different glucose concentrations

ROS production by human CD4⁺ T cells was tested in the presence of different glucose concentrations. T cells were cultured for 16h in 1, 5 and 25mM glucose with and without anti-CD3/CD28 Dynabeads stimulation (Figure 26). The representative FACS plots indicates that TCR stimulation increased ROS production independent of the local glucose availability (Figure 26A). Figure 26B shows the increased ROS production upon activation and the glucose independent ROS production for 1mM glucose (unstimulated vs stimulated p=0.0182), 5mM glucose (unstimulated vs stimulated p=0.0054) and 25mM glucose (unstimulated vs stimulated p=0.0028). These results are in line with the observation, that increasing glucose concentrations do not further increase T cell respiration

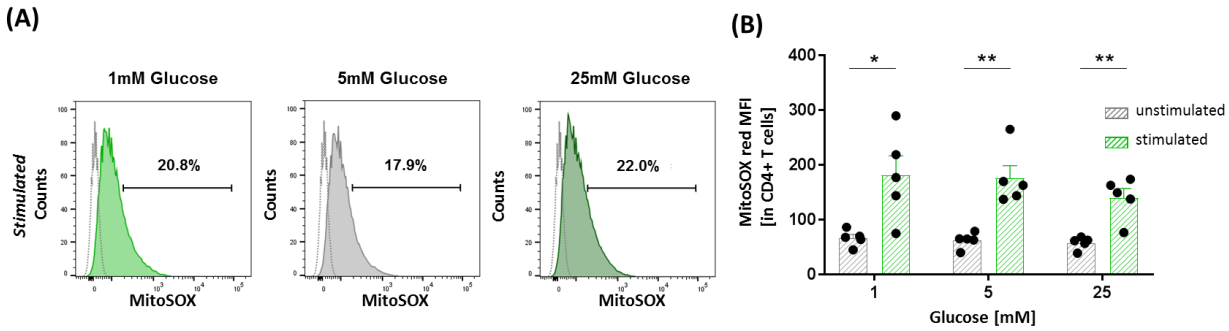

Figure 26: CD4⁺ ROS production in unstimulated and stimulated condition in the presence of different glucose concentrations. Human CD4⁺ T cells were cultured in 1mM, 5mM and 25mM glucose for 16h with and without anti-CD3/CD28 Dynabeads stimulation. Reactive oxygen species (ROS) production was measured by flow cytometry using MitoSOX red. (A) Representative FACS plots of stimulated T cells in different glucose concentrations. (B) MFI of MitoSOX red of unstimulated and stimulated T cells after exposure to various glucose levels. Each dot represents one donor (N=5). Each condition was performed in technical duplicates. Paired t-test of stimulated vs unstimulated T cells was performed for each glucose concentration (unstimulated vs stimulated) individually. 1mM glucose p=0.018; 5mM glucose p=0.0054; 25mM glucose p=0.0028.

3.10.3 T cell function in the presence of different glucose concentrations

The previous experiments indicate that low glucose concentrations affected T cell metabolism. The following experiments aimed to reveal if the detected metabolic alterations were also reflected on T cell functionality. The effect of different glucose concentration was tested on short- and long-term activation status, proliferation capacity and effectors function represented by cytokine secretion.

Short term T cell activation markers were unaffected by glucose concentrations. Only a slight decrease in CD4⁺ T cell positive for CD25 in hyperglycemic conditions was detected (25mM glucose p=0.021). The number of CD154 positive cells slightly decreased with 0mM of glucose (p=0.2521) and increased in hyperglycemic condition (25mM glucose p=0.3805). CD69⁺ positive T cells were maintained (Figure 27A).

Cytokine production was unaffected by glucose concentrations (Figure 27B). In contrast, proliferation was highly glucose-dependent (Figure 27C). Hypoglycemia inhibited T cell proliferation (0mM glucose p=0.000.; 1mM glucose p=0.0001 and 2mM p=0.0001). Activation marker expression after 72h of stimulation revealed a decrease in CD154⁺ T cells in the presence of 0mM glucose (p=0.0001; Figure 27D).

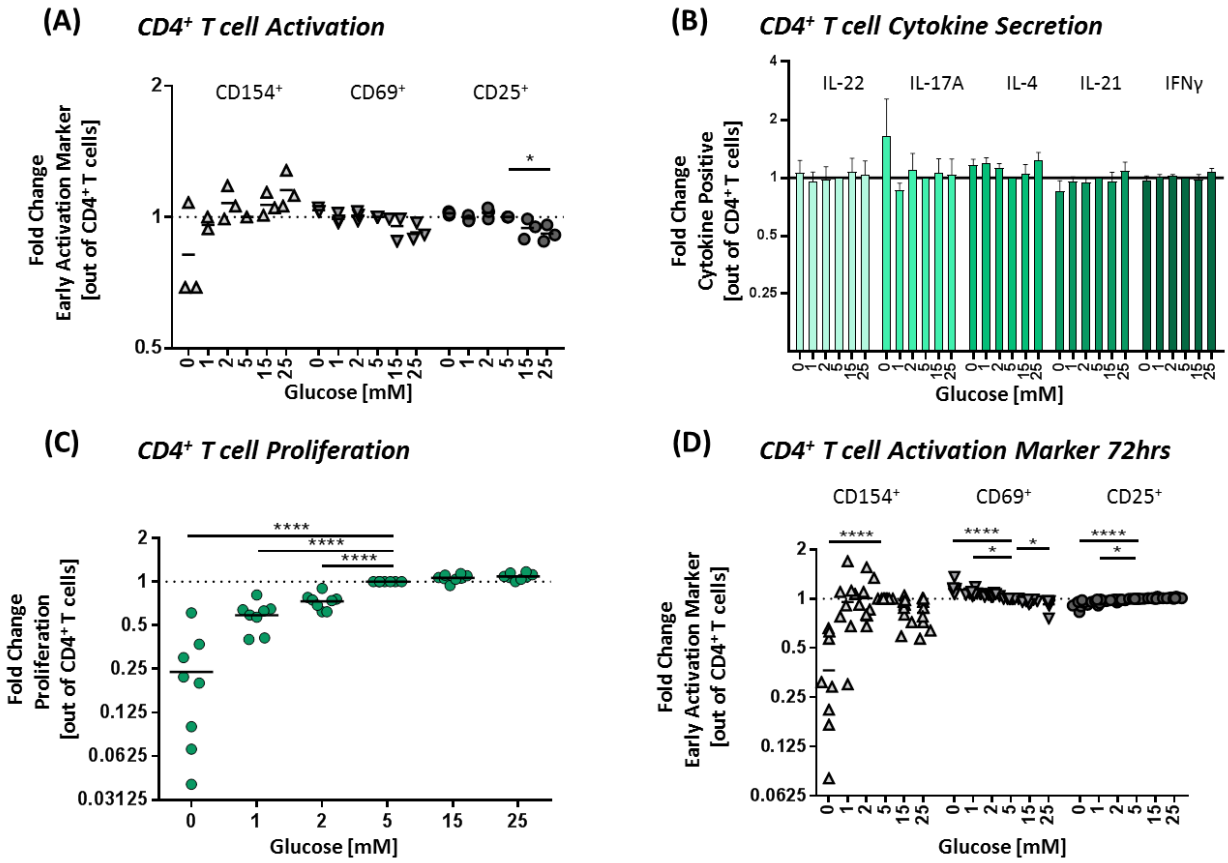

Figure 27: The effect of glucose availability on various T cell function. Human CD4+ T cells were cultured in varying glucose concentration and stimulated with anti-CD3/CD28 Dynabeads. (A) Glucose availability was tested on T cell activation after 16h of stimulation. Expression of CD69, CD25 and CD154 was investigated. (B) Cytokine secretion was analyzed by intracellular staining and flow cytometric measurements. T cells were stimulated for 6h, the last 4h in the presence of Brefeldin A. (C) For T cell proliferation analysis, the cells were cultured for 72h and proliferation cycles were followed by labelling cells with the proliferation marker eFluor450. (D) Activation marker expression was investigated after 72h. Ordinary one-way ANOVA and Dunnett's multiple comparisons test with a single pooled variance was performed (*P ≤0.05; ** P≤0.01; *** P≤0.001; **** P≤0.0001). T cell activation: CD25 25mM p=0.021; T cell proliferation: 0mM p=0.0001; 1mM p=0.0001; 2mM p=0.0001; T cell activation 72h: CD154 0mM p=0.0001, CD69 0mM p=0.0001, 1mM p=0.010, 25mM p=0.025.

3.11 Low glucose levels exacerbate the effect of mitochondrial dysfunction

Mitochondrial stress impaired considerable aspects of T cell function as evident from the Figure 20, Figure 21 and Figure 22. Varying glucose concentrations instead were mostly compensated to maintain T cell function (displayed in Figure 27). In the following experiments, the combined effects of mitochondrial dysfunction and glucose availability was tested to further understand the importance of stable glucose levels for T cell functionality in changing microenvironments.

T cell function was again represented by activation, proliferation and cytokine production. Glucose concentrations from 0 – 25mM glucose were tested in combination with 0.1µM and 1µM of oligomycin and rotenone. Surprisingly low glucose concentration (0-2mM) exacerbates the effect of mitochondrial dysfunction and hyperglycemia (15-25mM) improved the effect of mitochondrial stress as reported in Figure 28. (CD69: oligomycin and 1mM glucose p=0.018; rotenone and 0mM p=0.0032; CD25:

oligoymcin at 0mM glucose p=0.029; rotenone at 0mM glucose p=0.0001; CD154: Oligomycin at 0mM p=0.0036; Rotenone at 0mM p=0.0011).

As shown in the previous section, proliferation capacity is decreased in hypoglycemic conditions. Oligomycin alone decreased T cell proliferation at concentration of 0.1µM of oligomycin (Figure 21B). In combination with different glucose concentrations, oligomycin inhibits proliferation independently of glucose availability (Figure 28D). Rotenone treatment instead depicted an impairment of proliferation especially in low glucose levels (0 – 2mM) (Rotenone at 2mM, p=0.041). Physiological glucose concentration substantially ameliorates the effect of mitochondrial stress (Figure 28D). This data highlights the remarkable need for stable glucose levels for maintained T cell function in hostile microenvironments.

In order to test if the divergent results of rotenone and oligomycin originate from efficiency or specificity, the same experiments were performed with higher concentrations of inhibitors [1µM] (Figure 29). Strikingly, rotenone approximated the activation marker expression pattern to the expression pattern caused by oligomycin. Proliferation in the presence of 1µM of oligomycin and rotenone equally inhibited T cell proliferation independently of the glucose concentration. These results suggest a more general acclimatization mechanism of increasing glucose concentration and mitochondrial dysfunction. The presented data further highlights the importance of revealing specific adaptation mechanism present by increasing glucose concentration in order to understand T cells capability of maintained function in changing environmental conditions.

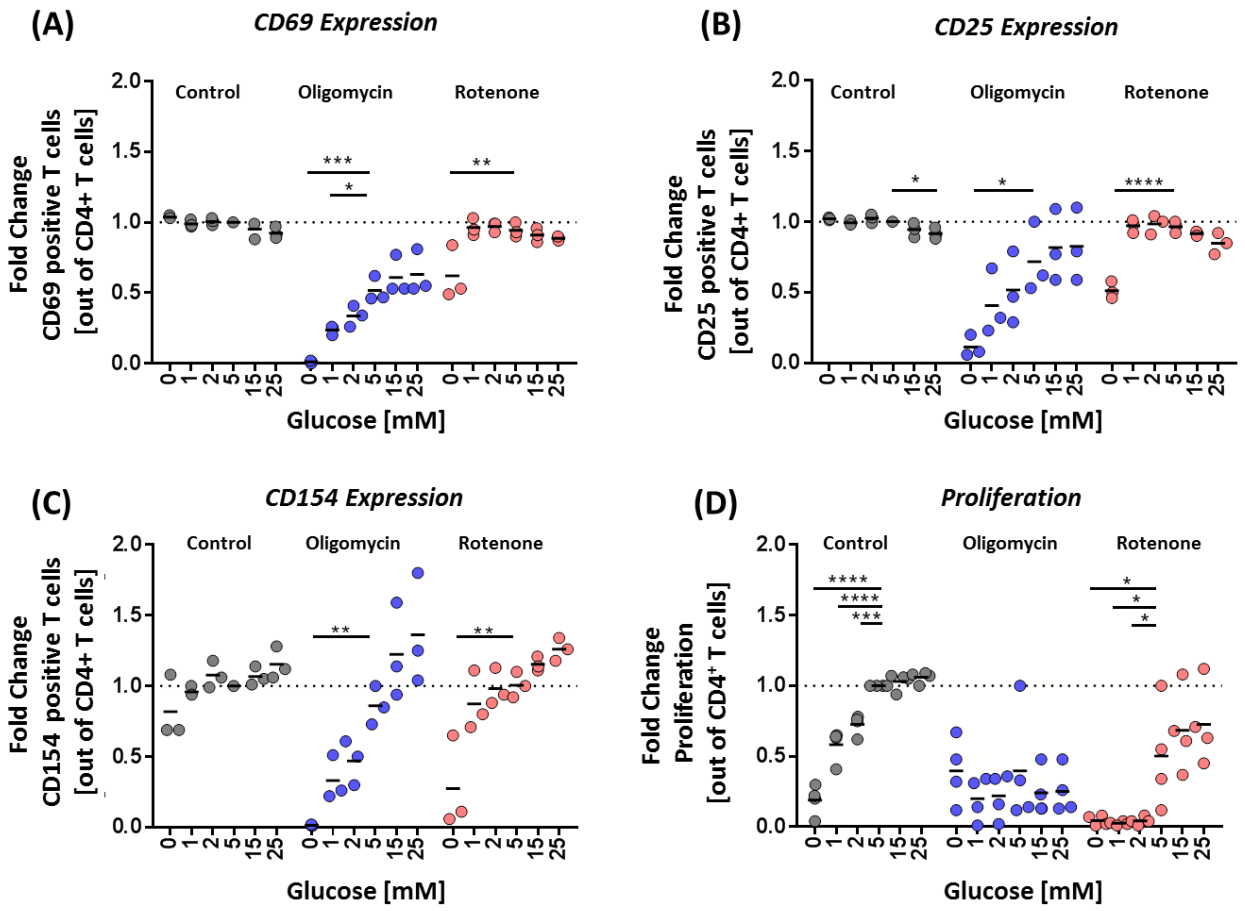

Figure 28: Early Activation of T cells under mitochondrial stress and various glucose concentrations. T cells were cultured and stimulated for 16h for T cell activation assay and 72h for T cell proliferation assay with different glucose concentration and treated with low concentration of mitochondrial inhibitors [0.1µM] oligomycin and rotenone. One point represents one donor (N=3). Data is represented as fold change to 5mM glucose out of $CD4^+$ T cells in the absence of mitochondrial inhibitor (*P ≤ 0.05; ** P≤0.01; *** P≤0.001; **** P≤0.0001). Ordinary one-way ANOVA; Dunnett's multiple comparisons test, with a single pooled variance was performed. CD69 expression: Oligomycin, 0mM p=0.0002, 1mM p=0.018; Rotenone 0mM p=0.0032; CD25 expression: Control, 25mM p=0.021; Oligomycin, 0mM p=0.029; Rotenone, 0mM p=0.0001; CD154 expression: Oligomycin, 0mM p=0.0036; Rotenone, 0mM p=0.0011; Proliferation: Control, 0mM p=0.0001, 1mM p=0.0001, 2mM p=0.0004, Rotenone: 0mM p=0.042, 1mM p=0.033, 2mM p=0.041.

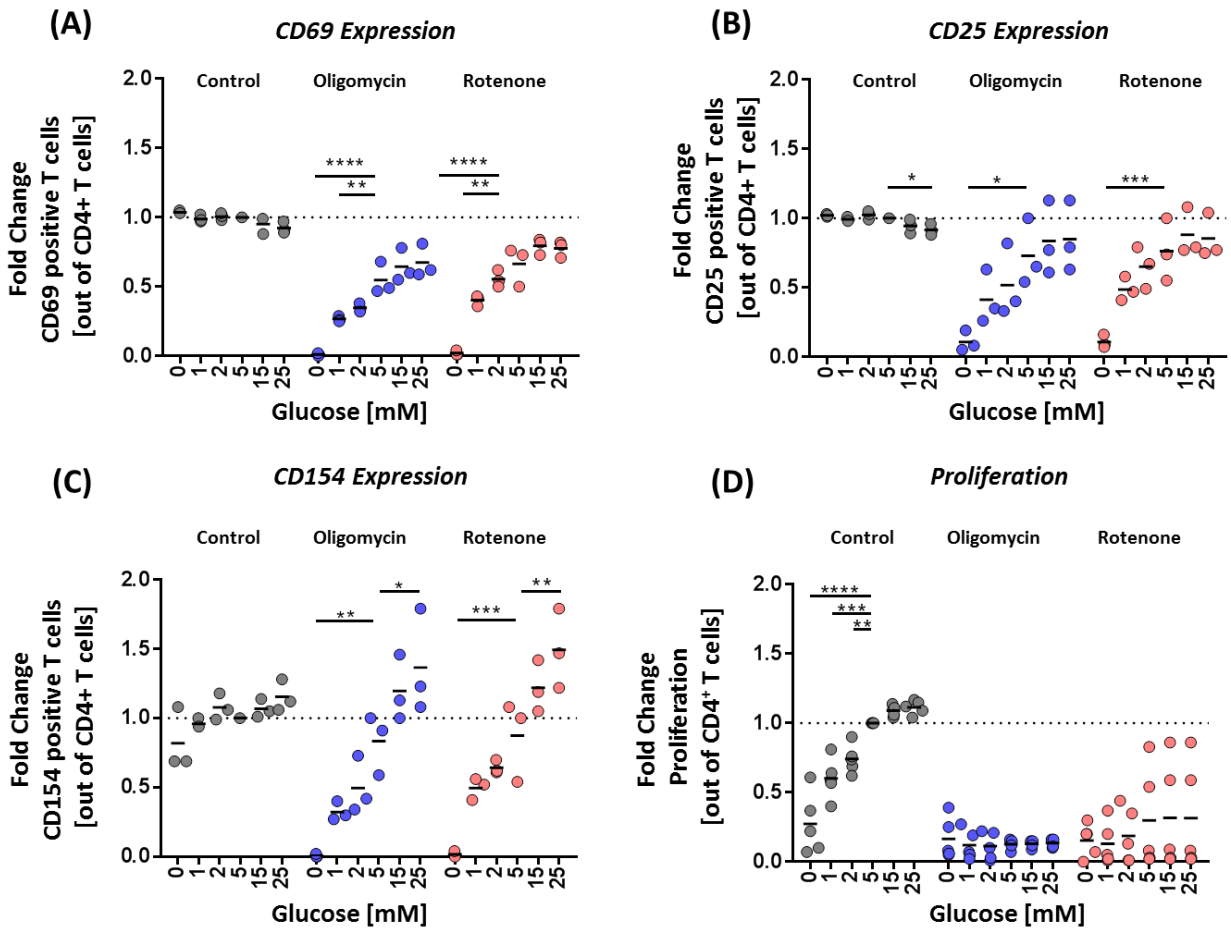

Figure 29: : Early Activation of T cells under mitochondrial stress and various glucose concentrations. T cells were cultured and stimulated for 16h for T cell activation assay and 72h for T cell proliferation assay with different glucose concentration and treated with low concentration of mitochondrial inhibitors [1µM] oligomycin and rotenone. One point represents one donor (N=3). Data is represented as fold change to 5mM glucose out of $CD4^+$ T cells in the absence of mitochondrial inhibitor (*P ≤ 0.05; ** P≤0.01; *** P≤0.001; **** P≤0.0001). Ordinary one-way ANOVA; Dunnett's multiple comparisons test, with a single pooled variance was performed. CD69 expression: Oligomycin, 0mM p=0.0001, 1mM p=0.0070; Rotenone 0mM p=0.0001; 1mM p=0.0041; CD25 expression: Control, 25mM p=0.021; Oligomycin, 0mM p=0.022; Rotenone, 0mM p=0.0009; CD154 expression: Oligomycin, 0mM p=0.0025, 25mM p= 0.044; Rotenone, 0mM p=0.0005; 25mM p=0.0065; Proliferation: Control, 0mM p=0.0001, 1mM p=0.0001, 2mM p=0.0098.

3.11.1 Mitochondrial dysfunction in combination with glucose starvation interferes with cytokine secretion

Cytokine secretion of $CD4^+$ T cells was shown to be more robust towards mitochondrial alterations and glucose scarcity (Figure 24B, C; Figure 27B). The combined effect of varying glucose levels and mitochondrial inhibitors illustrated in Figure 30 depict a decrease of cytokine positive cells upon low glucose levels and mitochondrial stress on the assessed cytokines, except for IL-17A. IL-22 was only marginally affected (IL-22: Oligomycin 0mM p=0.014). T cells positive for IL-4, IL-21 and IFNγ dramatically decreased in the presence of low glucose and mitochondrial stress conditioned by oligomycin and rotenone (IL-4: Oligomycin 1mM p=0.0043, Rotenone 0mM p=0.0025; IL-21:

Oligomycin 0mM p=0.0001, Rotenone 0mM p=0.038; IFNγ: Oligomycin 1mM p=0.0056; Rotenone 0mM p=0.0001).

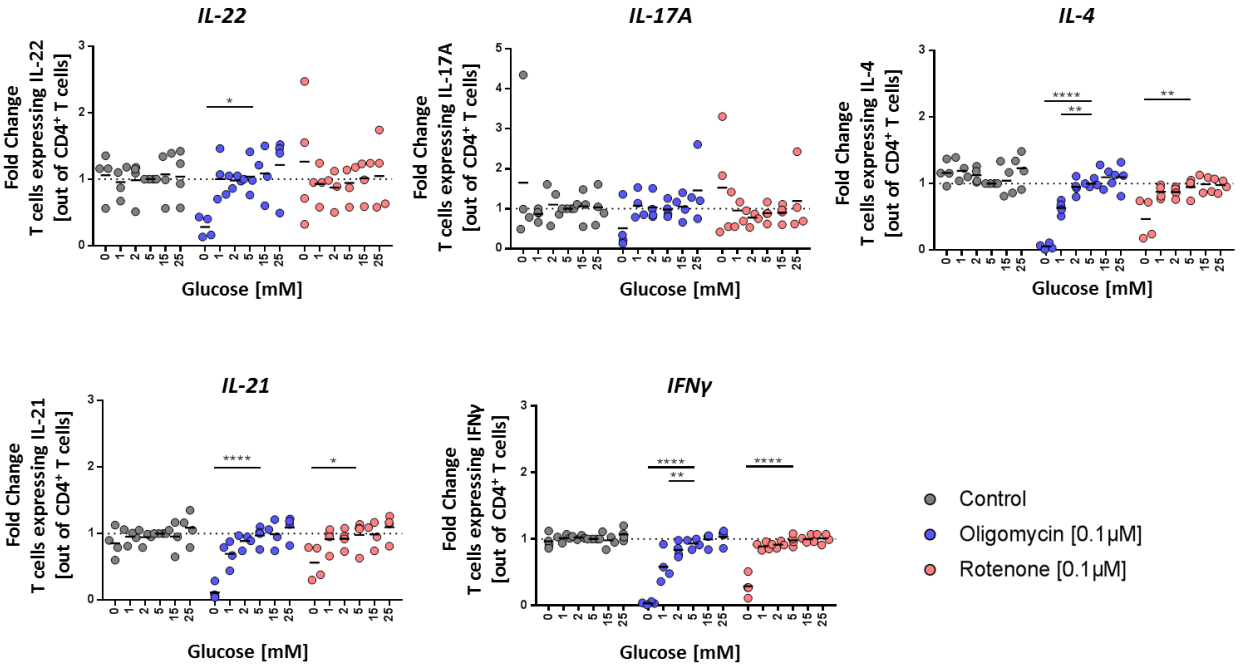

Figure 30: CD4⁺ T cell cytokine secretion in the presence of varying glucose concentration and mitochondrial dysfunction. CD4⁺ T cells were stimulated with anti-CD3/CD28 Dynabeads for 6h. The last 4h in the presence of the transport inhibitor Brefeldin A. Intracellular cytokine staining was performed of the following signature cytokines: IL-22; IL-17A; IL-4; IL-21 and IFNγ. Data is presented as fold change to 5mM glucose and out of CD4⁺ T cells (* P ≤ 0.05; ** P≤0.01; *** P≤0.001; **** P≤0.0001). Ordinary one-way ANOVA and Dunnett's multiple comparisons test with a single pooled variance was performed. One point represents one donor (N=4). IL-22: Oligomycin 0mM p=0.014; IL-4: Oligomycin 0mM p=0.0001, 1mM p=0.0043; Rotenone 0mM p=0.0025; IL-21: Oligomycin 0mM p=0.0001, Rotenone 0mM p=0.038; IFNγ: Oligomycin 0mM p=0.0001, 1mM p=0.0056; Rotenone 0mM p=0.0001.

3.12 Increased insulin levels increase glycolytic rates but maintain T cell function

In the next section I wanted to investigate the effect of T cell sensitivity in the presence of increasing insulin concentrations. Low glucose levels mainly affected T cell proliferation. Insulin is needed for an adequate glucose uptake into the cell. The following experiments aim to test, if increasing insulin levels alter T cell metabolism and function. Up to date, insulin sensitivity in T cells was not shown and its effect on their function remains widely unexplored. The effect of different insulin concentrations was tested on T cell metabolism, activation, and proliferation and effectors functions. The insulin concentration ranged up to 300µg/mL. Along with these experiments I further tested the solvent of insulin, DMSO. High concentrations of insulin were added to the cell culture, subsequently the highest DMSO concentration constituted 1%. Also lower concentration of DMSO on T cell functional and metabolic assays were tested upon polyclonal stimulation. Due to the unexpected strong effects of DMSO at concentration ranges which were reported to be nonhazardous to T cell function, the results

are presented here. For a more detailed analysis of this study I refer to my published paper (Holthaus et al., 2018).

3.12.1 Low concentration of DMSO inhibits T cell function

The activation markers CD69, CD25 and CD154 were upregulated within 16 h post-stimulation with plate-bound anti-CD3. The frequency of cells that expressed CD69 was decreased in the presence of 1% of DMSO (86.1 ± 7.7% of value without DMSO; p=0.0013). $CD25^+$ T cells were attenuated in the presence of 0.5% DMSO (81.7 ± 6.1 %; p=0.0002) and $CD154^+$ T cells were already reduced in the presence of 0.1% DMSO (83.4 ± 9.7%; p=0.0125) and almost completely abolished in the presence of 1% DMSO (9.7 ± 4.7%; p=0.0001). The effect of DMSO on human $CD4^+$ T cell cytokine production was determined after stimulation of T cells with anti-CD3/CD28 Dynabeads for 6 h with the addition of a transport inhibitor for the last 4 h before intracellular cytokine staining. The presence of DMSO resulted in a decrease in $CD4^+$ T cells positive for IL-4 and IL-21, but no effect was observed on IFNγ positive $CD4^+$ T cells (Figure 31).

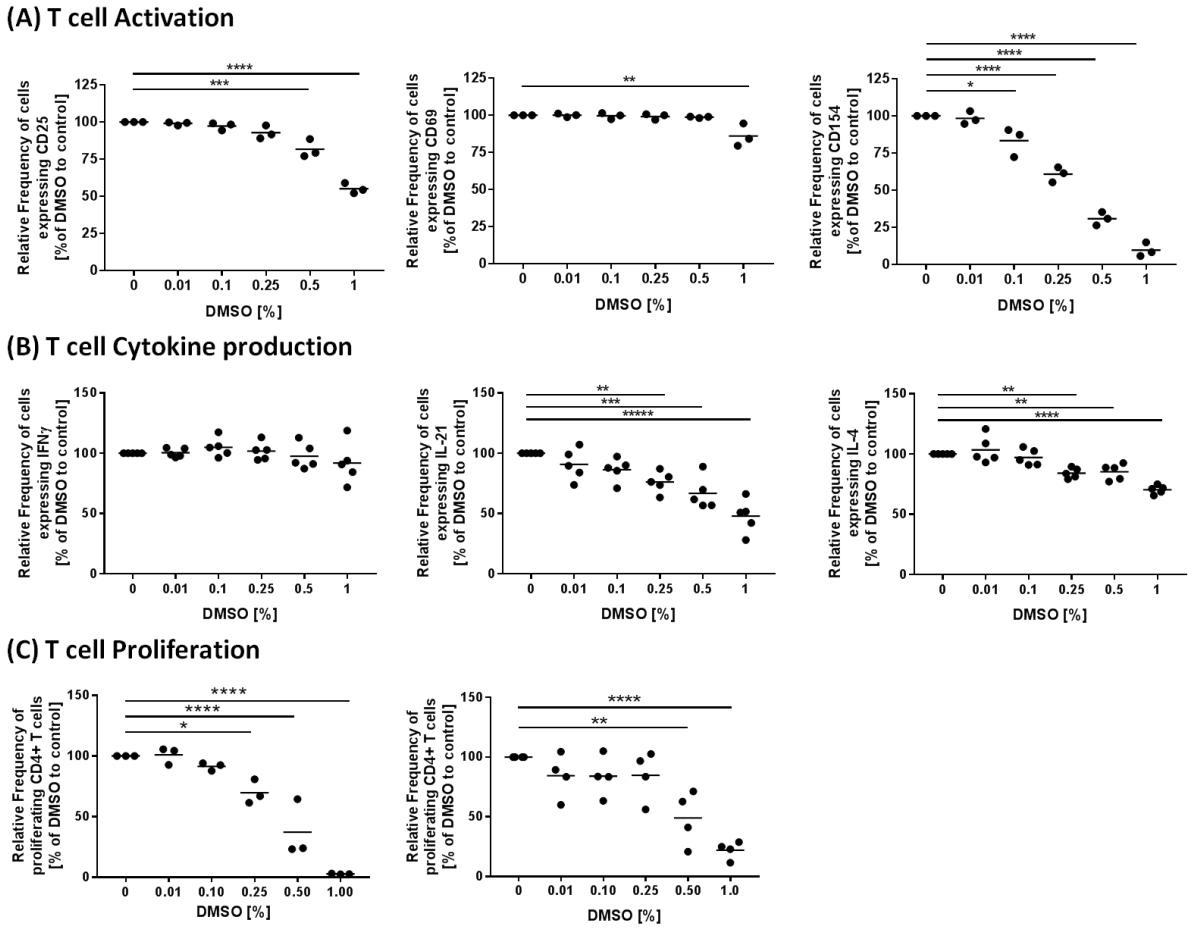

Figure 31: CD4⁺ T cell function is inhibited by low concentration of DMSO. CD4⁺ T cells were stimulated by plate-bound anti-CD3 antibody in the presence of increasing DMSO concentrations and surface expression of the activation markers CD69, CD25, and CD154 measured by flow cytometry after 16 h is shown. the quantitative data from three independent experiments using different donors expressed as the frequency of activation marker positive cells relative to the value at 0% DMSO is shown. (B) CD4⁺ T cells positive for cytokine expression of IL-21, IL-4 and IFNγ is shown. Cells were stimulated with anti-CD3/CD28 Dynabeads for 6 h in the presence of increasing DMSO concentrations. Brefeldin A was added for the last 4 h of culture before intracellular cytokine staining of cells and analysis by flow cytometry. Quantitative data from five independent experiments using different donors each performed with technical duplicates are shown. The data is expressed as the relative frequency of cytokine positive cells as compared to the value at 0% DMSO. (C) Proliferation was measured using eFluor450 labelled CD4⁺ T cells upon stimulation with plate-bound anti-CD3 for three days or eFluor450-labeled peripheral blood mononuclear cells stimulated with Tetanus toxoid for five days. Both experiments were performed in the presence of increasing DMSO concentrations. The quantitative data from 3 (anti-CD3 stimulation) and 4 (tetanus toxoid stimulation) independent experiments using different donors, each with technical duplicates are shown. The data is expressed as the relative frequency of dye-diluted cells as compared to the value at 0% DMSO. * P ≤ 0.05; ** P ≤ 0.01; **** P ≤0.0001; two-tailed one-way ANOVA.

3.12.2 DMSO affects cellular glucose uptake and increases glycolytic rates

In line with the inhibition of activation, the presence of 1% DMSO during plate-bound anti-CD3 stimulation reduced glucose uptake by CD4⁺ T cells during 16 hours of incubation (Figure 30A). Mitochondrial respiration and glycolysis were investigated by extracellular flux analysis 48 hours after polyclonal stimulation of CD4⁺ T cells with anti-CD3/CD28 Dynabeads. Mitochondrial oxidative phosphorylation, represented by ATP-linked respiration and maximal substrate oxidation, represented

by maximal respiration, were unaffected by DMSO concentrations up to 1% (Figure 32B). Basal and oligomycin-induced glycolytic rates, represented by extracellular acidification rates, were also not significantly affected by DMSO.

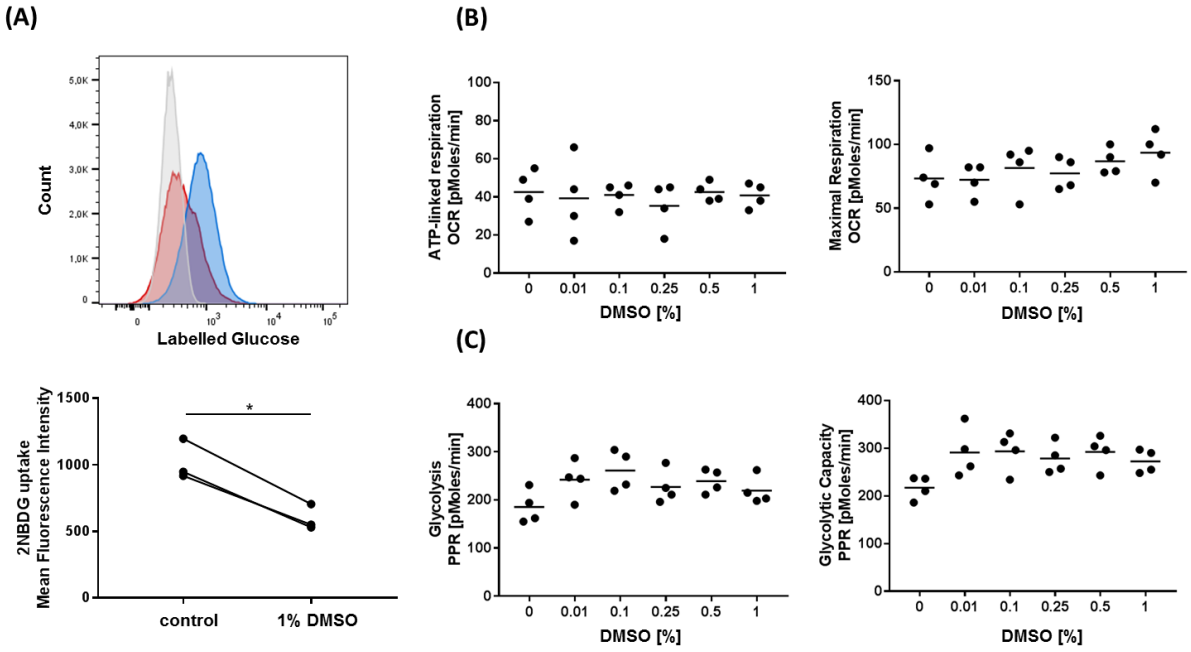

Figure 32: Glucose uptake in CD4⁺ T cells in the presence of DMSO. CD4⁺ T cells were stimulated with anti CD3/CD28 beads in the presence of increasing DMSO concentration up to 1%. (A) Glucose uptake was measured using labeled glucose (2NBDG) after stimulation of CD4⁺ T cells or 16 hours without and in the presence of 1% of DMSO (N=3). Representative FACS data is shown (gray curve represents the unstimulated control, blue curve cells without DMSO and the red curve the cell subsets measured in the presence of 1% of DMSO). The Mean Fluorescence Intensity of 2NBDG with and without DMSO is shown in the lower panel. (B) T cell OXPHOS rates (OCR) of ATP-linked respiration and maximal respiration, and (C) Glycolysis and glycolytic capacity of the CD4⁺ T cells after 48 hours stimulation with anti CD3/CD28 beads in the presence of increasing DMSO concentration. Each point represents one independent experiment from different donors (N=4). * P ≤ 0.05; paired t-test.

3.12.3 DMSO affects CD4⁺ T cell activation and function pathways

RNA sequencing was performed on CD4⁺ T cells that had been activated with anti CD3/CD28 Dynabeads in the presence or absence of 1% DMSO. Differential gene expression analysis using DESEQ2 identified 309 genes that are significantly up-regulated and 468 genes that are down-regulated in cells in the presence of 1% DMSO (p-value adjusted for multiple testing < 0.05; Figure 33A). Consistent with the data of protein and functional assays, KEGG pathway analysis of the down-regulated genes identified enrichment of cytokine-cytokine receptor interaction (hsa04060), T-cell receptor signaling (hsa04660), and NFκB signaling (hsa04064) pathways. No pathway enrichment was observed for the up-regulated genes.

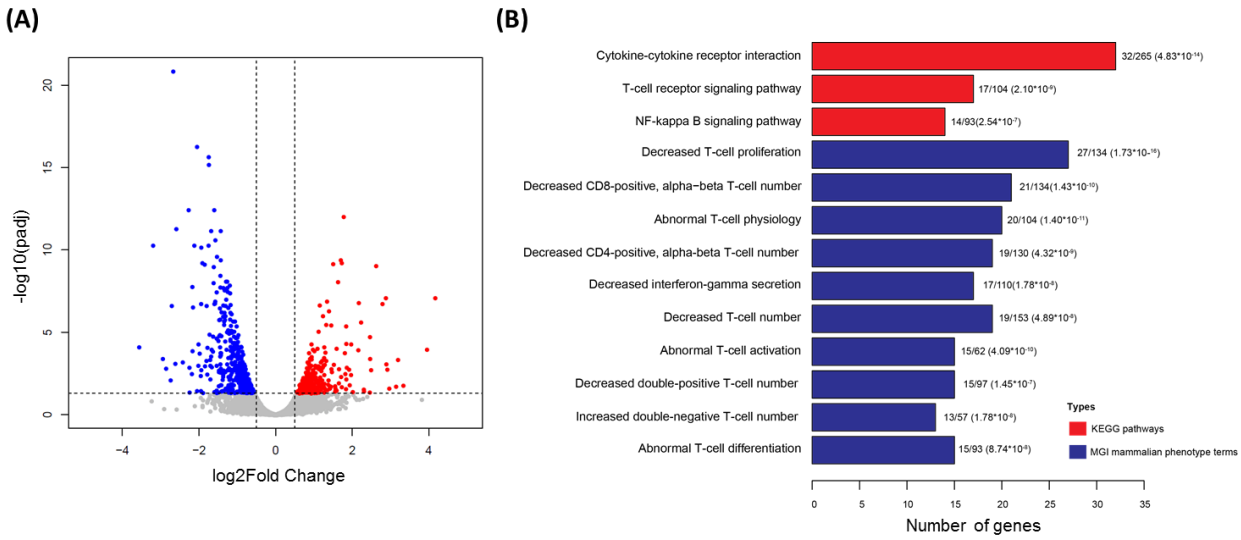

Figure 33: Volcano plot of RNAseq data and pathway analysis. Volcano plot of RNAseq data comparing CD4$^+$ T cell stimulated with plate bound anti-CD3 in the presence and absence of 1% DMSO. Blue dots represents downregulated genes, red dots are upregulated genes (P<0.05). Genes that are either not significant or show less than 1-5 fold changes are indicated in grey. The horizontal broken line represents a p value of 0.05 and the vertical broken lines represent a 1.5-fold change. (B) Results of enrichment pathway analysis; The KEGG pathway enrichment analysis identified three pathways which are downregulated by DMSO. The Mammalian phenotype terms are indicated as blue bars. The p value and the number of differently expressed genes are listed for each pathway.

3.12.4 Increasing insulin concentrations increases glycolytic rates

Considering the strong effect of the solvent DMSO, Insulin was dissolved in distilled water and stored on 20°C for eight weeks. Generally DMSO concentrations were minimized for the cell culture experiments to at least 0.25% or below. In the following the effect of different insulin concentration on T cell metabolism was tested by *xf* extracellular flux analysis after 48h of stimulation in the presence of insulin concentrations ranging from 0 – 300µg/mL. Figure 34 shows the respiration signature of the CD4$^+$ T cells. Neither ATP-linked respiration nor basal respiration was affected by insulin availability in the medium (Figure 34A and B). Glycolysis and glycolytic capacity were decreased at 0 and 300µg/mL of insulin as compared to all concentrations from 0.0003 to 30µg/mL (glycolysis: p=0.029; glycolytic reserve: p=0.022; Figure 34C, D).

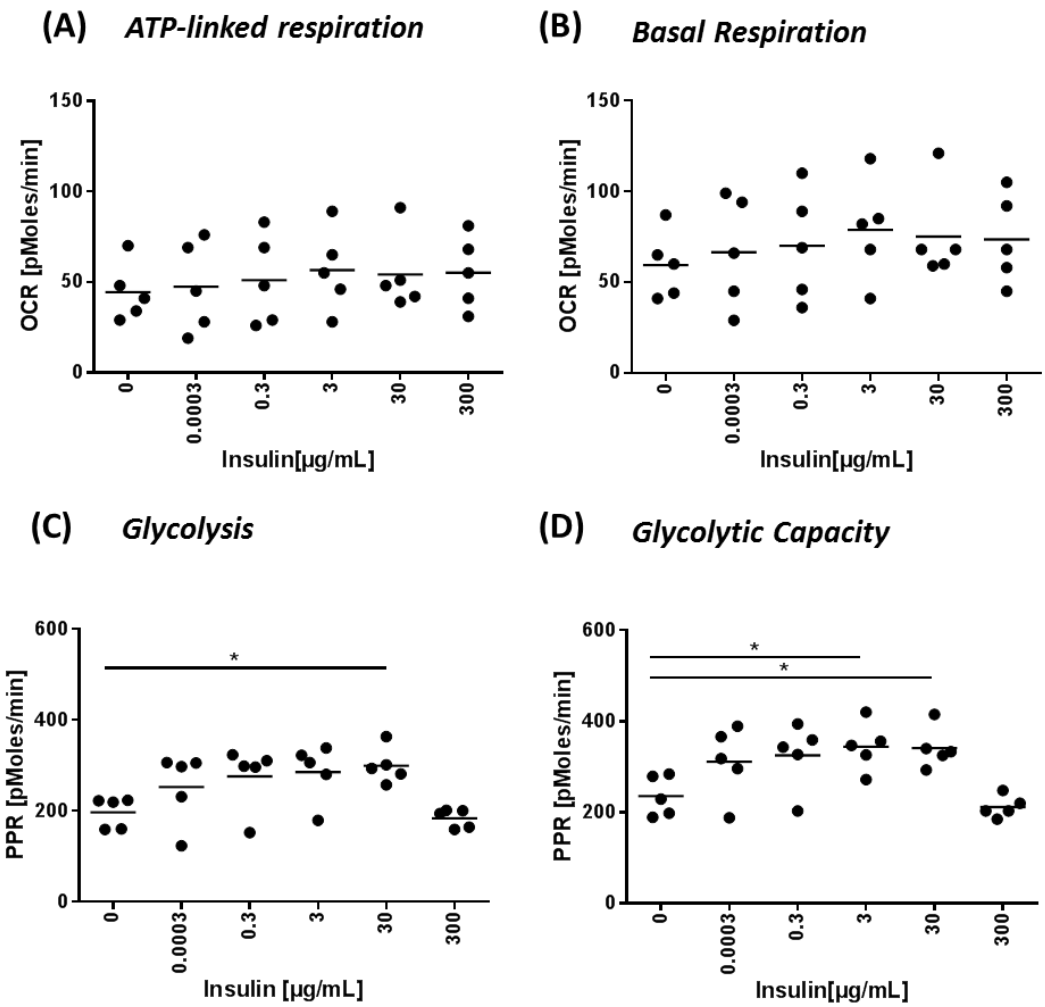

Figure 34: The effect of varying insulin levels on T cell metabolism. $CD4^+$ T cells were cultured for 48h in the presence of varying insulin concentrations. Anti-CD3/CD28 Dynabeads were used for TCR stimulation. ATP-linked and basal respiration was monitored as well as glycolysis and glycolytic flux by using xf extracellular flux analyzer. (n=5). Each point represents one independent experiment. Data is shown with mean. (*P≤0.05; ** P≤0.01; *** P≤0.001; **** P≤0.0001). Ordinary one-way ANOVA and Dunnett's multiple comparisons test with a single pooled variance was performed. Glycolysis: 30µg/mL p=0.029; Glycolytic Capacity: 3µg/mL p=0.0223, 30µg/mL p=0.027.

3.12.5 T cell function is maintained despite increased glycolysis

In order to reveal if increasing glycolytic rates were reflected by T cell function, the activation status, cytokine secretion and proliferation capacity together with long-term activation marker expression were tested (Figure 35). No effects of increasing insulin concentration on T cell activation phenotype, cytokine positive cells or proliferation were observed.

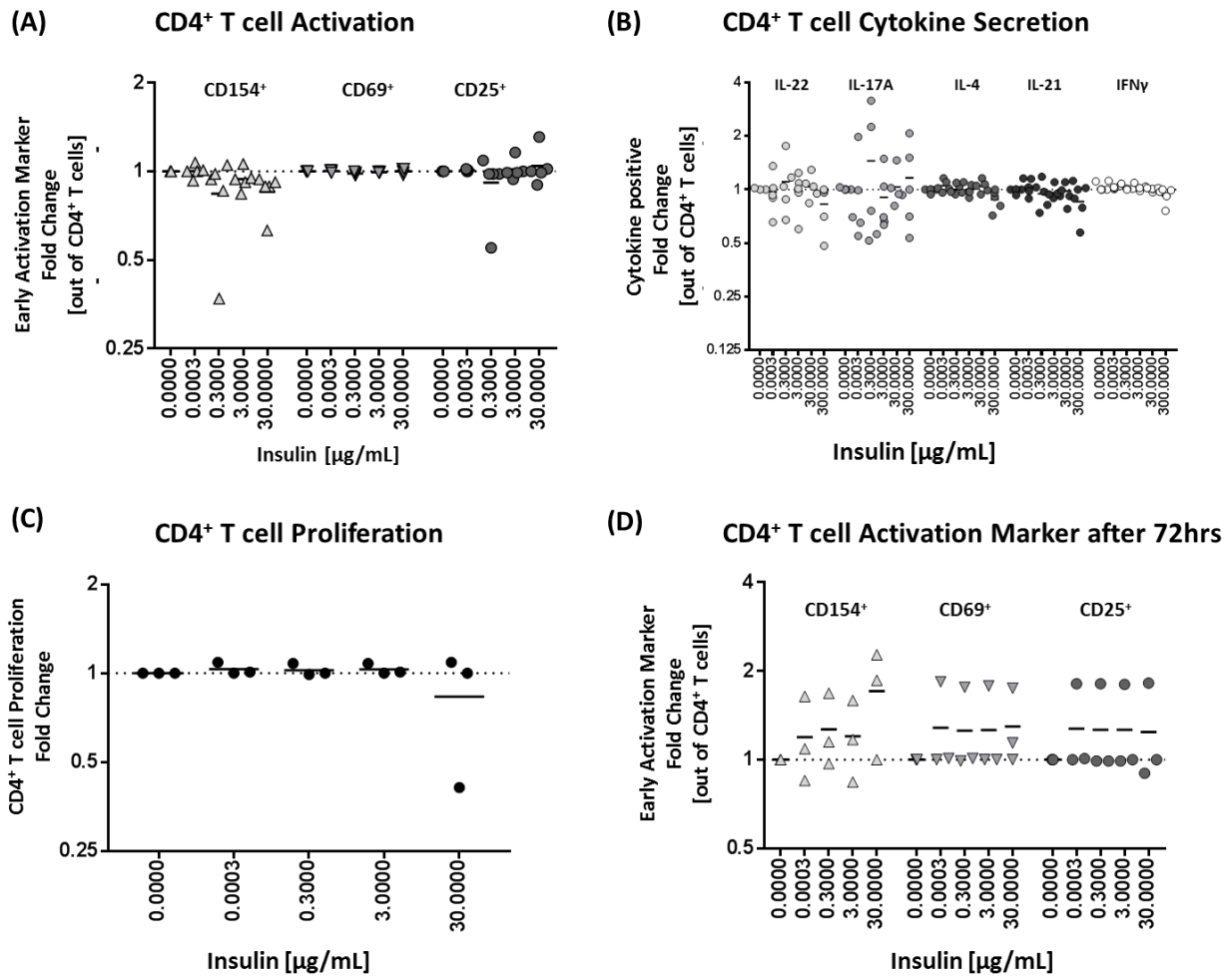

Figure 35 : Effect of varying insulin levels on T cell function. CD4+ T cells were cultured in 5mM glucose and varying insulin concentration. Anti-CD3/CD28 Dynabeads were used for TCR stimulation and analysis was performed using flow cytometry. (A) T cell activation was investigated after 16h and is represented by the surface expression of CD154, CD69 and CD25 (n=5 with mean). (B) T cell cytokine secretion was monitored after 6h of stimulation, the last 4h in the presence of Brefeldin A. Intracellular cytokine staining was performed for IL-22, IL-17A, IL-4, IL-21 and IFNγ (n=5 with mean). Proliferation was analyzed after 72h using the proliferation tracer eFluor450 (n=3 with mean). (D) Activation marker expression was again monitored during proliferation phase (after 72h) (n=3 with mean). Data is represented as fold change to the control condition. Ordinary one-way ANOVA with Dunnett's multiple comparisons test and a single pooled variance was performed.

3.12.6 The effect of varying insulin concentration and different metabolic conditions on T cell activation and proliferation

Previous data showed that insulin levels do not alter T cell function but increase glycolytic rates (Figure 34 and Figure 35). I assumed that insulin facilitates glucose uptake. In a next step I was aiming to understand if increasing insulin levels were advantageous under metabolic challenging conditions such as hypo- and hyperglycemia as well as mitochondrial dysfunction. T cell activation markers were analyzed after 16h of stimulation. Physiological glucose concentration (5mM glucose) and hyperglycemia (25mM glucose) in combination with insulin did not alter T cell activation marker expression (Figure 36A, B). Oligomycin and rotenone decreased T cell activation (Figure 20). This effect could not been recovered by increasing insulin concentrations (Figure 36).

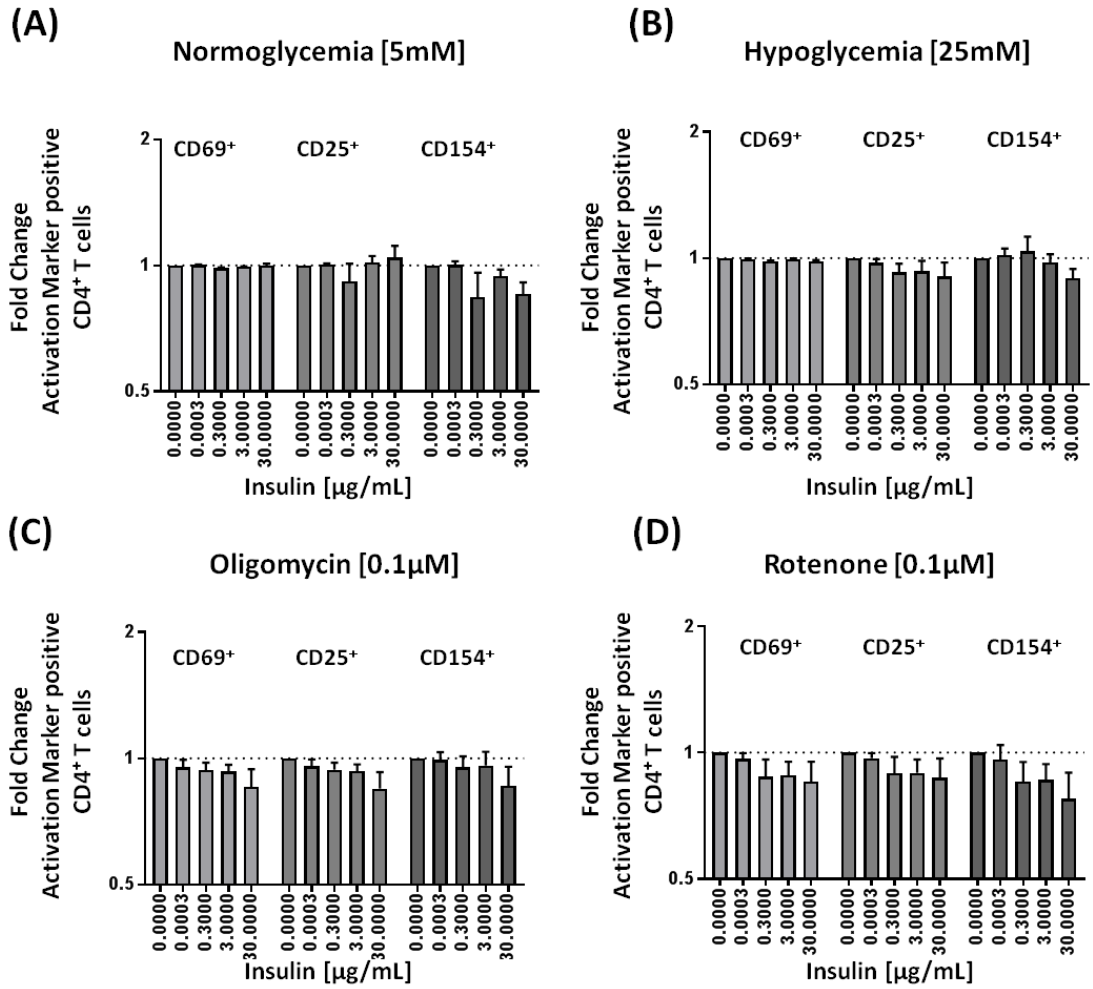

Figure 36: CD4⁺ T cell activation in the presence of insulin and metabolic stressors. CD4⁺ T cells were stimulated for 16h with anti-CD3/CD28 Dynabeads. The effect of different insulin concentration on T cells in the presence of 5mM Glucose (normoglycemia), 1mM glucose (hypoglycemia) or in the presence of the mitochondrial inhibitor oligomycin or rotenone was tested. (n=4). Data is shown as fold change of mean + SEM. Ordinary one-way ANOVA and Dunnett's multiple comparisons test with a single pooled variance was performed.

T cell proliferation and varying insulin levels in combination with hyperglycemia as well as mitochondrial stress showed similar results. No effect of varying insulin concentration was observed in the presence of metabolic stressors (Figure 37).

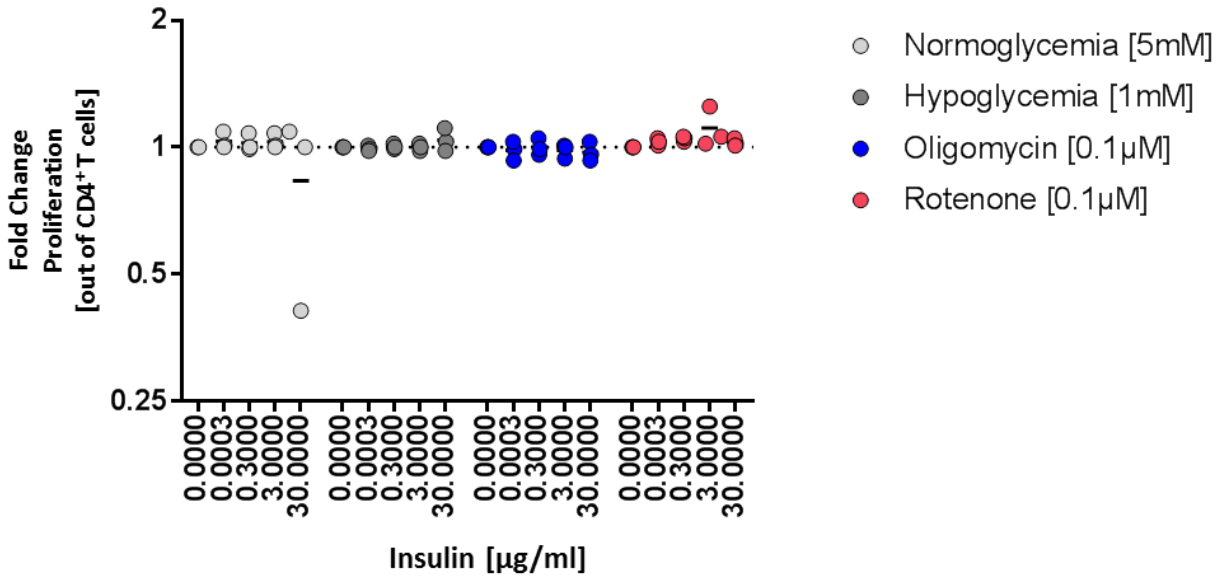

Figure 37: CD4⁺ T cell proliferation in the presence of different insulin and metabolic stressors. Human CD4⁺ T cells were stimulated using anti-CD3/CD28 Dynabeads and cultured in the presence of varying insulin levels and metabolic stressors. Hypoglycemia, oligomycin and rotenone were tested. (N=3) Data are shown as fold change to 0 µg/ml insulin for each of the four base conditions. The mean is indicated. Ordinary one-way ANOVA and Dunnett's multiple comparisons test with a single pooled variance was performed.

3.13 Naive and regulatory but not memory T cells are affected by mitochondrial dysfunction

To this point, whole CD4⁺ T cells were investigated. It has been shown that different T cell subsets engage different metabolic programs. To look further into CD4⁺ T cell energetics, I decided to distinguish between different CD4⁺ T cell subset to determine whether they show different sensitivities towards mitochondrial stress. FACS sorted memory, naive and regulatory T cells were tested for the effect of increasing rotenone concentrations. T cell activation was examined using CD69 expression. The data revealed a strong sensitivity of naive and regulatory T cells towards mitochondrial dysfunction. The frequency of CD69⁺ T cells was reduced by almost 50% (naive T cells: p=0.0017; regulatory T cells p=0.0008 for 1µM Rotenone). Memory T cells instead were more robust and no decrease in CD69⁺ cells were observed in the presence of 1µM rotenone treatment.

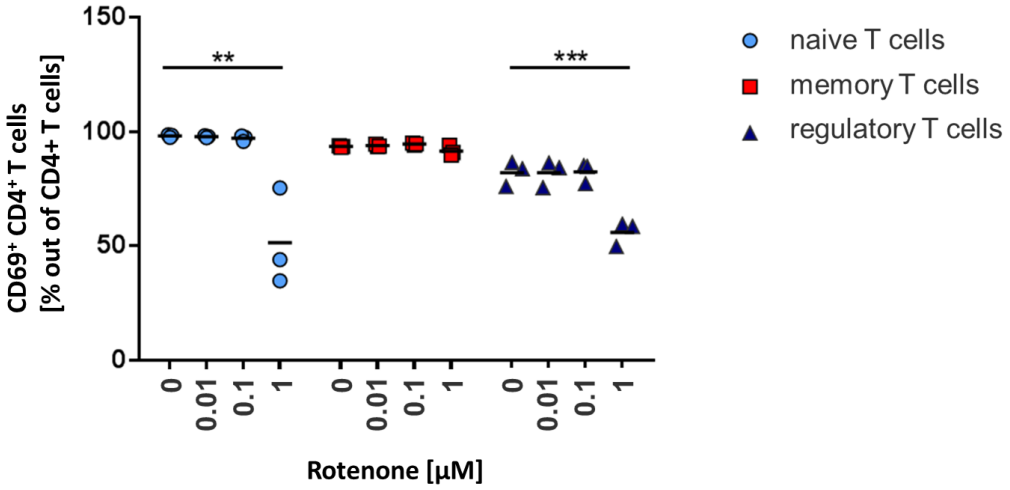

Figure 38: Mitochondrial Inhibitors on T cell subset early activation. Memory, naive and regulatory T cells were stimulated with anti-CD3/CD28 Dynabeads for 16h in the presence of rotenone. Early activation marker expression was investigated using flow cytometry (n=3 with mean). (*P ≤ 0.05; ** P≤0.01; *** P≤0.001; **** P≤0.0001) Ordinary one-way ANOVA with Dunnett's multiple comparisons test and with a single pooled variance was performed. Naive T cells: p=0.0017; Regulatory T cells: p=0.0008

3.13.1 CD4+ T cell subsets differ in their ROS production upon mitochondrial stress

The production of reactive oxygen species as an indicator of cellular stress was used in the following experiments to further evaluate the stress response of $CD4^+$ T cell subsets. $CD4^+$ T cells were stimulated for 16h in the presence of 0.1µM and 1µM oligomycin and 1 µM rotenone. Resveratrol was tested at a concentration of 50µM. ROS production was measured using MitoSOX red by flow cytometry on $CD25^+$ (regulatory) T cells; $CD45RO^+$ (memory) T cells and $CD45RO^-$ (naive) T cells. The influence of the mitochondrial inhibitors on ROS production was tested in an unstimulated (Figure 39) state as well as in the presence of polyclonal stimulation (Figure 40). The representative FACS plots in Figure 39A already highlight higher ROS production of the naive T cell subsets ($CD45RO^-$). The corresponding graph in Figure 39B reveals an increase of ROS production in the presence of 1µM oligomycin and rotenone. The naive T cells were substantially affected. $CD25^+$ and $CD45RO^+$ T cells depicted milder increases in ROS production.

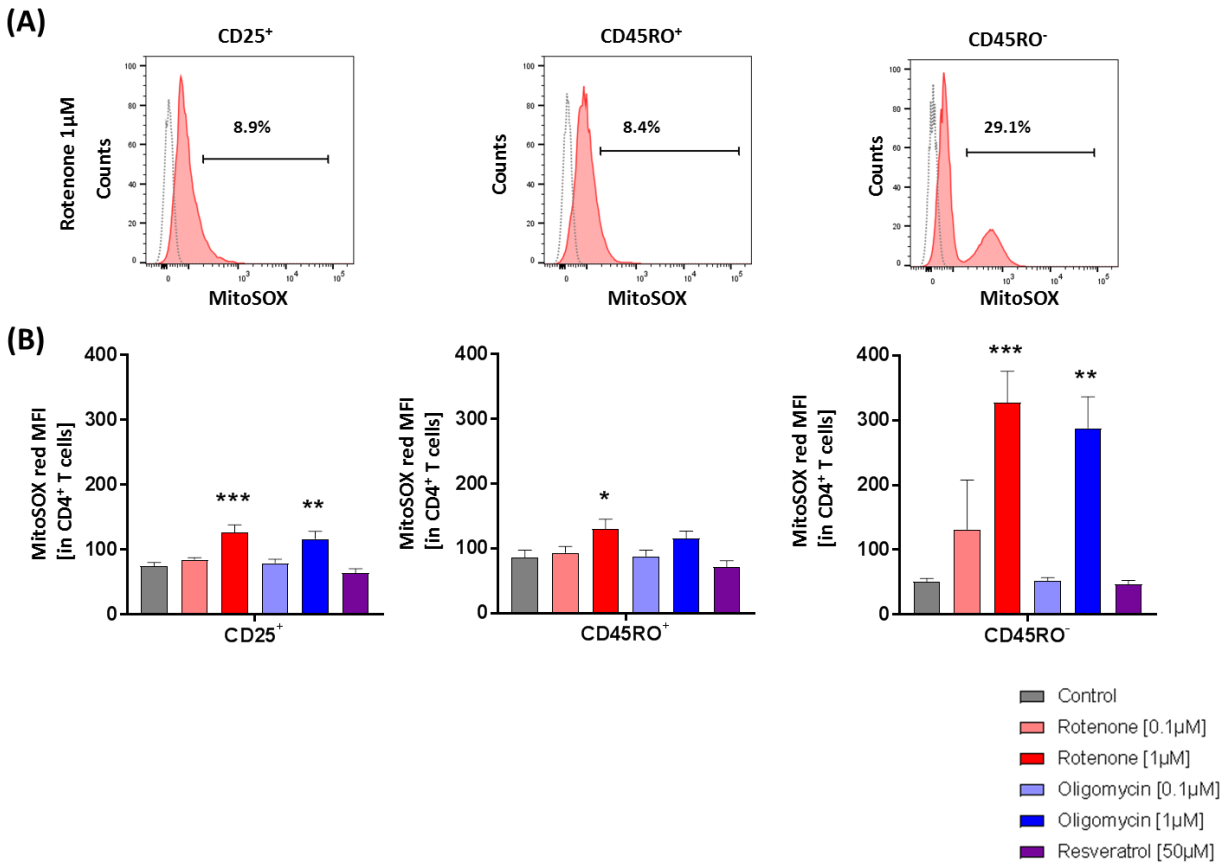

Figure 39: Production of reactive oxygen species (ROS) in unstimulated CD4⁺ T cell subsets in the presence of mitochondrial inhibitors. CD4⁺ T cells were cultured for 16h in the presence of different rotenone and oligomycin concentration [0.1 and 1µM] as well as 50µM of resveratrol. MitoSOX red was used to measure intracellular mitochondrial ROS production. (A) Depicts representative FACS plots of the different T cell subsets treated with 1µM of rotenone. (B) Shows the corresponding graph. Experiments were performed with individual donors in technical duplicates (N=5); (*P ≤ 0.05; ** P≤0.01; *** P≤0.001; **** P≤0.0001) Ordinary one-way ANOVA with Dunnett's multiple comparisons test and with a single pooled variance was performed. (CD25+: rotenone [1µM] p=0.0008, oligomycin p=0.0063; CD45RO+: rotenone [1µM] p=0.047; CD45RO-: rotenone [1µM] p=0.0005, oligomycin [1µM] p=0.0024.

A general enhancement of mitochondrial ROS production was observed in polyclonal stimulated cells (Figure 40). Also here, a higher stress response of the naive T cell fraction was observed as compared to the memory and regulatory T cell subsets (T cell subset, mean ± SEM: CD45RO⁻: control 140.4 ± 18.36; rotenone [1µM] 318.5 ± 28.84 (p=0.0005); oligomycin [1µM] 294.9 ± 27.199 (p=0.0024)). Furthermore, 16h of stimulation generally increased ROS production, and this increase was attenuated by 50µM resveratrol in all CD4⁺ T cell subsets (Inhibitor, T cell subset, mean ± SEM resveratrol: CD25⁺ control 182.6 ± 22.3, resveratrol 92.53 ± 7.8; CD45RO⁺ control 238.3 ± 38.8, resveratrol 123.6 ± 17.82; CD45RO⁻ control 140.4 ± 18.4, resveratrol 63.64 ± 7.42).

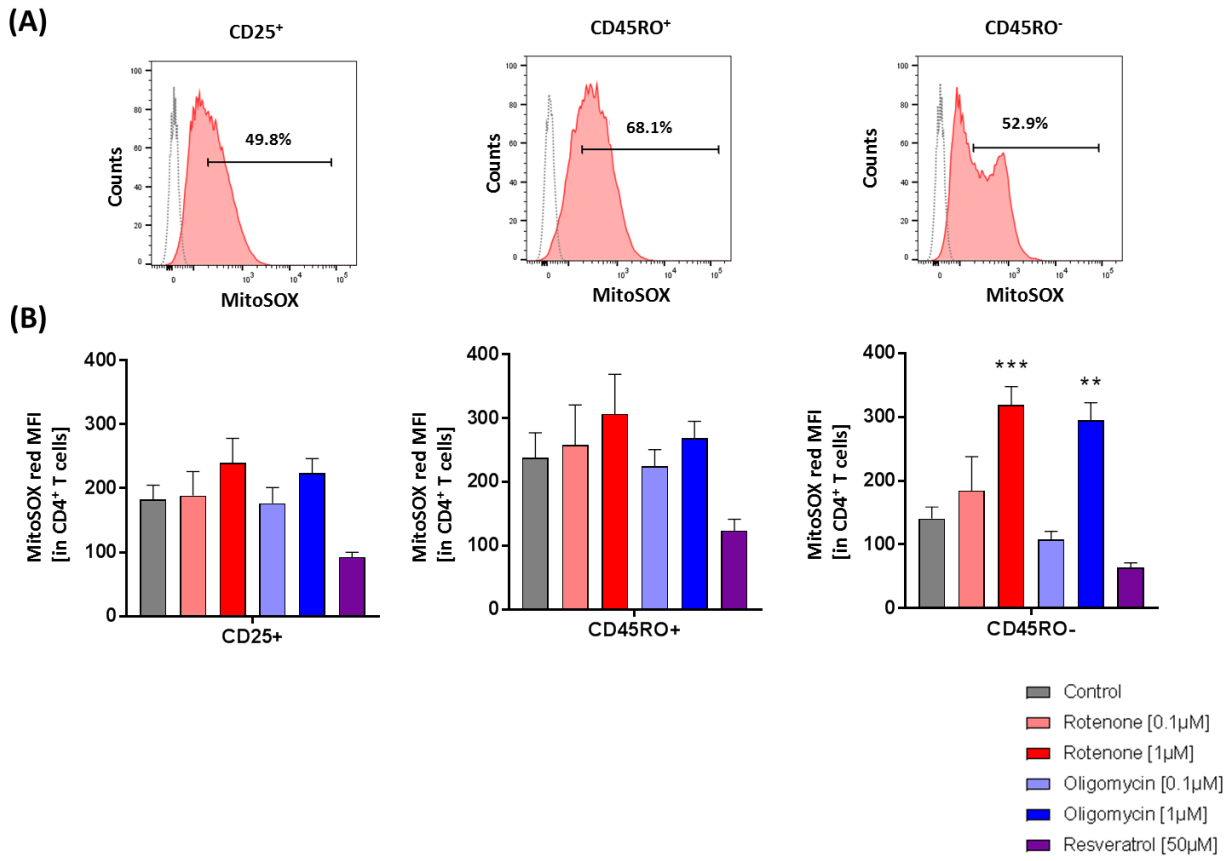

Figure 40: Production of reactive oxygen species (ROS) in stimulated CD4⁺ T cell subsets in the presence of mitochondrial inhibitors. CD4⁺ T cells were polyclonal stimulated for 16h using anti-CD3/CD28 Dynabeads in the presence of different rotenone and oligomycin concentration [0.1 and 1µM] as well as 50µM of resveratrol. MitoSOX red was used to measure intracellular mitochondrial ROS production. In (A) representative FACS plots of the different T cell subsets treated with 1µM of rotenone are shown. In (B) the corresponding graph is shown. Experiments were performed with individual donors in technical duplicates (N=5); (*P ≤ 0.05; ** P≤0.01; *** P≤0.001; **** P≤0.0001) Ordinary one-way ANOVA with Dunnett's multiple comparisons test and with a single pooled variance was performed. (CD45RO⁻, rotenone [1µM] p=0.0009; oligomycin [1µM] p=0.0033).

3.14 RNAseq analysis of CD4⁺ T cell subsets in the presence of different inhibitors and glucose concentrations

To determine the most relevant pathways affected by mitochondrial stress, I performed RNA sequencing in CD4⁺ T cell subsets stimulated in the presence of the three metabolic inhibitors in 1mM and 5mM glucose (Table 2). Memory, naive and regulatory T cells were sorted at high purity based on their fluorescent characteristics by fluorescent activated cell sorting. The cells were stimulated for 6h with anti-CD3/CD28 Dynabeads in 1mM or 5mM glucose with rotenone [1µM], oligomycin [0.1µM] or resveratrol [50µM]. RNA isolation was performed and the samples were further processed by the Deep Sequencing Facility of Dr. Andreas Dahl at the BIOTEC in Dresden, Germany. RNAseq was performed by Illumina dye sequencing with a read length of 75bp and 30 million reads per sample. The analysis is ongoing with the help of Dr. Virag Sharma (CRTD) and preliminary findings are presented in this thesis.

Table 12: Illustration of the various conditions for RNAseq. Naive, memory and regulatory $CD4^+$ T cells were sorted and stimulated for 6h in the presence of 1mM or 5mM glucose with no inhibitor or in the presence of defined inhibitor concentrations.

	Naive T cells		Memory T cells		Regulatory T cells	
Glucose	1mM	5mM	1mM	5mM	1mM	5mM
No Inhibitor	X	X	X	X	X	X
Oligomycin [0.1µM]	X	X	X	X	X	x
Rotenone [1µM]	X	X	X	X	X	X
Resveratrol [50µM]		X		X		X

3.14.1 Principal Component Analysis

Principal component analysis (PCA) was used to describe differences between different donors and conditions (Figure 41). The experiments were performed in technical duplicates. Blue dots represent control conditions in 5mM glucose and red dots are treated samples in the presence of 5mM glucose. Substantial differences between the donors were identified. However, for each inhibitors, consistent directional changes in all donors were identified.

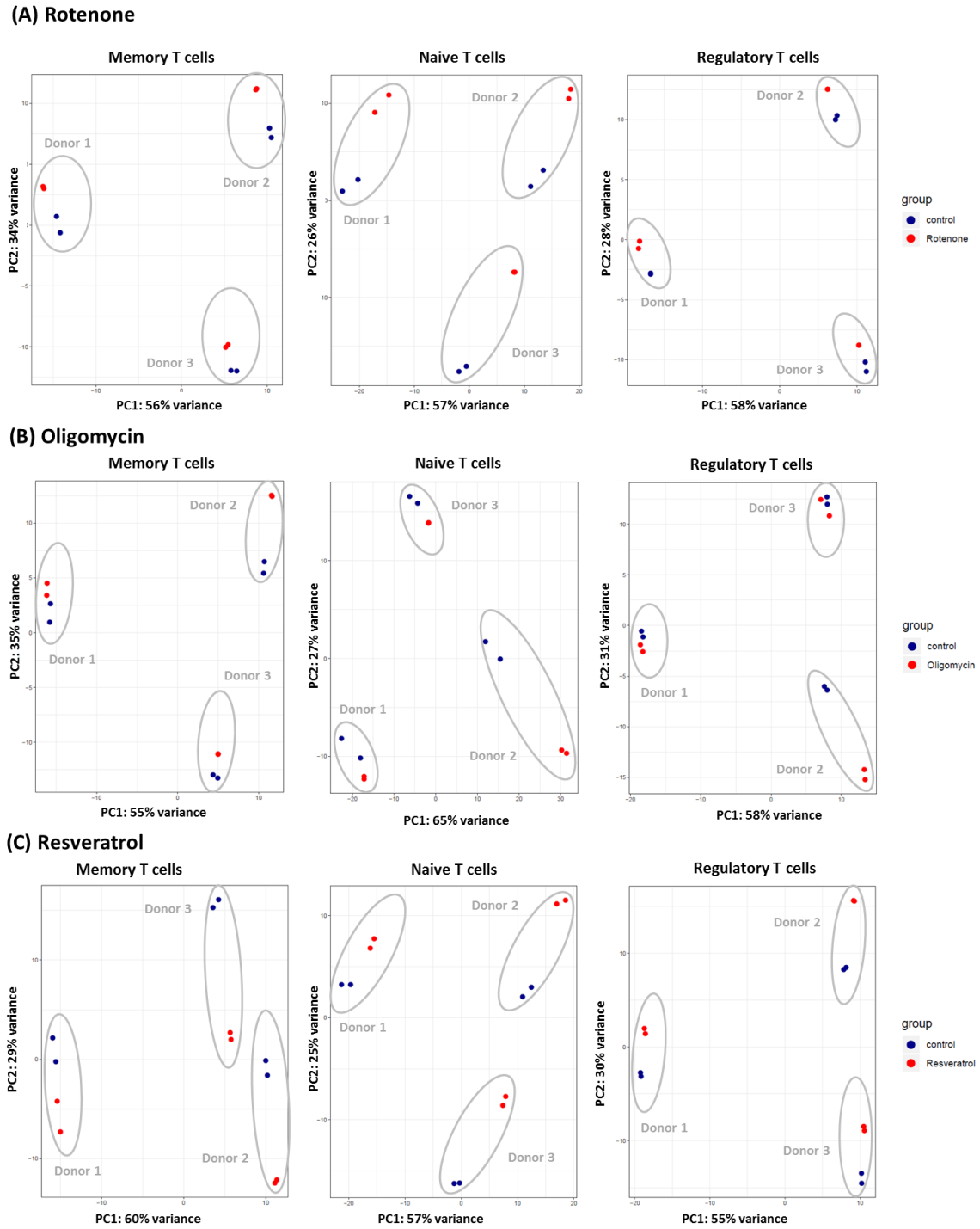

Figure 41: Principle Component Analysis (PCA) of the T cell subsets treated with (A) rotenone vs control (B) oligomycin vs control and (C) resveratrol vs control. Each colored point represents one donor. Blue dots are control conditions without inhibitor in the presence of 5mM glucose. Red dots represent treated samples with the different inhibitors. Individual donors are indicated by grey circles. The experiment was performed using technical duplicates, each of which is shown as a point.

3.14.2 Differently expressed genes

Volcano plots were used to identify differently expressed genes between the treated and the control condition for each T cell subset (Figure 42). One gene is represented by one point. The threshold for

differently expressed genes is an adjusted p value of <0.05 and is indicated by dotted lines. Differentially expressed genes were observed for each condition.

Venn diagrams illustrate the distribution of significantly up and down regulated genes ($p<0.05$) for each inhibitor in the three T cell subsets (Figure 43). There were relatively few genes that were differentially expressed in all the subsets. Naive T cells depict higher numbers of differentially expressed genes for all three inhibitors compared to memory and naive T cells. Only resveratrol treatment led to more up regulated genes in memory T cells (Figure 43F). Oligomycin treatment resulted in the fewest changes of differentially expressed genes (Figure 43C,D).

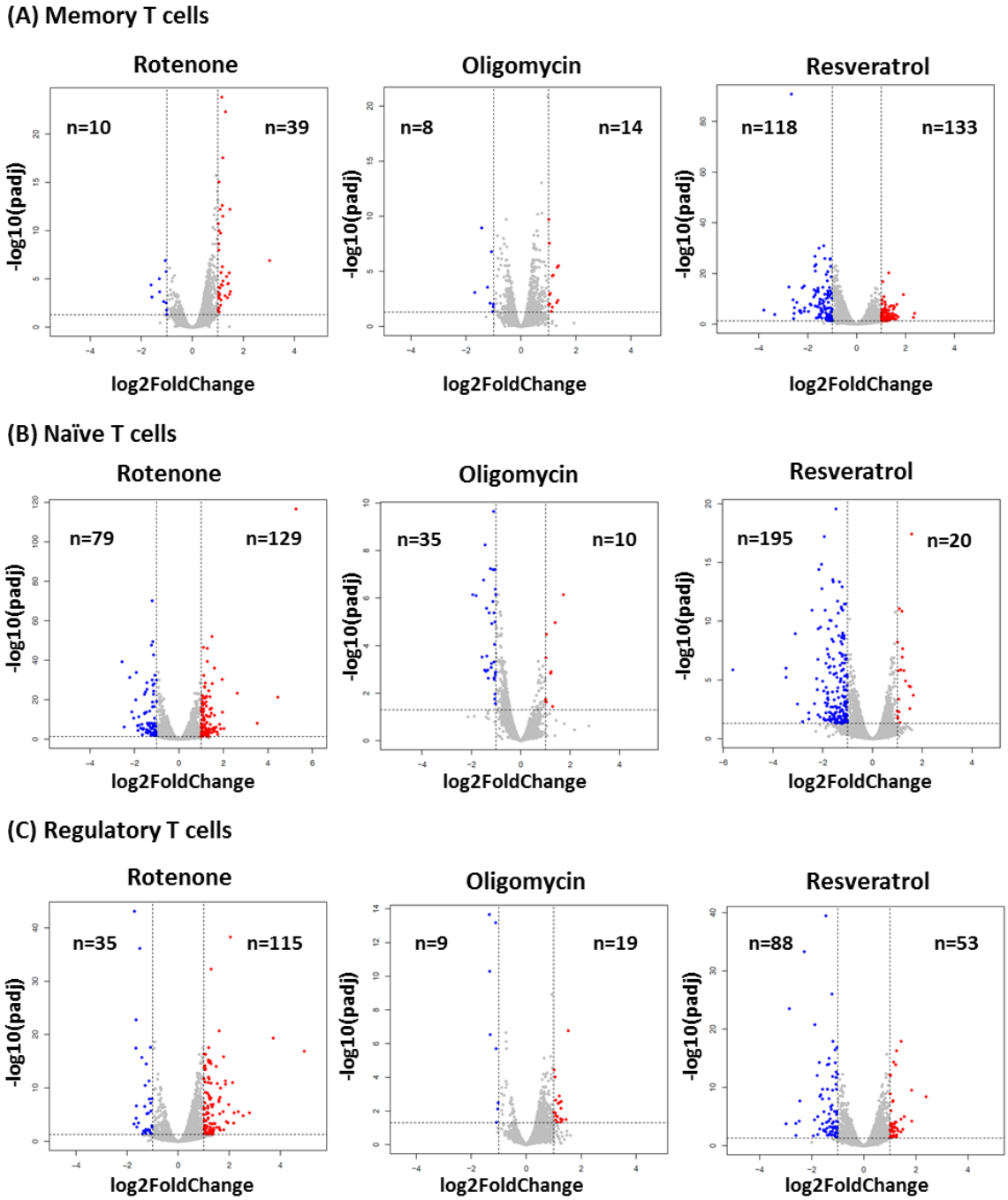

Figure 42: Differently expressed genes for each CD4⁺ T cell subset and condition are illustrated by volcano plots. The volcano plots show the fold change (log2 Ratio) against the absolute confidence (-log10 adjusted p-value). One gene is represented by one point. The threshold for differently expressed genes was chosen at an adjusted p value of <0.05 and a >2 fold change in expression. Both are indicated by the broken lines. Blue points indicate genes which are significantly down regulated compared to the control conditions, red points indicate significantly up regulated genes. The numbers of significantly altered genes are indicated.

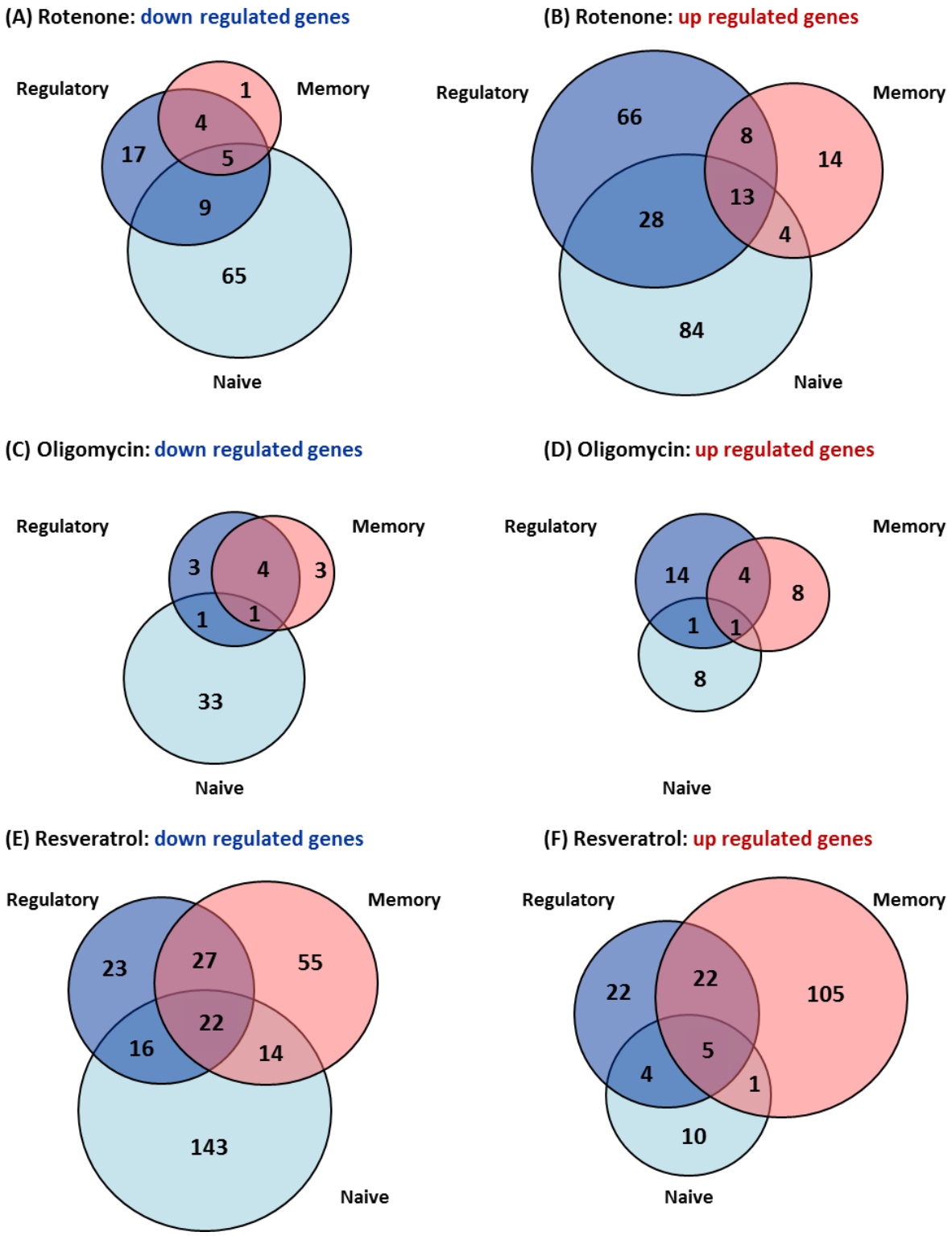

Figure 43: Venn diagram of down and up regulated genes in CD4⁺ T cell subsets stimulated in the presence of inhibitors. Distribution of down and up regulated genes in the presence of (A,B) 1µM rotenone; (C,D) 0.1µM oligomycin; (E,F) 50µM resveratrol among CD4⁺ T cell subsets.

3.14.3 Mitochondrial dysfunction does not change metabolic gene expression but causes a redox imbalance

The effects of molecular stress on T cell function was further investigated by analyzing the expression of key metabolic genes involved in glycolysis, TCA cycle and the malate-aspartate shuttle. The selected metabolic genes remained largely unaffected at the transcriptional level in the presence of all inhibitors (Figure 44). No significant alterations in the expression of glycolytic genes were detected. This is consistent with the functional data, which revealed stable glycolytic flux in the presence of mitochondrial dysfunction (Figure 16). However, to further understand why T cell proliferation is affected by mitochondrial dysfunction, redox balance effectiveness was investigated. Deregulated NAD/NADH ratios not only affect mitochondrial processes but also TCA cycle activity and glycolytic pathway engagement necessary for cell growth and proliferation. Oligomycin treatment is reported to alter the mitochondrial membrane potential and to lead to an accumulation of NADH in the inner mitochondrial matrix (Figure 45A). FCCP was used in the following experiment to uncouple electron transport chain function from ATP synthase activity by transporting protons across the inner mitochondrial membrane and depolarizing the membrane potential, reversing the effect of oligomycin. Early activation of T cells was used as a read out. Figure 45B shows a rescue of activation using 1.5µM FCCP. T cell activation, measured by the number of T cells positive for CD69 and CD25, was significantly increased in the presence of FCCP ($CD69^+$ p=0.006; $CD25^+$ p=0.027). However, genes of the malate-aspartate-shuttle remained unaffected. The malate-aspartate shuttle is responsible of the transport of NADH into the mitochondria and NAD^+ back into the cytosol and hence an important checkpoint for maintained redox balance. The stable expression of genes involved in glycolysis, TCA cycle and malate-aspartate shuttle instead suggests a regulatory mechanism on a post-transcriptional level (Figure 44).

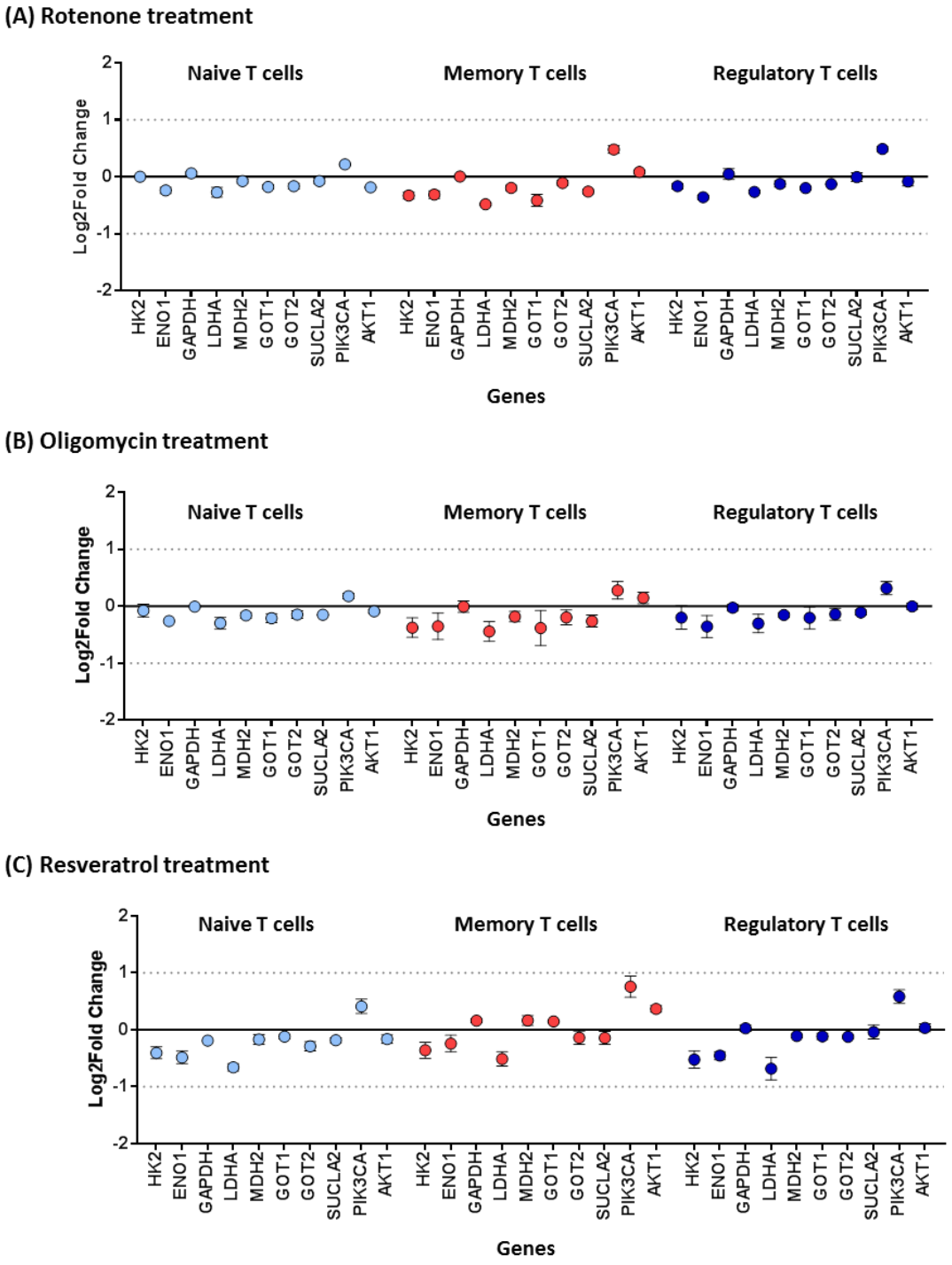

Figure 44: Fold change RNA expression of metabolic genes in the presence of metabolic inhibitor compared to control. The effect of (A) Oligomycin (B) Rotenone and (C) Resveratrol treatment on naive, memory and regulatory T cells is shown. The Log2Fold Change expression of treated vs control conditions of metabolic genes (HK2; ENO1; GAPDH; LDHA), genes related to the malate-aspartate-shuttle (MDH2; GOT1; GOT2), a TCA cycle gene (SUCLA2) and metabolic checkpoint genes (PIK3CA; AKT1) are illustrated as mean ± SEM of n=3 donors.

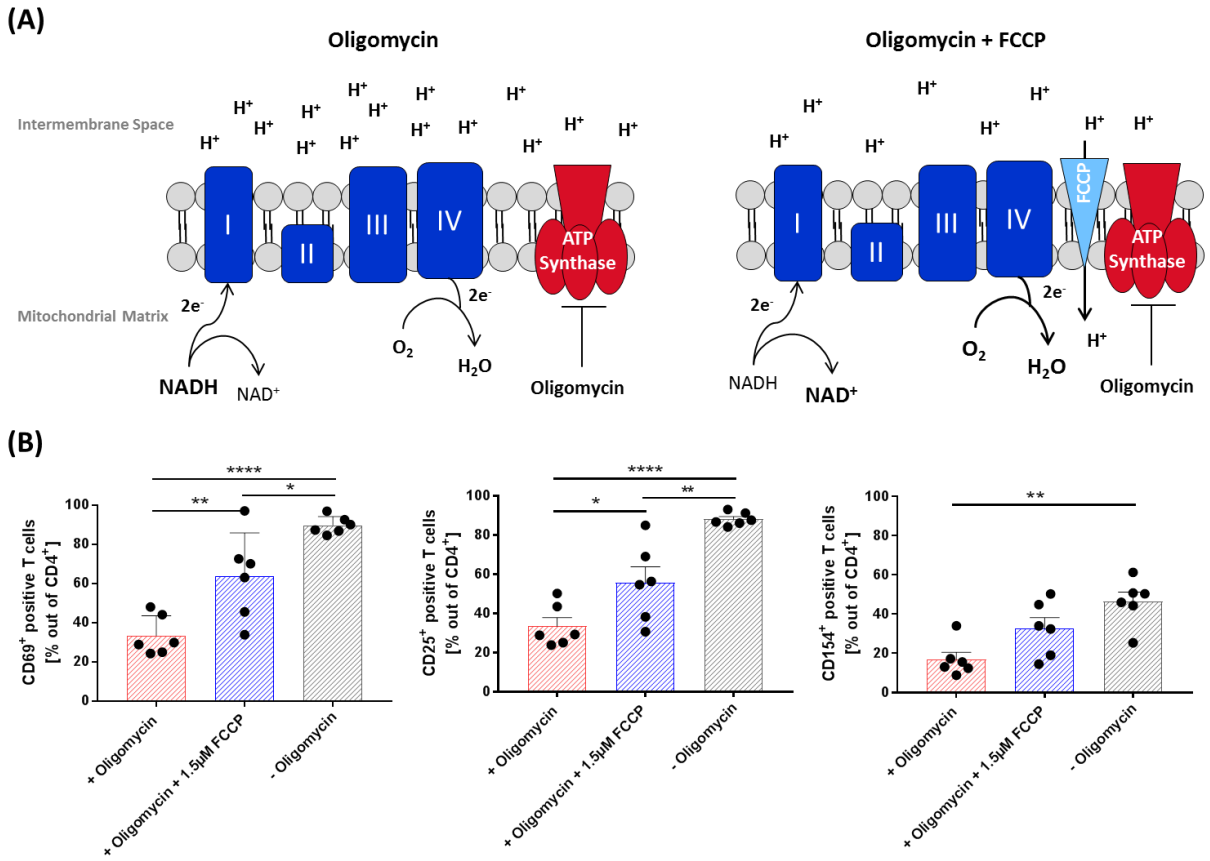

Figure 45: Rescue experiment after oligomycin treatment using FCCP. (A) Illustration of the effect of oligomycin on in the mitochondria and upon addition of FCCP. (B) T cells were stimulated for 16h using anti-CD3/CD28 Dynabeads in the presence (red bars) or absence (grey bars) of 0.1µM oligomycin and for the rescue experiment, 0.1µM oligomycin plus 1.5µM FCCP (blue bars). Cells positive for CD69, CD25 and CD154 were measured. Each point represents one independent experiment, performed in technical duplicates (N=5). (*P ≤ 0.05; ** P≤0.01; *** P≤0.001; **** P≤0.0001) Ordinary one-way ANOVA with Turkey's multiple comparisons test and with a single pooled variance was performed. (+ Oligomycin vs + Oligomycin and FCCP: CD69+ p=0.006; CD25+ p=0.0271. + Oligomycin vs – Oligomycin: CD69+ p<0.0001; CD25+ p<0.0001; CD154+ p=0.0016. + Oligomycin and FCCP vs – Oligomycin: CD69+ p=0.0172; CD25+ p=0.0018).

3.14.4 Rotenone and oligomycin cause an impairment of Type I and Type II IFN signaling in all investigated T cell subsets

Preliminary pathway analysis was conducted by the Reactome Pathway Database (Fabregat et al., 2018). It was performed against Reactome Version 67 on 03/02/2019. Genes that were down regulated more than 2 fold were examined. The most relevant pathways belong to the IFN signaling pathway. A list of the affected genes with their Log2Fold change, p-value and adjusted p-value can be found in the appendix of the thesis. Most of the down regulated IFN pathway genes are induced by both types of interferons. These include genes encoding for OAS proteins, IFITs and GBPs. Interferon Type II specific induced genes that were affected include XAF1, IFI6, RSAD2, ICAM1 and USP18 (Figure 46 and Figure 47).

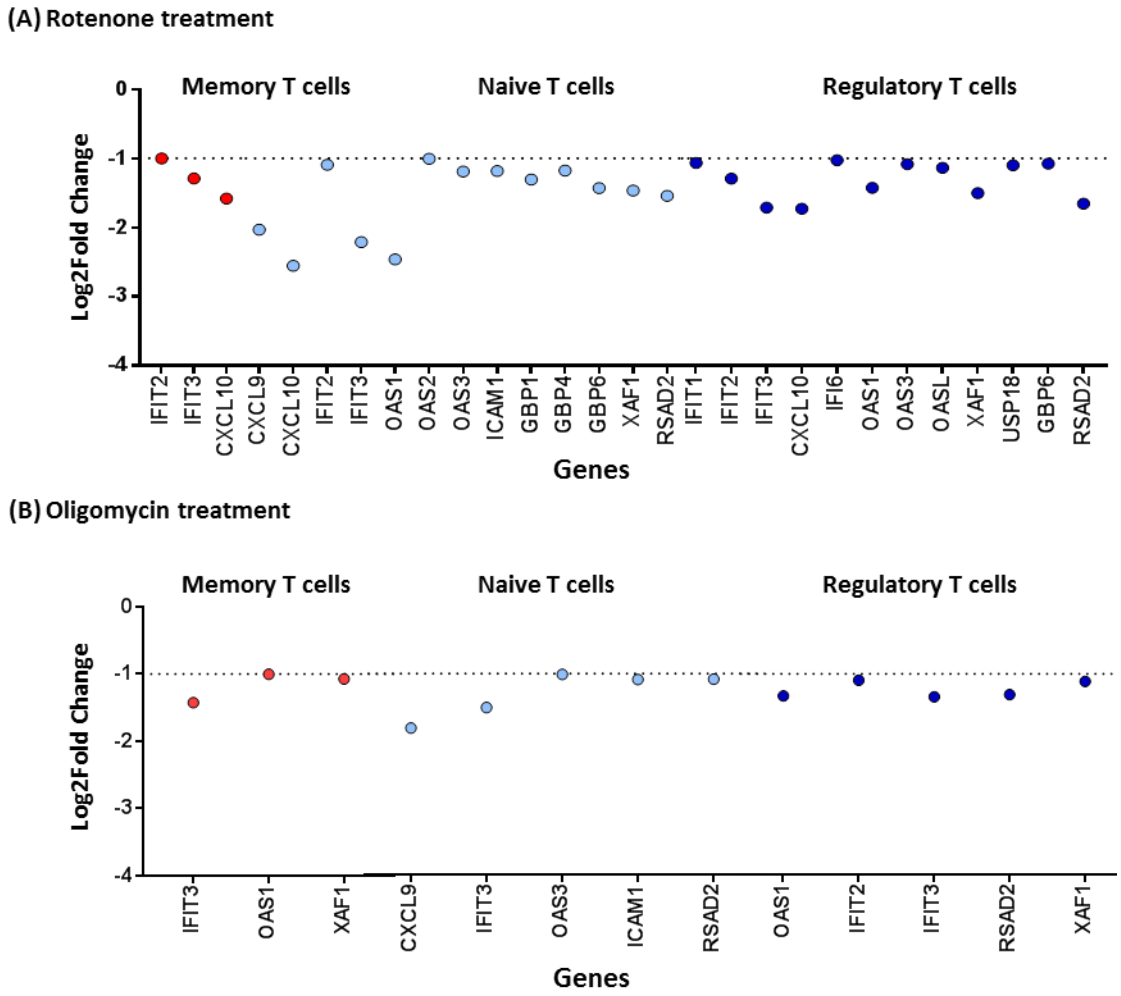

Figure 46: Downregulated genes related to IFN signaling in the presence of rotenone and oligomycin. Affected genes in memory $CD4^+$ T cell subset are indicated with red dots. Affected genes in the naive $CD4^+$ T cell subsets are indicated in light blue and affected genes in regulatory T cells are marked with dark blue dots. Genes are considered as differentially expressed with $p \leq 0.05$.

Preliminary pathway analysis of the significantly up regulated genes in the presence of rotenone revealed increases in genes encoding heat shock proteins (HSPs). The number of up regulated genes in the presence of oligomycin was too low for further pathway analysis. Memory and regulatory T cells increased the gene expression of molecular chaperones belonging to the heat shock family A (HSP70) or related HSPs. DNAJB1 (DnaJ Heat Shock Protein Family (Hsp40) Member B1) does not directly belong to the HSP70 family but interacts with it. Naive T cells additionally increased HSPB1 (HSP20) which was shown to be induced by environmental stress. The presented RNAseq data analysis again supports the functional observation of the particular sensitivity of the naive T cells and partially also of regulatory T cells already reported in previous experiments (Figure 38 and Figure 39).

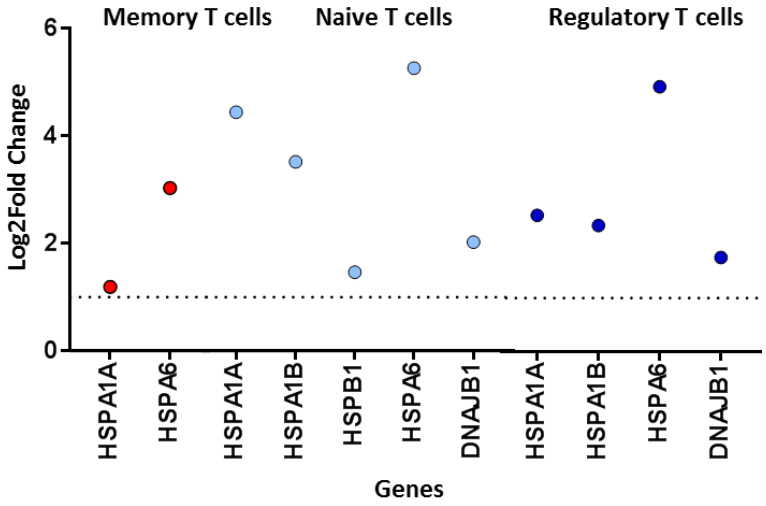

Figure 47: Up regulated genes encoding several heat shock proteins (HSP) in the presence of rotenone. Affected genes in memory CD4⁺ T cell subset are indicated with red dots. Affected genes in the naive CD4⁺ T cell subsets are indicated in light blue and affected genes in regulatory T cells are marked with dark blue dots. Genes are considered as differentially expressed with p≤0.05.

3.14.5 Resveratrol dampens cytokine and chemokine signaling in CD4⁺ T cell subsets

Preliminary RNAseq analysis of resveratrol treated samples was conducted by the Reactome Pathway database (Fabregat et al., 2018). The analysis was further performed against Reactome Version 67 on 03/02/2019. The most relevant affected pathway constitutes cytokine signaling, specifically signaling of interleukins. Genes related to chemokine signaling were also shown to be affected (Figure 48). A list of the shown affected genes with Log2Fold Change, p-value and adjusted p-value can be found in the appendix of the thesis. The RNAseq data supports the functional analysis of resveratrol on T cell function, which showed a dose-dependent decrease of cytokine production (Figure 24). Members of the TNF receptor superfamily (TNFRSF8; TNFRSF15 and TNFRSF21) were significantly down regulated (Figure 48). Members of this family are activators of NFκB. NFκB is a critical modulator of the immune response as it is involved in the transcriptional regulation of cytokine and chemokine expression.

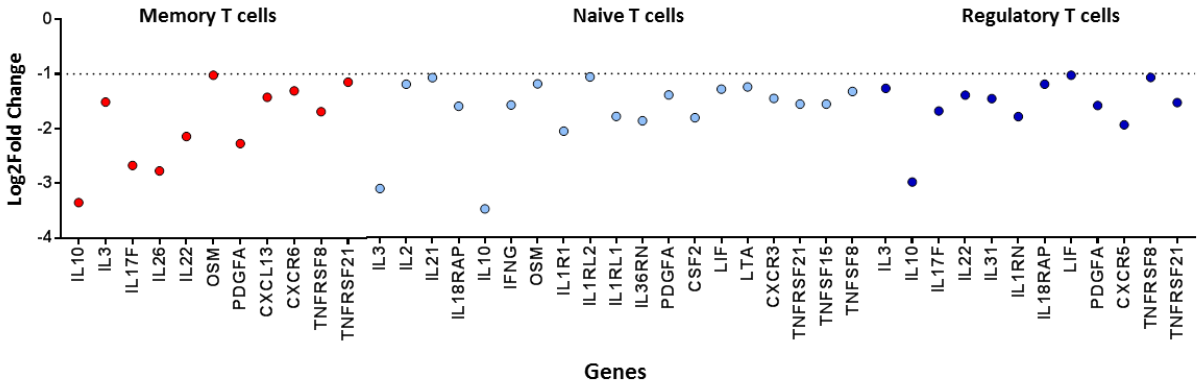

Figure 48: Genes of cytokine and chemokine signaling affected in the presence of resveratrol. Down regulated genes in memory $CD4^+$ T cell subset are indicated with red dots. Affected genes in the naive $CD4^+$ T cell subsets are indicated in light blue and affected genes in regulatory T cells are marked with dark blue dots. Genes are considered as differentially expressed with $p \leq 0.05$.

4 DISCUSSION

I studied the requirement of mitochondrial pathways and glycolysis for T cell function. Specific mitochondrial inhibitors targeting oxidative phosphorylation were used to define the importance of ETC function and mitochondrial ATP production for T cell activation, proliferation and cytokine secretion. I chose human $CD4^+$ T cells and developed an *in vitro* model and methods to link T cell respiratory signatures to $CD4^+$ T cell function. I discovered that intact mitochondrial ETC was critical for competent $CD4^+$ T cell activation and, in contrast to previous reports, that ATP synthase was required in both activation and $CD4^+$ T cell proliferation, the latter also markedly affected by limiting the availability of glucose. The effects of mitochondrial inhibition were associated with ROS production. Cytokine production was unaffected by ETC, ATP synthase or glucose availability. Different to other cell types (Keuper et al., 2014; Liemburg-Apers et al., 2015), I found that human $CD4^+$ T cells demonstrated little or no compensatory increase of glycolysis for mitoenergetic dysfunction. Moreover, although limiting glucose availability alone did not affect $CD4^+$ T cell activation or cytokine production, low glucose had a marked synergistic role together with ETC or ATP synthase inhibitors on T cell function. Gene expression validated the lack of effect on glycolysis associated with ETC and ATP synthase inhibition. Finally, I was able to discern clear differences in how activation of memory, naive and regulatory $CD4^+$ T cells is affected by mitochondrial dysfunction. Along the course of my thesis I also discovered that resveratrol does not affect mitochondrial function, but has profound effects on T cell proliferation and cytokine production, most likely through an inhibition of NFκB, and that the commonly used cryopreservative DMSO has marked inhibitory effects on T cell metabolism and function even at very low concentrations.

My thesis has a number of strengths. The interplay of metabolism and function was performed on human samples. This is the first detailed analysis of energy requirements for human $CD4^+$ T cells. Previous reports were predominantly in mouse T cells and I was unable to confirm all of the previous findings using human T cells. The assays I developed and used allowed an assessment of three stages in $CD4^+$ T cell function with clear differences in the effects of metabolic perturbation. In particular, my inclusion of a range of concentrations of different inhibitors with known specific targets enabled me to link metabolic checkpoints to $CD4^+$ T cell function. I was also able to investigate the effects using multiple methods that included the expression of protein markers, functional outputs and transcription analyses. Finally, in performing my thesis I considered and began to address that different $CD4^+$ T cell subsets may have different sensitivities to mitochondrial perturbation.

It is also important to acknowledge the limitations of the thesis. Although, I performed both technical replicates and performed experiments on multiple donors, for some of the experiments there was variation between the results of each donor. This was particularly true for some of the metabolic

measurements and the transcriptional analyses. Thus, a number of experiments are likely to have limited power to exclude differences. I did not determine whether the observed variation was associated with assay or donor variation or both. Some of the variation may have been due to biology and genetics, which could have been discerned if a much larger number of individuals were tested. The findings were all based on *in vitro* experiments. Therefore, I cannot assume that analogous perturbations in patients or with drug treatment will have similar effects. I was also unable to examine perturbation by knockdown of specific genes in the *in vitro* assays and lacked this set of validation experiments. My experimental design did examine time course to choose time points that reflected the functional outputs, but I did not perform perturbation experiments over a dynamic time range and, therefore, have only limited information as to the sequence of events that are affected. Moreover, metabolic alterations were mainly confined to respiratory flux analysis. Metabolic flux analysis of different carbon sources such as glutamine or fatty acid was neglected, and a description of the incorporation of glucose into precursors such as amino acids was not performed. It would also be interesting to evaluate mitochondrial function for precursor synthesis such as aspartate or serine to support anabolic processes.

A major finding of my work was that both ETC and ATP synthase were critical for $CD4^+$ T cell activation and proliferation. The metabolic requirements of T cells change depending upon the stage of T cell activation and function. I divided the process of activation through to function into three stages – activation, proliferation, and effector function. A first metabolic remodeling is necessary when resting T cells move out of quiescence. It was previously reported that the activation process requires purinergic signaling by increasing concentrations of ATP. Furthermore, Ca^{2+} increase at the immune synapse was shown to depend on mitochondria that function as a local buffer system. Mitochondrial ROS acts as a signaling molecule important for the activation process (Ledderose et al., 2014; L. A. Sena et al., 2013). The importance for mitochondrial pathways was also confirmed in the scope of this thesis. Inhibition of the mitochondrial electron transport chain or ATP synthase markedly decreased T cell activation.

The second major metabolic rewiring and the most investigated transition is the switch from activated to proliferating T cells. This transition is mediated by a shift from OXPHOS to glycolysis (Pearce et al., 2013). This model is further supported by results of this thesis. The glucose uptake assay reflects the proposed increase in glycolysis for proliferation, illustrated by a major increase in incorporated glucose after 72h (proliferation stage) and only minor increases of glucose uptake after 16h of stimulation (activation stage). I also showed that glucose restriction only affected T cell proliferation. Mitochondrial pathways were also previously shown to be crucial and increased in activated T cells to support proliferation. Mitochondrial pathways were shown to provide biosynthetic branches for the production of precursor within the TCA cycle. Furthermore the mitochondrial role for maintaining the

redox balance is essential for glycolytic flux and TCA cycle engagement (Dimeloe et al., 2017). Disrupting mitochondrial membrane potential and redox imbalance was shown to impair the synthesis of aspartate needed for anabolic cell growth (Birsoy et al., 2015; Sullivan et al., 2015). The role for maintained redox balance was further proven to be crucial also for T cell activation in this thesis by the rescue experiment using FCCP. Moreover, mitochondrial functional and morphological remodeling was further reported to support the switch from catabolic to anabolic metabolism (Buck et al., 2016; Rambold and Pearce, 2018; Ron-Harel et al., 2016). In the course of this thesis, an additional mitochondrial requirement for T cell proliferation was identified. Unexpectedly, mitochondrial ATP was shown to be crucial for T cell proliferation. Mitochondrial inhibition impaired the proliferation process. Clearly, impaired activation affects downstream proliferation, but I demonstrated that proliferation was impaired also when the inhibition of ATP synthase was performed subsequent to activation, thereby identifying an independent need for mitochondrial ATP.

The data from my thesis also define a metabolic uncoupling of glycolytic pathways and mitochondrial pathways for T cell function. This first became evident in the glucose deprivation data. Proliferation, but not activation, was affected by hypoglycemic conditions. The same was true in the presence of resveratrol, which is suggested to interfere with mitochondrial pathways. In contrast, mitochondrial ATP was required for activation and proliferation. However, the purpose for this requirement is different. The switch from resting to activation state requires ATP as a signaling molecule to initiate purinergic cascades as an important checkpoint for activation (Ledderose et al., 2014; Schenk et al., 2008). ATP for T cell proliferation is rather suggested as an energy source. The classical model of T cell metabolic rewiring claims that the required energy is provided by engaging aerobic glycolysis (Dimeloe et al., 2017; Pearce et al., 2013; Pearce and Pearce, 2013). I reported an impairment of T cell proliferation in the presence of mitochondrial inhibition although glycolytic flux remained stable. This is particularly interesting because it also questions the reported need of aerobic glycolysis for T cell proliferation. A common feature of many other cell types such as adipocytes and muscle cells is a compensatory increase of glycolysis for mitoenergetic dysfunction (Keuper et al., 2014; Liemburg-Apers et al., 2015). Instead, T cells did not compensate the loss of mitochondrial ATP with increasing glycolysis. This independency of mitochondrial function and glycolysis was supported by the performed RNAseq data. Representative metabolic genes of glycolysis, TCA cycle and the malate-aspartate-shuttle remained stable. These data suggest that first, glycolytic derived ATP is dispensable for activation, proliferation and effector function. Furthermore, it supports the hypothesis that the regulation of metabolic adaptation rather happens on a post-transcriptional level. The Illustration below (Figure 49), summarizes the different mitochondrial properties involved in T cell function. I was able to expand the known requirement with the need for mitochondrial ATP for T cell proliferation as well as the importance for redox balance for activation. Furthermore, the previously reported need for ROS

production for T cell activation is questioned here. The illustrated role of mitochondria for cell polarization during migration was not further discussed in the scope of this thesis, but is included in the figure for completeness.

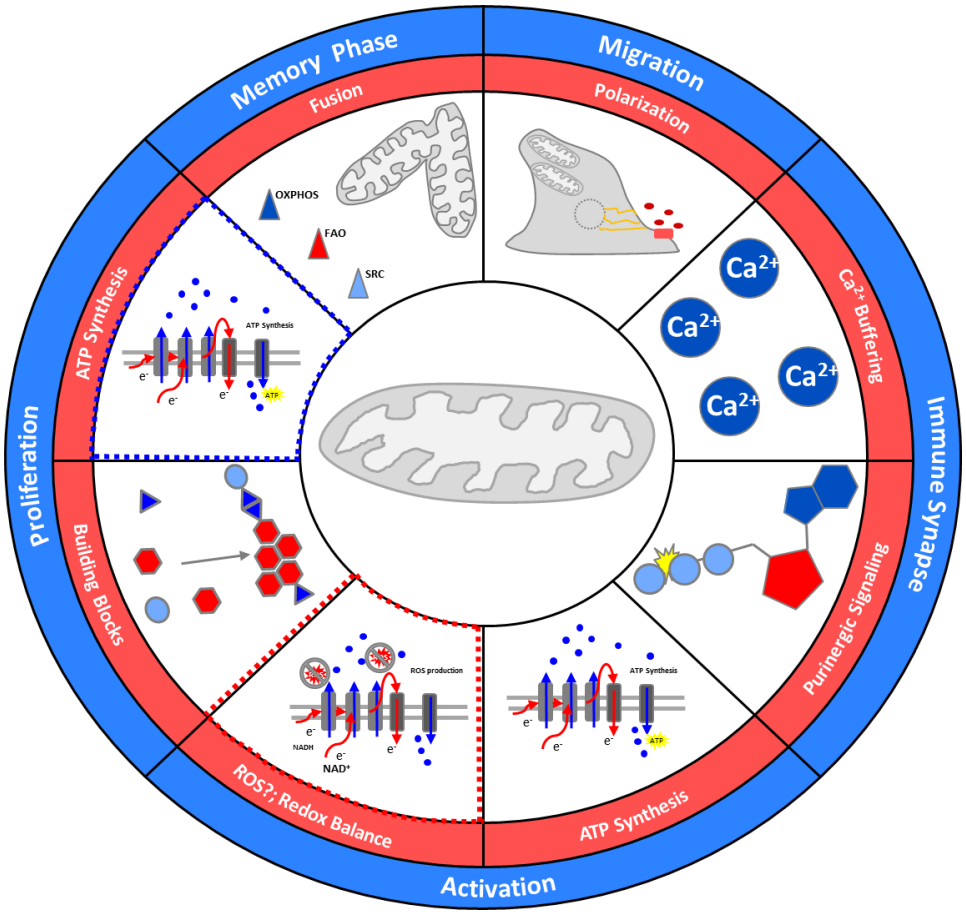

Figure 49: Required mitochondrial function for T cell activation and functional stages. Mitochondria are needed for T cell migration upon chemotactic activation. TCR ligation initiates calcium signaling and localizes mitochondria to the immune synapse where they act as a local buffer, induce additional purinergic signaling and provide energy in the form of ATP. Reactive oxygen species were shown to be important for activation signaling, a finding that is not supported by data from my thesis. Redox balance was further shown to be crucial for T cell activation. Mitochondria act as a biosynthetic hub for proliferation by producing important precursor molecules necessary for cell expansion. Mitochondrial ATP was further shown in my thesis to be an essential energy source for proliferation. Differentiation into memory T cells were linked to mitochondrial morphological rewiring resulting in fused mitochondrial with respiratory super chain complex for increased OXPHOS and spare respiratory capacity (SRC). Dashed lines marked the updated components of mitochondrial function by this thesis (modified from Desdín-Micó et al., 2018).

A second major finding of my work regards the metabolic independency of short term cytokine secretion which is a read out of T cell effector function *in vitro*. It was previously shown that effector phase T cells engage glycolysis and that OXPHOS is dispensable. Even in microenvironments with sufficient oxygen supply, cytokine producing cells were shown to ferment glucose into lactate (Chang et al., 2013; Kim and Dang, 2006). This engagement of glycolytic flux was reported to rapidly meet the cell's increasing energy demand and to further delegate differentiation and support cytokine synthesis on a translational level (Chang et al., 2013; Palmer et al., 2015). The functional relevance of glycolysis for cytokine production substantiates in an epigenetic and post-transcriptional control (Peng et al.,

2016; van der Windt et al., 2013). I was able to show the independency of effector function of mitochondrial pathways. Inhibition of the mitochondrial ETC and ATP synthase activity did not affect short-term cytokine production as measured by cytokine positive cells. Interestingly, alterations in glucose levels ranging from hyperglycemia (25mM) to hypoglycemia and glucose depleted conditions also did not affect cytokine production. These results contradict with existing mouse T cell data (Blagih et al., 2015; Cham et al., 2008). Nutrient availability was reported to induce a glucose-sensitive metabolic checkpoint controlled by AMPK. Overnight glucose starvation decreased the levels of IFNγ after 5h of re-stimulation (Blagih et al., 2015). I could not identify an effect on short-term IFNγ production in the presence of low or no glucose. Of interest, a recent report identified a rapid activation-induced engagement of glycolysis in mouse $CD8^+$ T cells, which occurs instantly after TCR ligation. It was further claimed that this short-term glycolytic flux differs from aerobic glycolysis engaged in actively proliferating cells. Apparently this rapid-induced glycolysis occurs independently of transcriptional and translational modification and does not depend on elevated glucose uptake (Menk et al., 2018). The observed independency of glucose availability of short-term cytokine production reported in this thesis substantiates that hypothesis also for human $CD4^+$ T lymphocytes. Furthermore, my data highlight a general robustness of cytokine production in broad ranges of cellular stress. I identified three conditions that affected cytokine production. These were the presence of DMSO, the combination of glucose deprivation and mitochondrial inhibition (as opposed to either of these alone), and treatment with resveratrol, which was reported to interfere with mitochondrial pathways (Gledhill et al., 2007; Kulkarni and Cantó, 2015; Park et al., 2016). Considering the independence of cytokine production to OXPHOS, the finding using resveratrol is highly interesting. It either suggests an underestimated role of mitochondrial pathways beyond ATP production for effector function or questions the published mechanistic targets of resveratrol.

Based on the conducted experiments, I propose a mechanism of action of resveratrol upstream of mitochondrial pathways. Transcriptional and functional analysis suggested an immune-suppressive effect mediated by inhibition of NFκB signaling. Many beneficial health effects are attributed to resveratrol and it therefore gained a lot of interest also in immune cell biology. Among the beneficial effects are anti-inflammatory properties, protection against oxidative cell damage and induction of tumor cell death as well as reversing obesity-induced metabolic disturbance (de Ligt et al., 2015; Park et al., 2016; Szkudelski and Szkudelska, 2015). The proposed mechanism of action of resveratrol suggests either a direct or indirect interference with mitochondrial pathways. A variety of potential targets of resveratrol were reported. The most frequent discussed targets are complex I or the ATP synthase (Gledhill et al., 2007; Gueguen et al., 2015), interference with mTOR, Sirt1-mediated AMPK activation or inhibition of NFκB signaling (Ma et al., 2015; Park et al., 2016; Price et al., 2012). In particular, a recent analysis by *Craveiro and colleagues* (Craveiro et al., 2017), indicates that resveratrol

activates the deacetylase Sirt1. This showed that high and low concentrations of resveratrol were shown to have opposing effects. The reported high concentration of 100µM resveratrol had toxic effects in the framework of my work and precipitated in DMSO. In the published data, a low concentration of 20µM resulted in increasing expression of Sirt1 and induced genotoxic stress with engagement in DNA damage response pathways. The concomitant activation of p53 in T cells was shown to be linked to a metabolic reprogramming characterized by decreased glycolytic rates and a shift to OXPHOS. They report an antioxidant effect by decreased ROS levels in a high concentration of resveratrol, but showed an increase of ROS at low concentration. They demonstrate a subsequent enhanced effector function of naive and memory $CD4^+$ T cells with increased IFNγ. The data of my thesis highly contradict these findings. First, resveratrol did not affect T cell respiration upon direct injection during extracellular flux analysis. I found decreased ROS production at 50µM of resveratrol, I did not identify a decreased activation capacity which was claimed in their study using 100µM of resveratrol, and in contrast to their findings, I observed a dose-dependent decrease of cytokine secretion. Finally, transcriptional analysis on $CD4^+$ T cell subset in my work did not identify an increase of Sirt1. Instead I found a decrease in expression of various cytokine genes, which further supports the decrease I observed at the protein level. Furthermore, known activators of NFκB were down regulated. Summing up, my data suggest a mechanism of action upstream of mitochondrial function. A direct interference with mitochondrial pathways is unlikely due to maintained metabolic flux after direct injection of resveratrol. Instead 16h of incubation decreases mitochondrial respiration and glycolysis. The dual effectiveness of OXPHOS and glycolysis after long-term incubation first suggests a mechanisms upstream of mitochondrial pathways and further argues against the metabolic shift from OXPHOS towards glycolytic flux proposed by Craveiro et al. Functional analysis revealed a dose-dependent effect on cytokine secretion and proliferation, but no effect on T cell activation. Furthermore, beneficial effects on mitochondrial function as previously reported (Craveiro et al., 2017; Price et al., 2012) is unlikely considering the present data. Solely increased SRC may be advantageous for T cell biology. However, higher SRC levels remained without functional consequences in human $CD4^+$ T cells in the present work.

This thesis provides new insights into the role of ROS in human $CD4^+$ T cells. Inhibition of complex I and ATP synthase increased ROS levels. These findings contradict with previous research, suggesting a decrease of ROS levels upon dysfunctional ETC. ROS are byproducts of aerobic respiration and mostly produced in mitochondria. Different ROS species possess diverse chemical properties that mediate reactivity to different biological targets. High levels of ROS are associated with oxidative stress causing damage in lipids, proteins and DNA. However, ROS is also associated with the induction of signaling pathways. In immune biology, ROS mediated signaling illustrates an interesting example of metabolic mediated signaling (Mehta et al., 2017). It was previously discussed that TCR ligation initiates T cell

activation and induce metabolic remodeling to promote anabolic growth by engaging glycolysis and TCA cycle activity. The initiation of T cell activation requires extended signaling activity and mitochondrial ROS was shown to be an important modulator of this signaling cascade (L. A. Sena et al., 2013; Weinberg et al., 2015). Impairment of complex III of the ETC inhibited the translocation of NFAT to the nucleus and led to an impaired induction of IL-2 production and up regulation of CD25 (L. A. Sena et al., 2013). It was shown that activation impairment was rescued by adding H_2O_2 and that treatment with antioxidants further impaired T cell activation. The inhibition of complex I and ATP synthase in my thesis increased mitochondrial ROS levels. Indeed, ETC dysfunction resulted in impaired activation. I was unable to link this inhibition to decreased ROS levels. Furthermore inhibition of complex III and the subsequent reported impairment of ROS production were dispensable for proliferation process. Instead, I reported impaired proliferation upon inhibition of complex I and ATP synthase accompanied by increased ROS production. This discrepancy is particularly interesting because it either suggests a different importance of complex I and III produced ROS for T cell function or it describes differences in mouse as compared to human T cells. Similar effects of ROS originating from complex I and complex III was suggested, but lacks comprehensive evidences (Kamiński et al., 2012; Mehta et al., 2017; L. A. Sena et al., 2013). Another compelling finding is the maintained activation capacity with lowered ROS levels. As discussed, resveratrol had an antioxidant effect without affecting T cell activation. These results challenge a previous study using a complex III knock-out mice strain, in which decreased ROS levels were linked to impaired activation (L. A. Sena et al., 2013).

An unexpected finding of this thesis and different to findings in mice, was the robustness of T cell function in the presence of fluctuating glucose concentrations. T cells use glucose and glutamine as primary nutrient sources. Especially glucose was shown to be essential for cell survival, growth, activation and cytokine production. A subsequent adequate nutrient balance is needed to engage the metabolism that supports their function (Chang et al., 2013; Cohen et al., 2017; Maciver et al., 2008). However, T cells often operate in environmental conditions where they have to compete for nutrients (Buck et al., 2017; Chang et al., 2015). A scarcity of glucose was associated with mouse T cell hyporesponsiveness (Chang et al., 2015). Activation, proliferation, effector function and cell survival was shown to be impaired (Blagih et al., 2015; Cham et al., 2008; Chang et al., 2013; Maciver et al., 2008). Glucose deprivation inhibited gene expression of IFNγ, TNFα and GM-CSF but not IL-2. Genes involved in cell cycle progression were impaired as well as cytolytic activity in mouse $CD8^+$ T cells. (Cham et al., 2008; Cham and Gajewski, 2005). However, a certain adaptive capacity must be present if T cells are to be effective in sites of inflammation and infection. Indeed it was shown, that murine T cells engage glutamine-dependent OXPHOS to maintain ATP concentration and survival in response to nutrient restriction. However, this metabolic adaptation did not support T cell function (Blagih et al., 2015).

The described sensitivity of T cells in response to glucose starvation was not entirely supported for human T cells by the findings of my thesis. T cell activation and cytokine secretion were shown here to be particularly robust in the presence of low glucose. The current data rather proposes a larger tolerable range of glucose fluctuation for immune function than previously reported for mice. Only proliferation decreased in a dose-dependent manner. Furthermore a lack of glucose not only inhibited glycolysis but also impaired OXPHOS rates. Maintained activation in glucose-free conditions supports the idea that activated T cells do not need glycolysis for the activation process but solely rely on mitochondrial pathways. Activation independency from glycolysis was further suggested by *Sena and colleagues* (L. A. Sena et al., 2013). Pyruvate was shown to bypass glycolysis and maintained T cell activation. Hence glycolysis was suggested to be only crucial for activation as a supplier of pyruvate. Likewise to mitochondrial dysfunction, glycolytic impairment also did not affect short-term cytokine secretion in the scope of this thesis. This is another hint for the independency of cytokine production from main cellular energy resources.

Glucose depletion is only one component of the local environment of immune function. I extended the *in vitro* model of nutrient scarcity and further induced mitochondrial stress. Strikingly, the combination of glucose deprivation and increased cellular stress, measured by increasing ROS concentration highly affected all aspects of T cell function. An exacerbating effect of mitochondrial stress in hypoglycemic conditions was observed. A possible explanation may be the lack of fuel for mitochondrial processes when these are already compromised. Glucose deprivation had a more severe effect on T cell activation when ATP synthase was inhibited compared to complex I, possibly because electrons from $FADH_2$ can still charge the ETC at complex II when complex I is blocked, potentially allowing ATP production. The exacerbated effect on proliferation is expected since it was affected by glucose deprivation, ETC or ATP synthase inhibition alone. In contrast, effector function was unaffected by these conditions, but was strongly affected by low glucose and different kinds of mitochondrial stress. In summary it can be concluded that human $CD4^+$ T cells can function over a wide range of glucose concentrations, but are grossly impaired under conditions of low glucose and cellular stress, which may be encountered in diseases such as diabetes and cancer.

Finally, I revealed a specific sensitivity of naive T cells in the presence of metabolic stress. I showed that memory, naive and regulatory T cells were differently affected by metabolic stress. ETC inhibition strongly affected activation of naïve $CD4^+$ T cells, less so regulatory $CD4^+$ T cells, and minimally, if at all, memory $CD4^+$ T cells. Naive $CD4^+$ T cells had a higher increase of ROS production in the presence of mitochondrial inhibition with or without stimulation, and had more differentially expressed genes than memory $CD4^+$ T cells in the presence of mitochondrial inhibition. Many of these genes were IFN response genes. Regulatory T cells were not sorted into memory and naïve T cells, which may explain their intermediate sensitivity. The maintained cytokine secretion upon mitochondrial dysfunction and

glucose scarcity might be explained by the robustness of memory T cells to these conditions, since cytokine positive cells are almost exclusively memory $CD4^+$ T cells. The underlying molecular mechanisms that may explain subset sensitivity were further analyzed by RNA sequencing. Rotenone and to lesser extend also oligomycin treatment led to a substantial increase of molecular heat shock proteins. Especially naive T cells up regulated a variety of molecular chaperone belonging to the Hsp70 family of heat shock proteins as well as Hsp20, a known chaperone activated in the presence of environmental stress. The increase in heat shock proteins is an induced stress response to the mitochondrial impairment. It confirms the observation of increasing stress levels measured by ROS production and further substantiates the sensitivity of naive T cells.

The thesis presents a detailed analysis, which describes human $CD4^+$ T cell responses to metabolic perturbations. The thesis gained some important findings to fill the gap of the link between metabolic and functional T cell adaptation specifically emphasizing T cell signaling cascades in stress response and IFN signaling. This results are relevant because they are based on human $CD4^+$ T cells, which were shown here to differ in their metabolic requirements in many aspects from murine immune cells. It is hoped that the findings with respect to the different responses to metabolic perturbations at each stage of T cell activation and function, and with respect to different human $CD4^+$ T cell subsets may be of value for developing therapies to correct human T cell responses that give rise to disease.

5 REFERENCES

Adriouch, S., Hubert, S., Pechberty, S., Koch-Nolte, F., Haag, F., Seman, M., 2007. NAD+ Released during Inflammation Participates in T Cell Homeostasis by Inducing ART2-Mediated Death of Naive T Cells In Vivo. J. Immunol. 179, 186–194.

Alayev, A., Berger, S.M., Holz, M.K., 2015. Resveratrol as a novel treatment for diseases with mTOR pathway hyperactivation. Ann. N. Y. Acad. Sci. 1348, 116–123.

Almeida, L., Lochner, M., Berod, L., Sparwasser, T., 2016. Metabolic pathways in T cell activation and lineage differentiation. Semin. Immunol. 28, 1–11.

Andrzejewski, S., Gravel, S.-P., Pollak, M., St-Pierre, J., 2014. Metformin directly acts on mitochondria to alter cellular bioenergetics. Cancer Metab. 2, 12.

Angelin, A., Gil-de-go, L., Dahiya, S., Wallace, D.C., Hancock, W.W., Beier, U.H., 2017. Foxp3 Reprograms T Cell Metabolism to Function in Article Foxp3 Reprograms T Cell Metabolism to Function in Low-Glucose , High-Lactate Environments 1–12.

Araki, K., Turner, A.P., Shaffer, V.O., Gangappa, S., Keller, S.A., Bachmann, M.F., Larsen, C.P., Ahmed, R., 2009. mTOR regulates memory CD8 T-cell differentiation. Nature 460, 108–112.

Arcaro, A., Gregoire, C., Boucheron, N., Stotz, S., Palmer, E., Malissen, B., Luescher, I.F., 2000. Essential Role of CD8 Palmitoylation in CD8 Coreceptor Function. J. Immunol. 165, 2068–2076.

Arpaia, N., Campbell, C., Fan, X., Dikiy, S., Van Der Veeken, J., Deroos, P., Liu, H., Cross, J.R., Pfeffer, K., Coffer, P.J., Rudensky, A.Y., 2013. Metabolites produced by commensal bacteria promote peripheral regulatory T-cell generation. Nature 504, 451–455.

Bai, A., Yong, M., Ma, A.G., Ma, Y., Weiss, C.R., Guan, Q., Bernstein, C.N., Peng, Z., 2010. Novel anti-inflammatory action of 5-aminoimidazole-4-carboxamide ribonucleoside with protective effect in dextran sulfate sodium-induced acute and chronic colitis. J. Pharmacol. Exp. Ther. 333, 717–25.

Balmer, M.L., Ma, E.H., Bantug, G.R., Grählert, J., Pfister, S., Glatter, T., Jauch, A., Dimeloe, S., Slack, E., Dehio, P., Krzyzaniak, M.A., King, C.G., Burgener, A.V., Fischer, M., Develioglu, L., Belle, R., Recher, M., Bonilla, W. V., Macpherson, A.J., Hapfelmeier, S., Jones, R.G., Hess, C., 2016. Memory CD8+ T Cells Require Increased Concentrations of Acetate Induced by Stress for Optimal Function. Immunity 44, 1312–1324.

Bar-Peled, L., Sabatini, D.M., 2014. Regulation of mTORC1 by amino acids. Trends Cell Biol. 24, 400–406.

Battaglia, M., Stabilini, A., Migliavacca, B., Horejs-Hoeck, J., Kaupper, T., Roncarolo, M.-G., 2006. Rapamycin Promotes Expansion of Functional CD4+CD25+FOXP3+ Regulatory T Cells of Both Healthy Subjects and Type 1 Diabetic Patients. J. Immunol. 177, 8338–8347.

Battaglia, M., Stabilini, A., Roncarolo, M.G., 2005. Rapamycin selectively expands CD4+CD25+FoxP3 + regulatory T cells. Blood 105, 4743–4748.

Berg, J.M., Tymoczko, J.L., Stryer, L., Gatto, G.J., 2010. Biochemistry, 7th Editio. ed. W. H. Freeman.

Berod, L., Friedrich, C., Nandan, A., Freitag, J., Hagemann, S., Harmrolfs, K., Sandouk, A., Hesse, C., Castro, C.N., Bähre, H., Tschirner, S.K., Gorinski, N., Gohmert, M., Mayer, C.T., Huehn, J., Ponimaskin, E., Abraham, W.-R., Müller, R., Lochner, M., Sparwasser, T., 2014. De novo fatty acid synthesis controls the fate between regulatory T and T helper 17 cells. Nat. Med. 20, 1327–1333.

Birsoy, K., Wang, T., Chen, W.W., Freinkman, E., Abu-Remaileh, M., Sabatini, D.M., 2015. An Essential Role of the Mitochondrial Electron Transport Chain in Cell Proliferation Is to Enable Aspartate Synthesis. Cell 162, 540–551.

Blagih, J., Coulombe, F., Vincent, E.E., Dupuy, F., Galicia-Vázquez, G., Yurchenko, E., Raissi, T.C., van der Windt, G.J.W., Viollet, B., Pearce, E.L., Pelletier, J., Piccirillo, C.A., Krawczyk, C.M., Divangahi, M., Jones, R.G., 2015. The Energy Sensor AMPK Regulates T Cell Metabolic Adaptation and Effector Responses In Vivo. Immunity 42, 41–54.

Brown, E.J., Albers, M.W., Shin, T.B., Ichikawa, K., Keith, C.T., Lane, W.S., Schreiber, S.L., 1994. A mammalian protein targeted by G1-arresting rapamycin-receptor complex. Nature 369, 756–758.

Buck, M.D., O'Sullivan, D., Pearce, E.L., 2015. T cell metabolism drives immunity. J. Exp. Med. 212,

1345–1360.
Buck, M.D., Sowell, R.T., Kaech, S.M., Pearce, E.L., 2017. Metabolic Instruction of Immunity. Cell 169, 570–586.
Buck, M.D.D., O'Sullivan, D., Klein Geltink, R.I.I., Curtis, J.D.D., Chang, C.H., Sanin, D.E.E., Qiu, J., Kretz, O., Braas, D., van der Windt, G.J.J.W., Chen, Q., Huang, S.C.C., O'Neill, C.M.M., Edelson, B.T.T., Pearce, E.J.J., Sesaki, H., Huber, T.B.B., Rambold, A.S.S., Pearce, E.L.L., 2016. Mitochondrial Dynamics Controls T Cell Fate through Metabolic Programming. Cell 166, 63–76.
Cham, C.M., Driessens, G., O'Keefe, J.P., Gajewski, T.F., 2008. Glucose deprivation inhibits multiple key gene expression events and effector functions in CD8+ T cells. Eur. J. Immunol. 38, 2438–2450.
Cham, C.M., Gajewski, T.F., 2005. Glucose Availability Regulates IFN- Production and p70S6 Kinase Activation in CD8+ Effector T Cells. J. Immunol. 174, 4670–4677.
Chandel, N.S., 2015. Evolution of Mitochondria as Signaling Organelles. Cell Metab. 22, 204–206.
Chang, C.H., Curtis, J.D., Maggi, L.B., Faubert, B., Villarino, A. V., O'Sullivan, D., Huang, S.C.C., Van Der Windt, G.J.W., Blagih, J., Qiu, J., Weber, J.D., Pearce, E.J., Jones, R.G., Pearce, E.L., 2013. Posttranscriptional control of T cell effector function by aerobic glycolysis. Cell 153, 1239–1251.
Chang, C.H., Qiu, J., O'Sullivan, D., Buck, M.D., Noguchi, T., Curtis, J.D., Chen, Q., Gindin, M., Gubin, M.M., Van Der Windt, G.J.W., Tonc, E., Schreiber, R.D., Pearce, E.J., Pearce, E.L., 2015. Metabolic Competition in the Tumor Microenvironment Is a Driver of Cancer Progression. Cell 162, 1229–1241.
Chantranupong, L., Scaria, S.M., Saxton, R.A., Gygi, M.P., Shen, K., Wyant, G.A., Wang, T., Harper, J.W., Gygi, S.P., Sabatini, D.M., 2016. The CASTOR Proteins Are Arginine Sensors for the mTORC1 Pathway. Cell 165, 153–164.
Clever, D., Roychoudhuri, R., Constantinides, M.G., Askenase, M.H., Sukumar, M., Klebanoff, C.A., Eil, R.L., Hickman, H.D., Yu, Z., Pan, J.H., Palmer, D.C., Phan, A.T., Goulding, J., Gattinoni, L., Goldrath, A.W., Belkaid, Y., Restifo, N.P., 2016. Oxygen Sensing by T Cells Establishes an Immunologically Tolerant Metastatic Niche. Cell 166, 1117–1131.e14.
Cohen, S., Danzaki, K., MacIver, N.J., 2017. Nutritional effects on T-cell immunometabolism. Eur. J. Immunol. 47, 225–235.
Craveiro, M., Cretenet, G., Mongellaz, C., Matias, M.I., Caron, O., de Lima, M.C.P., Zimmermann, V.S., Solary, E., Dardalhon, V., Dulić, V., Taylor, N., 2017. Resveratrol stimulates the metabolic reprogramming of human CD4 + T cells to enhance effector function. Sci Signal 10, eaal3024.
Crise, B., Rose, J.K., 1992. Identificationof palmitoylation sites on CD4, the human immunodeficiency virus receptor. J. Biol. Chem. 267, 13593–13597.
Dang, E. V., Barbi, J., Yang, H.Y., Jinasena, D., Yu, H., Zheng, Y., Bordman, Z., Fu, J., Kim, Y., Yen, H.R., Luo, W., Zeller, K., Shimoda, L., Topalian, S.L., Semenza, G.L., Dang, C. V., Pardoll, D.M., Pan, F., 2011. Control of TH17/Treg balance by hypoxia-inducible factor 1. Cell 146, 772–784.
de Ligt, M., Timmers, S., Schrauwen, P., 2015. Resveratrol and obesity: Can resveratrol relieve metabolic disturbances? Biochim. Biophys. Acta 1852, 1137–1144.
DeBerardinis, R.J., Lum, J.J., Thompson, C.B., 2006. Phosphatidylinositol 3-kinase-dependent modulation of carnitine palmitoyltransferase 1A expression regulates lipid metabolism during hematopoietic cell growth. J. Biol. Chem. 281, 37372–37380.
Delgoffe, G.M., Kole, T.P., Zheng, Y., Zarek, P.E., Matthews, K.L., Xiao, B., Worley, P.F., Kozma, S.C., Powell, J.D., 2009. The mTOR Kinase Differentially Regulates Effector and Regulatory T Cell Lineage Commitment. Immunity 30, 832–844.
Delgoffe, G.M., Pollizzi, K.N., Waickman, A.T., Heikamp, E., Meyers, D.J., Horton, M.R., Xiao, B., Worley, P.F., Powell, J.D., 2011. The kinase mTOR regulates the differentiation of helper T cells through the selective activation of signaling by mTORC1 and mTORC2. Nat. Immunol. 12, 295–304.
Desdín-Micó, G., Soto-Heredero, G., Mittelbrunn, M., 2018. Mitochondrial activity in T cells. Mitochondrion 41, 51–57.
Di Virgilio, F., Vuerich, M., 2015. Purinergic signaling in the immune system. Auton. Neurosci. Basic Clin. 191, 117–123.
Dimeloe, S., Burgener, A.V., Grählert, J., Hess, C., 2017. T-cell metabolism governing activation,

proliferation and differentiation; a modular view. Immunology 150, 35–44.

Dimeloe, S., Mehling, M., Frick, C., Loeliger, J., Bantug, G.R., Sauder, U., Fischer, M., Belle, R., Develioglu, L., Tay, S., Langenkamp, A., Hess, C., 2016. The Immune-Metabolic Basis of Effector Memory CD4 T Cell Function under Hypoxic Conditions. J. Immunol. 196, 106–114.

Divakaruni;, A.S., Paradyse;, A., Ferrick;, D.A., Murphy;, A.N., Jastroch;, M., 2014. Analysis and Interpretation of Microplate-Based Oxygen Consumption and pH Data. Methods Enzym. 547, 309–354.

Efeyan, A., Comb, W.C., Sabatini, D.M., 2015. Nutrient-sensing mechanisms and pathways. Nature 517, 302–310.

Endo, Y., Asou, H.K., Matsugae, N., Hirahara, K., Shinoda, K., Tumes, D.J., Tokuyama, H., Yokote, K., Nakayama, T., 2015. Obesity drives Th17 cell differentiation by inducing the lipid metabolic kinase, ACC1. Cell Rep. 12, 1042–1055.

Fabregat, A., Jupe, S., Matthews, L., Sidiropoulos, K., Gillespie, M., Garapati, P., Haw, R., Jassal, B., Korninger, F., May, B., Milacic, M., Roca, C.D., Rothfels, K., Sevilla, C., Shamovsky, V., Shorser, S., Varusai, T., Viteri, G., Weiser, J., Wu, G., Stein, L., Hermjakob, H., D'Eustachio, P., 2018. The Reactome Pathway Knowledgebase. Nucleic Acids Res. 46, D649–D655.

Fox, C.J., Hammerman, P.S., Thompson, C.B., 2005. Fuel feeds function: Energy metabolism and the T-cell response. Nat. Rev. Immunol.

Frauwirth, K.A., Riley, J.L., Harris, M.H., Parry, R. V, Rathmell, J.C., Plas, D.R., Elstrom, R.L., June, C.H., Thompson, C.B., 2002. The CD28 Signaling Pathway Regulates Glucose Metabolism 16, 769–777.

Gaud, G., Lesourne, R., Love, P.E., 2018. Regulatory mechanisms in T cell receptor signalling. Nat. Rev. Immunol. 18, 485–497.

Gaude, E., Schmidt, C., Gammage, P.A., Dugourd, A., Blacker, T., Chew, S.P., Saez-Rodriguez, J., O'Neill, J.S., Szabadkai, G., Minczuk, M., Frezza, C., 2018. NADH Shuttling Couples Cytosolic Reductive Carboxylation of Glutamine with Glycolysis in Cells with Mitochondrial Dysfunction. Mol. Cell 69, 648–663.e7.

Gerriets, V., Kishton, R., 2014. Metabolic programming and PDHK1 control CD4+ T cell subsets and inflammation. J. Clin. Invest. 125, 1–14.

Gledhill, J.R., Montgomery, M.G., Leslie, A.G.W., Walker, J.E., 2007. Mechanism of inhibition of bovine F1-ATPase by resveratrol and related polyphenols. Proc. Natl. Acad. Sci. U. S. A. 104, 13632–7.

Gualdoni, G.A., Mayer, K.A., Göschl, L., Boucheron, N., Ellmeier, W., Zlabinger, G.J., 2016. The AMP analog AICAR modulates the Treg/Th17 axis through enhancement of fatty acid oxidation. FASEB J. 30, 3800–3809.

Gueguen, N., Desquiret-Dumas, V., Leman, G., Chupin, S., Baron, S., Nivet-Antoine, V., Vessières, E., Ayer, A., Henrion, D., Lenaers, G., Reynier, P., Procaccio, V., 2015. Resveratrol directly binds to mitochondrial complex i and increases oxidative stress in brain mitochondria of aged mice. PLoS One 10, 1–19.

Harris, M., 1980. Pyruvate blocks expression of sensitivity to antimycin A and chloramphenicol. Somatic Cell Genet. 6, 699–708.

Hirayama, A., Kami, K., Sugimoto, M., Sugawara, M., Toki, N., Onozuka, H., Kinoshita, T., Saito, N., Ochiai, A., Tomita, M., Esumi, H., Soga, T., 2009. Quantitative metabolome profiling of colon and stomach cancer microenvironment by capillary electrophoresis time-of-flight mass spectrometry. Cancer Res. 69, 4918–4925.

Holthaus, L., Lamp, D., Gavrisan, A., Sharma, V., Ziegler, A., Jastroch, M., Bonifacio, E., 2018. CD4+ T cell activation, function, and metabolism are inhibited by low concentrations of DMSO. J. Immunol. Methods 463, 54–60.

Hubert, S., Rissiek, B., Klages, K., Huehn, J., Sparwasser, T., Haag, F., Koch-Nolte, F., Boyer, O., Seman, M., Adriouch, S., 2010. Extracellular NAD shapes the Foxp3 regulatory T cell compartment through the ART2 P2X7 pathway. J. Exp. Med. 207, 2561–2568.

Jaakkola, P., Mole, D.R., Tian, Y.-M., Wilson, M.I., Gielbert, J., Gaskell, S.J., Kriegsheim, A. v., Hebestreit, H.F., Mukherji, M., Schofield, C.J., Maxwell, P.H., Pugh, C.W., Ratcliffe, P.J., 2001. Targeting of HIF-alpha to the von Hippel-Lindau Ubiquitylation Complex by O2-Regulated Prolyl Hydroxylation.

Science (80-.). 292, 468–472.
Jacobs, S.R., Herman, C.E., Maciver, N.J., Wofford, J. a, Wieman, H.L., Hammen, J.J., Rathmell, J.C., 2008. Glucose uptake is limiting in T cell activation and requires CD28-mediated Akt-dependent and independent pathways. J. Immunol. 180, 4476–4486.
Kamiński, M.M., Sauer, S.W., Kamiński, M., Opp, S., Ruppert, T., Grigaravičius, P., Grudnik, P., Gröne, H.J., Krammer, P.H., Gülow, K., 2012. T cell Activation Is Driven by an ADP-Dependent Glucokinase Linking Enhanced Glycolysis with Mitochondrial Reactive Oxygen Species Generation. Cell Rep. 2, 1300–1315.
Kang, K.Y., Kim, Y.K., Yi, H., Kim, J., Jung, H.R., Kim, I.J., Cho, J.H., Park, S.H., Kim, H.Y., Ju, J.H., 2013. Metformin downregulates Th17 cells differentiation and attenuates murine autoimmune arthritis. Int. Immunopharmacol. 16, 85–92.
Kaveh, D.A., Whelan, A.O., Hogarth, P.J., 2012. The duration of antigen-stimulation significantly alters the diversity of multifunctional CD4 T cells measured by intracellular cytokine staining. PLoS One 7.
Kelly, B., Neill, L.A.J.O., 2015. Metabolic reprogramming in macrophages and dendritic cells in innate immunity. Nat. Publ. Gr. 25, 771–784.
Keuper, M., Jastroch, M., Yi, C.X., Fischer-Posovszky, P., Wabitsch, M., Tschöp, M.H., Hofmann, S.M., 2014. Spare mitochondrial respiratory capacity permits human adipocytes to maintain ATP homeostasis under hypoglycemic conditions. FASEB J. 28, 761–770.
Khan, M., Syed, G.H., Kim, S.J., Siddiqui, A., 2015. Mitochondrial dynamics and viral infections: A close nexus. Biochim. Biophys. Acta - Mol. Cell Res. 1853, 2822–2833.
Kidani, Y., Elsaesser, H., Hock, M.B., Vergnes, L., Williams, K.J., Argus, J.P., Marbois, B.N., Komisopoulou, E., Wilson, E.B., Osborne, T.F., Graeber, T.G., Reue, K., Brooks, D.G., Bensinger, S.J., 2013. Sterol regulatory element-binding proteins are essential for the metabolic programming of effector T cells and adaptive immunity. Nat. Immunol. 14, 489–499.
Kim, J.W., Dang, C. V., 2006. Cancer's molecular sweet tooth and the warburg effect. Cancer Res.
Kim, S.G., Buel, G.R., Blenis, J., 2013. Nutrient regulation of the mTOR complex 1 signaling pathway. Mol. Cells.
King, M., Attardi, G., 1989. Human cells lacking mtDNA: repopulation with exogenous mitochondria by complementation. Science (80-.). 246, 500–503.
Klein Geltink, R.I., Kyle, R.L., Pearce, E.L., 2018. Unraveling the Complex Interplay Between T Cell Metabolism and Function. Annu. Rev. Immunol. 36, 461–488.
Koegl, M., Zlatkine, P., Ley, S.C., Courtneidge, S.A., Magee, A.I., 1994. Palmitoylation of multiple Src-family kinases at a homologous N-terminal motif. Biochem. J. 303 (Pt 3, 749–53.
Kulkarni, S.S., Cantó, C., 2015. The molecular targets of resveratrol. Biochim. Biophys. Acta - Mol. Basis Dis. 1852, 1114–1123.
Kurebayashi, Y., Nagai, S., Ikejiri, A., Ohtani, M., Ichiyama, K., Baba, Y., Yamada, T., Egami, S., Hoshii, T., Hirao, A., Matsuda, S., Koyasu, S., 2012. PI3K-Akt-mTORC1-S6K1/2 Axis Controls Th17 Differentiation by Regulating Gfi1 Expression and Nuclear Translocation of RORγ. Cell Rep. 1, 360–373.
Ladygina, N., Martin, B.R., Altman, A., 2011. Dynamic Palmitoylation and the Role of DHHC Proteins in T Cell Activation and Anergy. Adv. Immunol. 109, 1–44. h
Laplante, M., Sabatini, D.M., 2012. MTOR signaling in growth control and disease. Cell.
Ledderose, C., Bao, Y., Lidicky, M., Zipperle, J., Li, L., Strasser, K., Shapiro, N.I., Junger, W.G., 2014. Mitochondria are gate-keepers of T cell function by producing the ATP that drives purinergic signaling. J. Biol. Chem. 289, 25936–25945.
Lee, K., Gudapati, P., Dragovic, S., Spencer, C., Joyce, S., Killeen, N., Magnuson, M.A., Boothby, M., 2010. Mammalian target of rapamycin protein complex 2 regulates differentiation of Th1 and Th2 cell subsets via distinct signaling pathways. Immunity 32, 743–753.
Liemburg-Apers, D.C., Schirris, T.J.J., Russel, F.G.M., Willems, P.H.G.M., Koopman, W.J.H., 2015. Mitoenergetic Dysfunction Triggers a Rapid Compensatory Increase in Steady-State Glucose Flux. Biophys. J. 109, 1372–1386.

Lochner, M., Berod, L., Sparwasser, T., 2015. Fatty acid metabolism in the regulation of T cell function. Trends Immunol. 1–11.

Lunt, S.Y., Vander Heiden, M.G., 2011. Aerobic Glycolysis: Meeting the Metabolic Requirements of Cell Proliferation. Annu. Rev. Cell Dev. Biol. 27, 441–464.

Ma, C., Wang, Y., Dong, L., Li, M., Cai, W., 2015. Anti-inflammatory effect of resveratrol through the suppression of NF-κB and JAK/STAT signaling pathways. Acta Biochim. Biophys. Sin. (Shanghai). 47, 207–213.

Macintvre, A.N., Gerriets, V. a, Able, E., Rathmell, J.C., 2012. Glucose uptake via GLUT1 maintains T cell survival during proliferative stress. BMC Proc. 6, P33.

Maciolek, J. a., Alex Pasternak, J., Wilson, H.L., 2014. Metabolism of activated T lymphocytes. Curr. Opin. Immunol. 27, 60–74.

Maciver, N.J., Jacobs, S.R., Wieman, H.L., Wofford, J. a, Coloff, J.L., Rathmell, J.C., 2008. Glucose metabolism in lymphocytes is a regulated process with significant effects on immune cell function and survival. J. Leukoc. Biol. 84, 949–957.

Mayer, A., Denanglaire, S., Viollet, B., Leo, O., Andris, F., 2008. AMP-activated protein kinase regulates lymphocyte responses to metabolic stress but is largely dispensable for immune cell development and function. Eur. J. Immunol. 38, 948–956.

Mehta, M.M., Weinberg, S.E., Chandel, N.S., 2017. Mitochondrial control of immunity: beyond ATP. Nat. Rev. Immunol.

Menk, A. V., Scharping, N.E., Moreci, R.S., Zeng, X., Guy, C., Salvatore, S., Bae, H., Xie, J., Young, H.A., Wendell, S.G., Delgoffe, G.M., 2018. Early TCR Signaling Induces Rapid Aerobic Glycolysis Enabling Distinct Acute T Cell Effector Functions. Cell Rep. 22, 1509–1521.

Michalek, R.D., Gerriets, V.A., Jacobs, S.R., Macintyre, A.N., MacIver, N.J., Mason, E.F., Sullivan, S.A., Nichols, A.G., Rathmell, J.C., 2011. Cutting Edge: Distinct Glycolytic and Lipid Oxidative Metabolic Programs Are Essential for Effector and Regulatory CD4+ T Cell Subsets. J. Immunol. 186, 3299–3303.

Murphy, K., 2012. Janeway's immunobiology 8th edition, 8th ed. Garland Science, Taylor and Francis Group, New York.

Murphy, K.P., 2011a. Janeway's Immunobiology, 8th ed. Garland Science, Taylor and Francis Group.

Murphy, K.P., 2011b. Janeway's Immunobiology - T cell-Mediated Immunity, in: Janeway's Immunobiology. p. 888.

Nath, N., Giri, S., Prasad, R., Salem, M.L., Singh, A.K., Singh, I., 2005. 5-Aminoimidazole-4-Carboxamide Ribonucleoside: A Novel Immunomodulator with Therapeutic Efficacy in Experimental Autoimmune Encephalomyelitis. J. Immunol. 175, 566–574.

Nomura, L.E., Walker, J.M., Maecker, H.T., 2000. Optimization of whole blood antigen-specific cytokine assays for CD4+ T cells. Cytometry 40, 60–68.

Nordlie, R.C., Foster, J.D., Lange, A.J., 1999. Regulation of Glucose Production By the Liver. Annu. Rev. Nutr. 19, 379–406.

O'Neill, L.A.J., Kishton, R.J., Rathmell, J.C., 2016. A guide to immunometabolism for immunologists. Nat. Rev. Immunol.

O'Neill, L.A.J., Pearce, E.J., 2015. Immunometabolism governs dendritic cell and macrophage function. J. Exp. Med. jem.20151570.

O'Sullivan, D., Van der Windt, G.W.J., Huang, S.C.C., Curtis, J.D., Chang, C.H., Buck, M.D.L., Qiu, J., Smith, A.M., Lam, W.Y., DiPlato, L.M., Hsu, F.F., Birnbaum, M.J., Pearce, E.J., Pearce, E.L., 2014. Memory CD8 T Cells Use Cell-Intrinsic Lipolysis to Support the Metabolic Programming Necessary for Development. Immunity 41, 75–88.

Olenchock, B.A., Rathmell, J.C., Vander Heiden, M.G., 2017. Biochemical Underpinnings of Immune Cell Metabolic Phenotypes. Immunity 46, 703–713.

Palmer, C.S., Ostrowski, M., Balderson, B., Christian, N., Crowe, S.M., 2015. Glucose metabolism regulates T cell activation, differentiation, and functions. Front. Immunol. 6, 1–6.

Park, D., Jeong, H., Lee, M.N., Koh, A., Kwon, O., Yang, Y.R., Noh, J., Suh, P.-G., Park, H., Ryu, S.H., 2016. Resveratrol induces autophagy by directly inhibiting mTOR through ATP competition. Sci. Rep. 6,

21772.
Pavlova, N.N., Thompson, C.B., 2016. The Emerging Hallmarks of Cancer Metabolism. Cell Metab. 23, 27–47.
Pearce, E., Pearce, E., 2013. Metabolic pathways in immune cell activation and quiescence. Immunity 38, 633–643.
Pearce, E.L., Poffenberger, M.C., Chang, C.-H., Jones, R.G., 2013. Fueling immunity: insights into metabolism and lymphocyte function. Science 342, 1242454.
Pearce, E.L., Walsh, M.C., Cejas, P.J., Harms, G.M., Shen, H., Wang, L.-S., Jones, R.G., Choi, Y., 2009. Enhancing CD8 T-cell memory by modulating fatty acid metabolism. Nature 460, 103–107.
Peng, M., Peng, M., Yin, N., Chhangawala, S., Xu, K., Leslie, C.S., Li, M.O., 2016. Aerobic glycolysis promotes T helper 1 cell differentiation through an epigenetic mechanism. Science (80-.). 6284, 481–485.
Pollizzi, K.N., Powell, J.D., 2015. Regulation of T cells by mTOR: The known knowns and the known unknowns. Trends Immunol. 36, 13–20.
Price, N.L., Gomes, A.P., Ling, A.J.Y., Duarte, F. V., Martin-Montalvo, A., North, B.J., Agarwal, B., Ye, L., Ramadori, G., Teodoro, J.S., Hubbard, B.P., Varela, A.T., Davis, J.G., Varamini, B., Hafner, A., Moaddel, R., Rolo, A.P., Coppari, R., Palmeira, C.M., De Cabo, R., Baur, J.A., Sinclair, D.A., 2012. SIRT1 is required for AMPK activation and the beneficial effects of resveratrol on mitochondrial function. Cell Metab. 15, 675–690.
Printz, R.L., Magnuson, M.A., Granner, D.K., 1993. Mammalian Glucokinase. Annu. Rev. Nutr. 463–496.
Rambold, A.S., Pearce, E.L., 2018. Mitochondrial Dynamics at the Interface of Immune Cell Metabolism and Function. Trends Immunol. 39, 6–18.
Rao, R.R., Li, Q., Odunsi, K., Shrikant, P.A., 2010. The mTOR Kinase Determines Effector versus Memory CD8+T Cell Fate by Regulating the Expression of Transcription Factors T-bet and Eomesodermin. Immunity 32, 67–78.
Rolf, J., Zarrouk, M., Finlay, D.K., Foretz, M., Viollet, B., Cantrell, D.A., 2013. AMPKα1: A glucose sensor that controls CD8 T-cell memory. Eur. J. Immunol. 43, 889–896.
Ron-Harel, N., Santos, D., Ghergurovich, J.M., Sage, P.T., Reddy, A., Lovitch, S.B., Dephoure, N., Satterstrom, F.K., Sheffer, M., Spinelli, J.B., Gygi, S., Rabinowitz, J.D., Sharpe, A.H., Haigis, M.C., 2016. Mitochondrial Biogenesis and Proteome Remodeling Promote One-Carbon Metabolism for T Cell Activation. Cell Metab. 24, 104–117.
Schenk, U., Westendorf, A.M., Radaelli, E., Casati, A., Ferro, M., Verderio, C., Buer, J., Scanziani, E., Grassi, F., 2008. Supplementary Materials for Purinergic Control of T Cell Activation by ATP Released Through. Analysis 1, 3–8.
Seman, M., Adriouch, S., Scheuplein, F., Krebs, C., Freese, D., Glowacki, G., Deterre, P., Haag, F., Koch-Nolte, F., 2003. NAD-induced T cell death: ADP-ribosylation of cell surface proteins by ART2 activates the cytolytic P2X7 purinoceptor. Immunity 19, 571–582.
Sena, L., Chandel, N., 2012. Physiological roles of mitochondrial reactive oxygen species. Mol. Cell 48, 158–167.
Sena, L., Li, S., Jairaman, A., Prakriya, M., 2013. Mitochondria are required for antigen-specific T cell activation through reactive oxygen species signaling. Immunity 38, 225–236.
Sena, L.A., Li, S., Jairaman, A., Prakriya, M., Ezponda, T., Hildeman, D.A., Wang, C.R., Schumacker, P.T., Licht, J.D., Perlman, H., Bryce, P.J., Chandel, N.S., 2013. Mitochondria Are Required for Antigen-Specific T Cell Activation through Reactive Oxygen Species Signaling. Immunity 38, 225–236.
Shi, L.Z., Wang, R., Huang, G., Vogel, P., Neale, G., Green, D.R., Chi, H., 2011. HIF1α–dependent glycolytic pathway orchestrates a metabolic checkpoint for the differentiation of $T_{H}17$ and T_{reg} cells. J. Exp. Med. 208, 1367–1376.
Smith-Garvin, J., Koretzky, G., 2009. T cell activation. Annu. Rev. Immunol. 27, 591–619.
Smith, P.M., Howitt, M.R., Panikov, N., Michaud, M., Gallini, C.A., Bohlooly-Y, M., Glickman, J.N., Garrett, W.S., 2013. The Microbial Metabolites, Short-Chain Fatty Acids, Regulate Colonic Treg Cell Homeostasis. Sci. Reports 569–574.
Son, H.J., Lee, J., Lee, S.Y., Kim, E.K., Park, M.J., Kim, K.W., Park, S.H., Cho, M. La, 2014. Metformin

attenuates experimental autoimmune arthritis through reciprocal regulation of Th17/Treg balance and osteoclastogenesis. Mediators Inflamm. 2014.

Sullivan, L.B., Gui, D.Y., Hosios, A.M., Bush, L.N., Freinkman, E., Vander Heiden, M.G., 2015. Supporting Aspartate Biosynthesis Is an Essential Function of Respiration in Proliferating Cells. Cell 162, 552–563.

Swamy, M., Pathak, S., Grzes, K.M., Damerow, S., Sinclair, L. V., Van Aalten, D.M.F., Cantrell, D.A., 2016. Glucose and glutamine fuel protein O-GlcNAcylation to control T cell self-renewal and malignancy. Nat. Immunol. 17, 712–720.

Szkudelski, T., Szkudelska, K., 2015. Resveratrol and diabetes: From animal to human studies. Biochim. Biophys. Acta - Mol. Basis Dis. 1852, 1145–1154.

Thorens, B., Mueckler, M., 2010. Glucose transporters in the 21st Century. Am. J. Physiol. Endocrinol. Metab. 298, E141-5.

van der Windt, G.J.W., O'Sullivan, D., Everts, B., Huang, S.C.-C., Buck, M.D., Curtis, J.D., Chang, C.-H., Smith, A.M., Ai, T., Faubert, B., Jones, R.G., Pearce, E.J., Pearce, E.L., 2013. CD8 memory T cells have a bioenergetic advantage that underlies their rapid recall ability. Proc. Natl. Acad. Sci. 110, 14336–14341.

Waickman, A.T., Powell, J.D., 2012. Mammalian Target of Rapamycin Integrates Diverse Inputs To Guide the Outcome of Antigen Recognition in T Cells. J. Immunol. 188, 4721–4729.

Wakil, S.J., Abu-Elheiga, L.A., 2009. Fatty acid metabolism: target for metabolic syndrome. J. Lipid Res. 50, S138–S143.

Walls, J., Sinclair, L., Finlay, D., 2016. Nutrient sensing, signal transduction and immune responses. Semin. Immunol. 28, 396–407.

Wang, R., Dillon, C.P., Shi, L.Z., Milasta, S., Carter, R., Finkelstein, D., McCormick, L.L., Fitzgerald, P., Chi, H., Munger, J., Green, D.R., 2011. The Transcription Factor Myc Controls Metabolic Reprogramming upon T Lymphocyte Activation. Immunity 35, 871–882.

Wang, R., Dillon, C.P., Shi, L.Z., Milasta, S., Finkelstein, D., Mccormick, L.L., Fitzgerald, P., Chi, H., Munger, J., Green, D.R., 2012. NIH Public Access 35, 871–882.

Ward, C., 2015. Fatty Acid Oxidation and Synthesis [WWW Document]. Diapedia. https://doi.org/https://doi.org/10.14496/dia.5105592814.23

Wei, J., Raynor, J., Nguyen, T.L.M., Chi, H., 2017. Nutrient and metabolic sensing in T cell responses. Front. Immunol. 8, 1–14.

Weinberg, S.E., Sena, L.A., Chandel, N.S., 2015. Mitochondria in the regulation of innate and adaptive immunity. Immunity 42, 406–417.

Wheaton, W.W., Weinberg, S.E., Hamanaka, R.B., Soberanes, S., Sullivan, L.B., Anso, E., Glasauer, A., Dufour, E., Mutlu, G.M., Scott Budigner, G.R., Chandel, N.S., 2014. Metformin inhibits mitochondrial complex I of cancer cells to reduce tumorigenesis. Elife 2014, 1–18.

Yang, K., Shrestha, S., Zeng, H., Karmaus, P.W.F., Neale, G., Vogel, P., Guertin, D. a., Lamb, R.F., Chi, H., 2013. T Cell Exit from Quiescence and Differentiation into Th2 Cells Depend on Raptor-mTORC1-Mediated Metabolic Reprogramming. Immunity 39, 1043–1056.

Yusuf, I., Fruman, D.A., 2003. Regulation of quiescence in lymphocytes. Trends Immunol. h

Zeng, H., Yang, K., Cloer, C., Neale, G., Vogel, P., Chi, H., 2013. MTORC1 couples immune signals and metabolic programming to establish Treg-cell function. Nature 499, 485–490.

Zhao, D., Long, X.D., Lu, T.F., Wang, T., Zhang, W.W., Liu, Y.X., Cui, X.L., Dai, H.J., Xue, F., Xia, Q., 2015. Metformin decreases IL-22 secretion to suppress tumor growth in an orthotopic mouse model of hepatocellular carcinoma. Int. J. Cancer 136, 2556–2565.

Zhu, J., Yamane, H., Paul, W.E., 2010. Differentiation of effector CD4 T cell populations (*). Annu. Rev. Immunol. 28, 445–489.

6 ACKNOWLEDGMENT

An dieser Stelle möchte ich meinen besonderen Dank nachstehenden Personen entgegen bringen, ohne deren Mithilfe die Anfertigung dieser Promotion nicht möglich gewesen wäre.

Mein ganz besonderer Dank gilt zunächst meinem Mentor Herrn Prof. Dr. Ezio Bonifacio, für die außergewöhnliche Betreuung, den steten konstruktiven und kreativen Austausch, der mir einen kritischen Zugang zu dem Thema ermöglichte. Vielen Dank für den Enthusiasmus und die Motivation für mein Promotionsthema.

Weiterhin möchte ich ganz besonders Frau Prof. Dr. Anette-Gabriele Ziegler für die Betreuung meiner Doktorarbeit danken. Vielen Dank für die hilfreichen Diskussionen und der kritischen Auseinandersetzung. Ich habe unglaublich viel gelernt in dieser Zeit.

Ich bedanke mich ganz herzlich auch bei Prof. Dr. Martin Hrabě de Angelis für die Betreuung meiner Doktorarbeit als Zweitbetreuer, für das Feedback und die interessanten Diskussionen in den Thesis Committee Meetings.

Ferner Danke ich Dr. Martin Jastroch für die vielen hilfreichen und vor allem lehrreichen Diskussionen und den konstruktiven Ideen zum Thema. In diesem Rahmen möchte ich mich ebenfalls bei Daniel Lamp für seine Mithilfe, Geduld und Ideenreichtum bei der Etablierung der metabolischen Experimente bedanken.

Weiterhin wäre diese Arbeit in dieser Form nicht möglich gewesen ohne die Hilfe der Mitarbeiter des IDF1. Danke für alle Blutabnahmen, Blutspenden sowie jegliche Unterstützung im Labor. Besonders möchte ich hierbei Anita, Marlon, Lorena, Cigdem, Lisa, Christina und Rainer danken. Ein spezieller Dank gilt ebenfalls allen StudienbetreuerInnen, ÄrztInnen und natürlich den StudienteilnehmerInnen.

In diesem Rahmen möchte ich auch meine Kolleginnen am CRTD Julia, Maria und Anne nennen. Ganz besonders möchte ich mich bei Dr. Virag Sharma für seine kompetente Analyse meiner RNAseq Daten bedanken.

Ein ganz besonderes Dankschön gilt an dieser Stelle meinen grandiosen und wunderbaren PhD-Kollegen und Freunden Martin, Jan und Markus. Ihr seid die Besten, vielen Dank für die unvergessliche Zeit!

Tief verbunden und Dankbar bin ich meinen Eltern, meiner Schwester und meinem Freund. Vielen Dank für eure Unterstützung, Geduld und Motivation. Danke, dass ihr immer für mich da seid und ich mich immer auf Euch verlassen kann.

7 APPENDIX

Table 13: Down regulated genes involved in cytokine-chemokine signaling in memory, naive and regulatory T cells in the presence of Resveratrol.

Gene Symbol	Memory T cells			Naive T cells			Regulatory T cells		
	Log2FoldChange	p-value	p-value adjusted	Log2FoldChange	p-value	p-value adjusted	Log2FoldChange	p-value	p-value adjusted
IL10	-3,350891458	1,07204E-05	0,000154828	-3,473896282	4,45527E-08	5,82009E-06	-2,980605077	3,71788E-06	0,000155554
IL3	-1,512468088	0,000135559	0,001269324	-3,102316958	2,46856E-12	1,13634E-09	-1,269545675	1,65541E-09	2,15558E-07
IL17F	-2,670010404	1,30192E-95	1,72986E-91				-1,681910508	1,5486E-11	3,29361E-09
IL26	-2,770280386	7,3165E-18	2,20942E-15						
IL31							-1,453544213	0,000229431	0,00386759
IL22	-2,143263591	2,68986E-18	9,16415E-16				-1,392697788	6,10466E-13	1,98407E-10
IL21				-1,072969142	3,22887E-05	0,001571015			
IFNG				-1,573281184	1,46649E-11	5,23171E-09			
IL2				-1,191403479	1,40414E-14	1,11317E-11			
IL18RAP				-1,594026636	1,15299E-17	2,74219E-14	-1,192976939	2,61102E-15	1,23404E-12
IL36RN				-1,86212886	4,1246E-07	4,2962E-05			
IL1R1				-2,050477083	3,85243E-19	1,37436E-15			
IL1RL1				-1,780563045	2,09629E-10	6,23209E-08			
IL1RL2				-1,056977607	0,000440213	0,012439299			
IL1RN							-1,786285419	1,79318E-15	9,15309E-13
LTA				-1,240070433	0,001077551	0,023839769			
LIF				-1,280066459	0,002198783	0,039919375	-1,028673229	0,000532285	0,007162682
CSF2				-1,806063175	5,31114E-06	0,00037335			
OSM	-1,021137835	5,40529E-13	6,24523E-11	-1,185122373	7,41167E-09	1,27427E-06			
PDGFA	-2,272478426	1,90616E-06	3,613E-05	-1,389753955	4,49523E-07	4,64832E-05	-1,581399384	6,21917E-13	1,98407E-10
CXCR3				-1,45291416	1,66844E-08	2,48895E-06			
CXCR5							-1,934036048	0,002292243	0,020441171
CXCL13	-1,424074157	6,58732E-08	2,05459E-06						
CXCR6	-1,306968334	9,56619E-15	1,51317E-12						
TNFRSF8	-1,687952376	1,27121E-24	1,05566E-21	-1,325878253	0,000447465	0,012442243	-1,066761079	6,82871E-14	2,72316E-11
TNFRSF21	-1,14803883	1,09397E-08	4,33898E-07	-1,55499693	0,000532749	0,014080493	-1,527539994	1,40523E-08	1,44614E-06
TNFSF15				-1,553552934	0,000670813	0,016912552			

Table 14: Down regulated genes involved in IFN signaling in memory, naive and regulatory T cells in the presence of Rotenone.

Gene Symbol	Memory T cells			Naive T cells			Regulatory T cells		
	Log2FoldChange	p-value	p-value adjusted	Log2FoldChange	p-value	p-value adjusted	Log2FoldChange	p-value	p-value adjusted
IFIT1							-1,065151292	0,003181841	0,030227489
IFIT2	-1,002065286	0,002522357	0,045209882	-1,093191298	6,37359E-05	0,000768316	-1,292746567	1,69322E-13	3,39895E-11
IFIT3	-1,291229493	6,88195E-08	9,28668E-06	-2,210555067	6,69543E-35	4,90064E-32	-1,711401325	5,99927E-48	8,30958E-44
IFI6							-1,023914997	8,85392E-11	1,03055E-08
CXCL9				-2,031793942	3,35675E-13	2,17187E-11			
CXCL10	-1,581601086	1,4296E-05	0,000752625	-2,554544029	4,77393E-43	5,59075E-40	-1,72908336	2,10869E-05	0,000551752
OAS1				-2,461582443	2,25746E-08	6,60929E-07	-1,423481364	2,7627E-19	1,9133E-16
OAS2				-1,004691654	4,23297E-22	7,29004E-20			
OAS3				-1,187053263	8,87926E-22	1,42445E-19	-1,082888444	1,60522E-21	2,47043E-18
OASL							-1,133624515	1,02745E-10	1,18594E-08
XAF1				-1,46623894	2,04995E-16	1,93605E-14	-1,502866057	1,577E-40	7,28103E-37
RSAD2				-1,541866322	5,77847E-16	5,20552E-14	-1,656439517	2,96016E-21	3,41676E-18
GBP1				-1,306144323	1,6181E-10	7,31643E-09			
GBP4				-1,175444386	1,21654E-53	3,56173E-50			
GBP6				-1,429016078	3,01859E-05	0,000404471	-1,07649592	6,91213E-10	6,51292E-08
USP18							-1,097053142	0,001996099	0,021057097
ICAM1				-1,182081867	2,63725E-19	3,59126E-17			

Table 15: Up regulated genes encoding heat shock proteins (HSPs) genes in memory, naive and regulatory T cells in the presence of rotenone.

Gene Symbol	Memory T cells			Naive T cells			Regulatory T cells		
	Log2FoldChange	p-value	p-value adjusted	Log2FoldChange	p-value	p-value adjusted	Log2FoldChange	p-value	p-value adjusted
HSPA1A	1,192574902	4,02341E-15	3,14899E-12	4,44836583	2,31949E-24	5,32619E-22	2,542757182	3,42199E-07	1,57993E-05
HSPB1				1,467510911	1,53737E-18	2,02294E-16			
HSPA6	3,030269607	3,97422E-10	1,22782E-07	5,266702817	1,8703E-121	2,1903E-117	4,937540353	1,32394E-20	1,30984E-17
HSPA1B				3,522222436	1,76104E-10	7,87156E-09			
DNAJB1				2,026011551	1,68033E-07	4,0742E-06	1,757483782	4,55557E-08	2,72619E-06
HSPA1B							2,351400271	4,56629E-08	2,72619E-06

Table 16: Down regulated genes involved in IFN signaling in memory, naive and regulatory T cells in the presence of Rotenone.

Gene Symbol	Memory T cells			Naive T cells			Regulatory T cells		
	Log2FoldChange	p-value	p-value adjusted	Log2FoldChange	p-value	p-value adjusted	Log2FoldChange	p-value	p-value adjusted
IFIT2							-1,093655371	1,81046E-09	1,99825E-06
IFIT3	-1,425659327	7,02629E-13	1,13866E-09	-1,504354588	1,30511E-10	1,71328E-07	-1,340563804	3,41827E-18	2,13731E-14
OAS1	-1,00115355	0,000252676	0,009157689				-1,328246028	1,65744E-14	5,03074E-11
OAS3				-1,012034484	7,43847E-10	7,05927E-07			
XAF1	-1,072020199	3,73076E-10	1,56747E-07				-1,110283927	1,63196E-17	6,60452E-14
ICAM1				-1,088581912	8,37572E-09	4,13453E-06			
RSAD2				-1,081515669	2,43315E-06	0,000473202	-1,308782037	1,93339E-10	2,93416E-07
CXCL9				-1,810705037	1,02897E-09	7,71878E-07			